SF 298 KEEP THIS COPY

REPORT DOCUMENTATION PAGE

Form Approved
OMB NO. 0704-0188

1. AGENCY USE ONLY (Leave blank)	2. REPORT DATE	3. REPORT TYPE AND DATES COVERED
	3/21/97	FINAL REPORT 15 Jul 96 - 14 Jul 97

4. TITLE AND SUBTITLE

Polarization Diversity Active Imaging

5. FUNDING NUMBERS

61102F
2301/FS

6. AUTHOR(S)

Russell A. Chipman, Pierre Yves Gerligand, Elizabeth Sornsin, and Matthew Smith.

7. PERFORMING ORGANIZATION NAMES(S) AND ADDRESS(ES)

University of Alabama in Huntsville
301 Sparkman Drive, Physics, OB318
Huntsville, Alabama 35899

AFOSR-TR-97

0321

9. SPONSORING / MONITORING AGENCY NAME(S) AND ADDRESS(ES)

Air Force Office of Scientific Research - NE
Bolling Air Force Base
Washington, D.C.

10. SPONSORING / MONITORING AGENCY REPORT NUMBER

F49620-96-1-0316

11. SUPPLEMENTARY NOTES

The views, opinions and/or findings contained in this report are those of the author(s) and should not be construed as an official Department of the Army position, policy or decision, unless so designated by other documentation.

12a. DISTRIBUTION / AVAILABILITY STATEMENT

Approved for public release: distribution unlimited.

12 b. DISTRIBUTION CODE

13. ABSTRACT (Maximum 200 words)

Polarization Diversity Active Imaging illuminates a scene or target with a sequence of polarization states and then measures images of the polarization state scattered from a scene or target. These polarization images are then analyzed to provide additional details in the optical signature of objects by quantifying the object interaction with polarized light.

The Mueller Matrix Imaging Polarimeter at The University of Alabama in Huntsville has been configured for bistatic scattering measurements of the Mueller matrices of small targets. The initial targets used were simple geometric shapes (spheres and cones). These targets were chosen because mathematical descriptions of their surfaces are easily obtained. Therefore, the measured polarization signatures can be compared with the known surface orientations.

Data obtained indicated the ability of the PDAI technique to measure polarimetric signatures of the spheres and cones made of different materials (metals, plastics, and wood). In that data, there were evident relationships between various polarization properties and an object's material and shape. The results demonstrated the feasibility and the strong potential of the PDAI technique to determine the shape and orientation of an object from its polarization properties.

14. SUBJECT TERMS

15. NUMBER IF PAGES
89

16. PRICE CODE

17 SECURITY CLASSIFICATION OR REPORT	18. SECURITY CLASSIFICATION OF THIS PAGE	19. SECURITY CLASSIFICATION OF ABSTRACT	20. LIMITATION OF ABSTRACT
UNCLASSIFIED	UNCLASSIFIED	UNCLASSIFIED	UL

Final Report

Polarization Diversity Active Imaging:

Mueller Matrix Imaging Polarimetry of Spheres and Cones

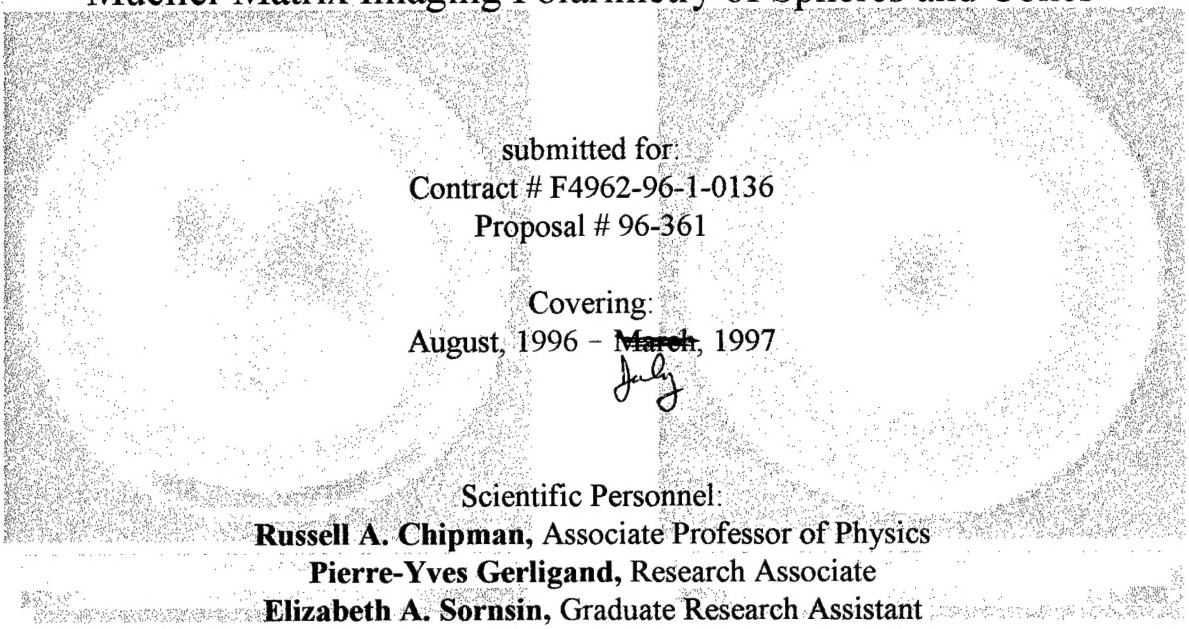

submitted for:
Contract # F4962-96-1-0136
Proposal # 96-361

Covering:
August, 1996 - ~~March~~ July, 1997

Scientific Personnel:
Russell A. Chipman, Associate Professor of Physics
Pierre-Yves Gerligand, Research Associate
Elizabeth A. Sornsin, Graduate Research Assistant
Matthew H. Smith, Research Scientist

Polarization and Lens Design Laboratory
Department of Physics
Optics Bldg. 318
The University of Alabama in Huntsville
Huntsville, AL 35899

telephone: (205)890-6417 ext. 318
facsimile: (205)890-6873
email: chipmanr@email.uah.edu

Contracting Office:
Captain William Arrasmith
Air Force Office of Scientific Research
Bolling Air Force Base
Washington, DC

Table of Contents

List of Figures

Appendices

1. Summary

This final report describes experiments into Polarization Diversity Active Imaging (PDAI) performed at the Physics Department of the University of Alabama in Huntsville (UAH).

Polarization Diversity Active Imaging illuminates a scene or target with a sequence of polarization states and then measures images of the polarization state scattered from a scene or target. These polarization images are then analyzed to provide additional details in the optical signature of objects by quantifying the object interaction with polarized light. These polarization images are then analyzed in the following sequence:

1. Measure the Mueller matrix image associated with the scene,
2. Map the retardance, diattenuation, and depolarization images for the scene,
3. Estimate the plane of incidence and target orientation pixel by pixel,
4. Obtain estimates of the refractive index of objects in the scene and other information relating to texture.

With a successful Polarization Diversity Active Imaging apparatus, a series of polarization images would be acquired, the image would be displayed, and then we could overlay images of the retardance, diattenuation, depolarization, orientation of the surface normal, and estimates of refractive index. These additional images would be useful for image interpretation tasks such as clutter rejection, target identification, target classification, target orientation, etc. Polarization Diversity Active Imaging may prove useful for many difficult imaging tasks such as satellite imaging, plume/hard body identification, hard body/wake, unresolved objects, and overcoming camouflage. But this present contract specifically aims to evaluate if Polarization Diversity Active Imaging could measure the orientation of bodies such as satellites in space and estimate their refractive index. Thus PDAI might allow the direction in which a space-based telescope or radar is pointing to be determined.

The Mueller Matrix Imaging Polarimeter at The University of Alabama in Huntsville has been configured for bistatic scattering measurements of the Mueller matrices of small targets. The initial targets used were simple geometric shapes (spheres and cones). These targets were chosen because mathematical descriptions of their surfaces are easily obtained. Therefore, the measured polarization signatures can be compared with the known surface orientations.

In an interim report submitted in November 1996, we presented early data indicating the ability of the PDAI technique to measure polarimetric signatures of the spheres and cones made of different materials (metals, plastics, and wood). In that data, there were evident relationships between various polarization properties and an object's material and shape. The results demonstrated the feasibility of the PDAI technique to determine the shape and orientation of an object from its polarization properties.

As an example, *with PDAI it was easy to distinguish metal spheres from metal cones* viewed nearly head-on. However, with simple intensity images of these objects it might be *impossible* to distinguish spheres from disks from head-on cones. This data makes a compelling argument for the continued study of PDAI as a means of estimating surface geometry and material.

This report completes the polarimetric analysis of the data sets, and presents a mathematical approach for comparing our measured polarization properties to the *known* geometry of the targets. For a number of spherical targets, diattenuation and retardance properties are correlated with the angle-of-incidence and angle of scatter of the target. It is shown that *strong* correlations exist between theory and measurement in a number of samples. For some samples, we were able to accurately estimate the angle between the illumination beam and the camera, *even though the angle was only ~10°*. It is unlikely this information could have been obtained through conventional intensity imaging, once again indicating the potential strength of the PDAI technique.

Polarization Diversity Active Imaging

R.A. Chipman, University of Alabama in Huntsville

Bistatic Configuration:

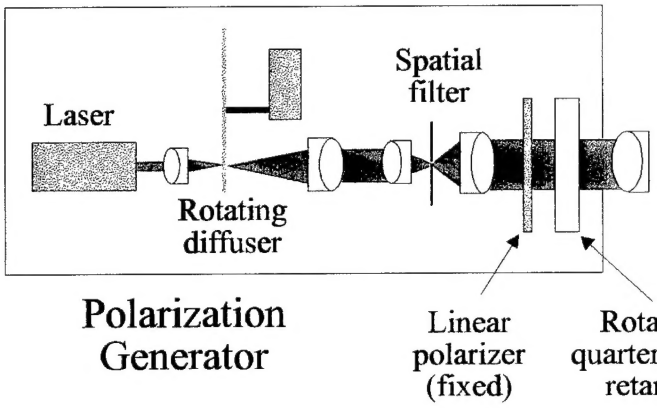

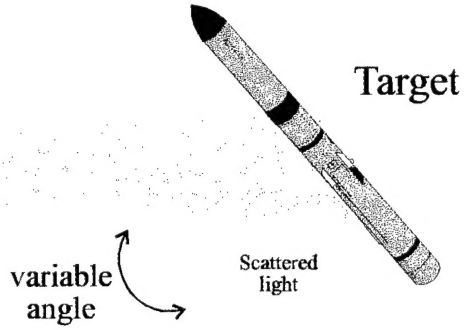

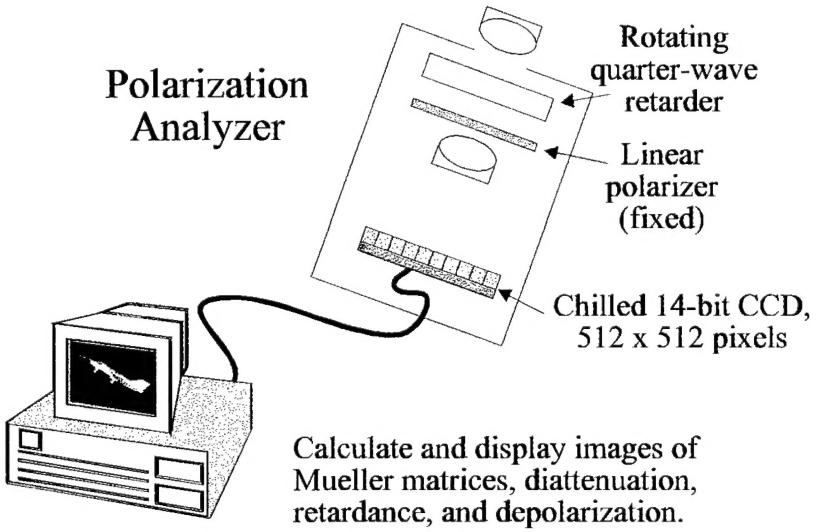

- Obtain Mueller matrix images of radiation scattered from scenes and targets.
- Investigate scatter polarization relationship to object geometry.
- Measure images of retardance, diattenuation, and depolarization.
- Estimate object orientation and refractive index.
- Classify target texture.

This final report documents the work as a whole performed under our AFOSR contract. Accomplishments include:

- Modified the Mueller Matrix Imaging Polarimeter for PDAI measurements
- Wrote data reduction and display software
- Measured the Mueller matrices of seven different models
  - stainless steel sphere
  - wooden sphere
  - smooth plastic sphere
  - ping-pong ball (diffuse plastic sphere)
  - aluminum cone w/ rounded tip (re-entry vehicle model) at 2 orientations
  - flat black coated cone w/ ridges around tip (re-entry vehicle model) at 2 orientations
  - brass (gold-toned) cone with rounded tip (re-entry vehicle model) at 2 orientations
- Determined the data integrity of our measurements
- Calculated polarization signatures of out targets
  - depolarization
  - diattenuation
  - retardance
  - polarizance
  - polarization crosstalk
- Developed technique for comparing measured signatures with mathematically predicted results

A couple of significant results were obtained during the course of this study that indicated the efficacy of the PDAI technique. These results include:

- Some materials (plastic, metal) were found to produce predictable polarization signatures, while other materials (wood) were less predictable.
- **The orientation and magnitude of linear diattenuation and linear retardance were**

observed to have distinctive patters that directly related the geometry of targets.

- High correlation was calculated between these polarization properties and the shape of the mathematically determined target surface.

In this **Summary** section we present some of the most interesting data sets that we measured. In the Experimental Methods section. These measurements were made with the bistatic configuration of the MMIP shown on the next page. In the **Experimental Methods** of this report, the measurement process and data reduction techniques are described in more detail. Finally, in the **Appendix** of this report, *all* of the data from this study is presented.

The first images in this section correspond to the *polarizance* of the sample. Data is shown from a ping-pong ball and from a stainless steel sphere. The next sets of images are of the *linear diattenuation* and the *linear retardance*. It is interesting to note that each of these three properties reveals information about the surface geometry. (See the **Experimental Methods** section of this report for full descriptions of these properties.)

To understand the relationship between these properties and the geometry of the targets, we developed a mathematical model of the angle-of-incidence and angle-of-scatter of spheres measured in our bistatic MMIP configuration. (See the **Experimental Methods** section of this report for a full description of this model.) Two figure are shown that demonstrate a strong correlation between the diattenuation orientation and the angle of incidence of a sphere.

The final figure demonstrates the power of the PDAI technique. Our measurements were made with a ~10° angle between the illumination beam and the camera. This figure plots the magnitude of the correlation between our measured orientation of diattenuation and the angle of scatter as a function of incident angle. *It is found that this correlation maximizes at an angle of ~10°.* Therefore, we were able to determine the angle of the illumination beam with respect to the camera location! It is very unlikely that this information could have been determined from simple intensity images.

Polarization Diversity Active Imaging

R.A. Chipman, University of Alabama in Huntsville

Polarizance Vector
Metal sphere

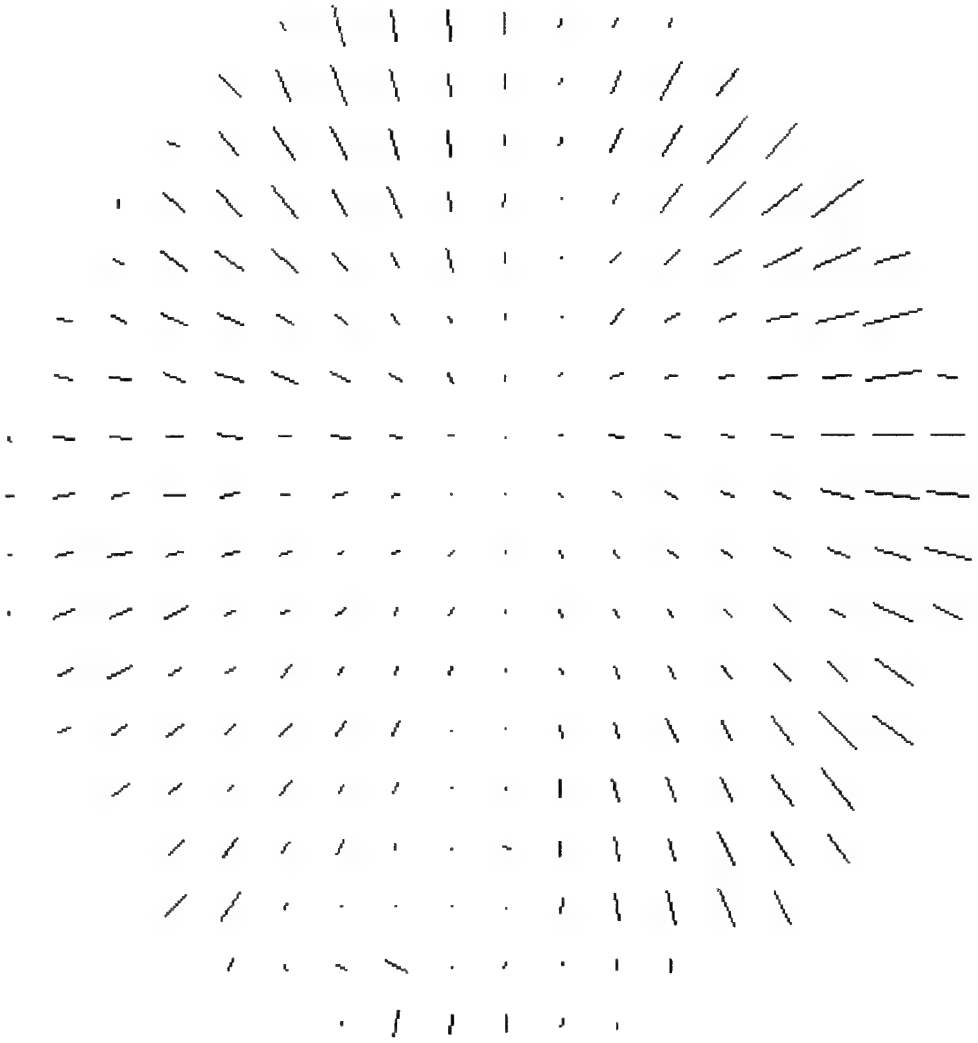

Polarization Diversity Active Imaging

R.A. Chipman, University of Alabama in Huntsville

Polarizance Vector
Ping-pong ball

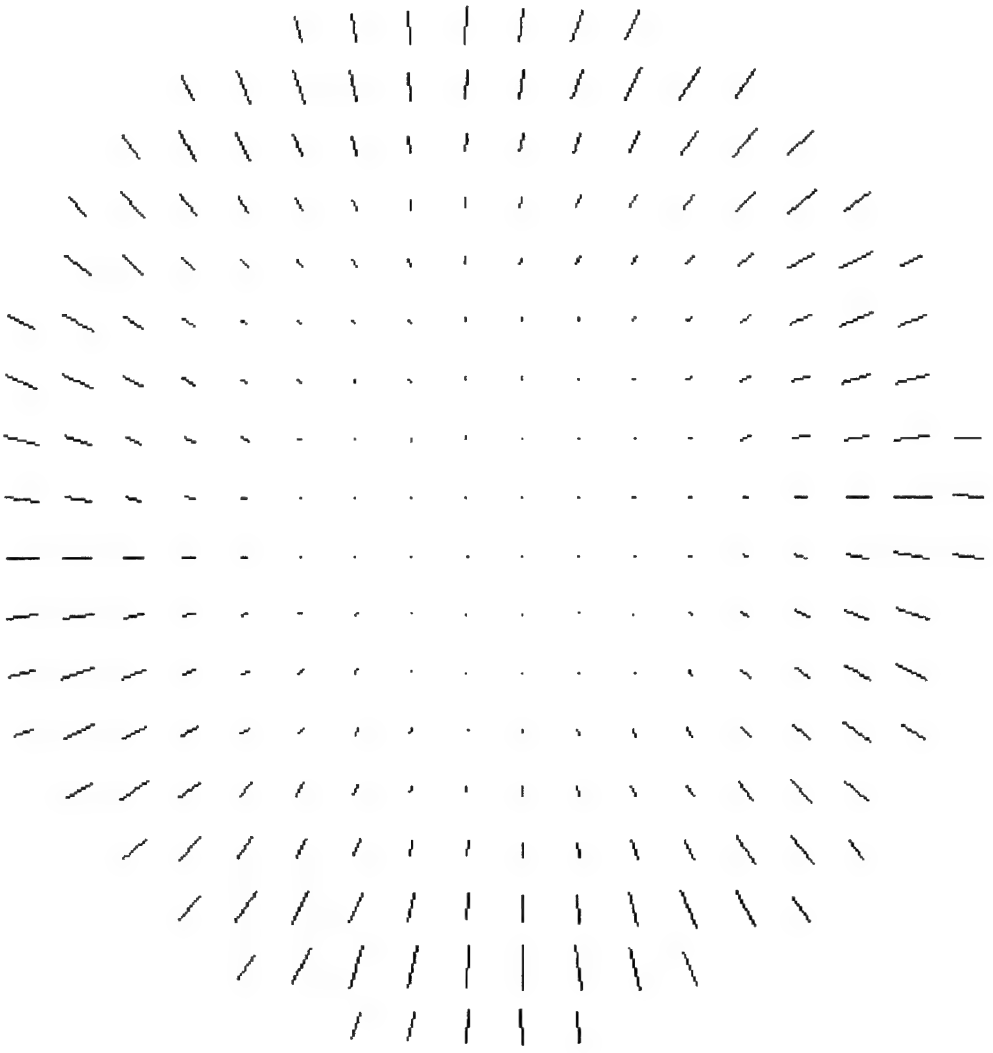

Polarization Diversity Active Imaging

R.A. Chipman, University of Alabama in Huntsville

Metal sphere

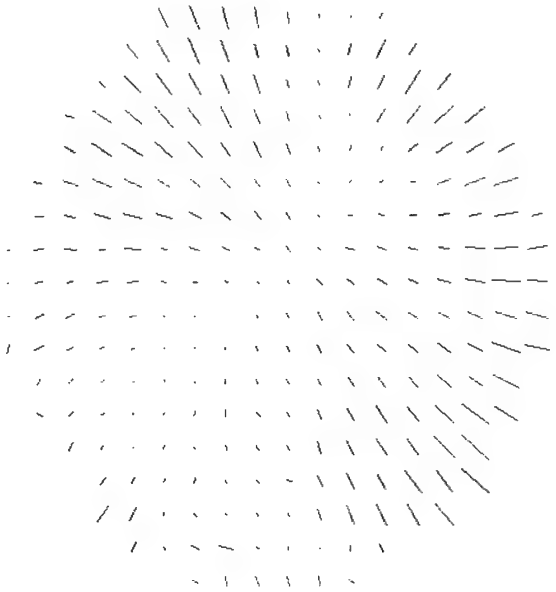

Orientation and Magnitude of the diattenuation

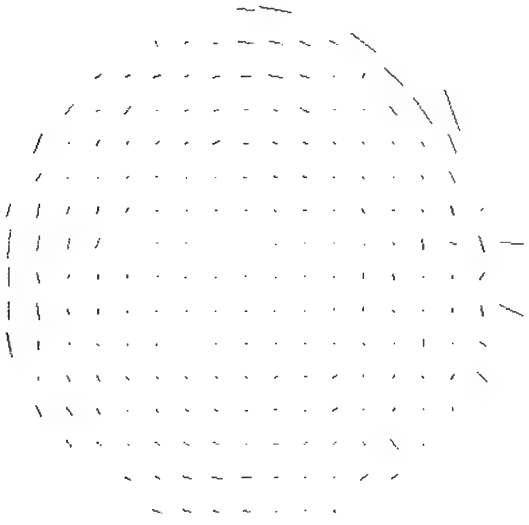

Orientation and Magnitude of the retardance

Polarization Diversity Active Imaging

R.A. Chipman, University of Alabama in Huntsville

Ping-pong ball

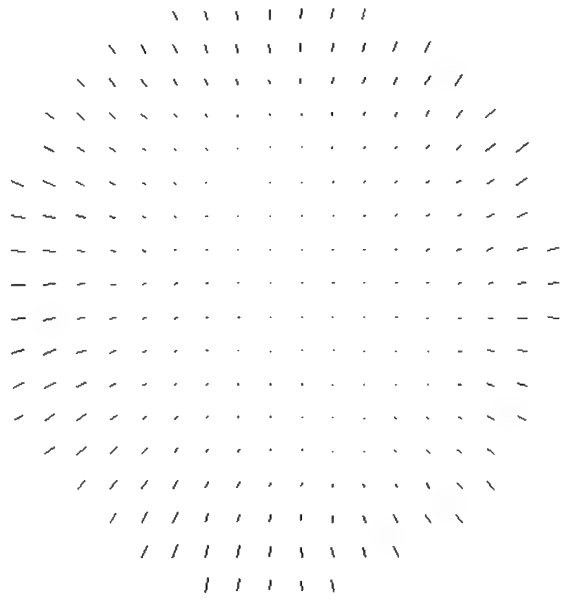

Orientation and Magnitude of the diattenuation

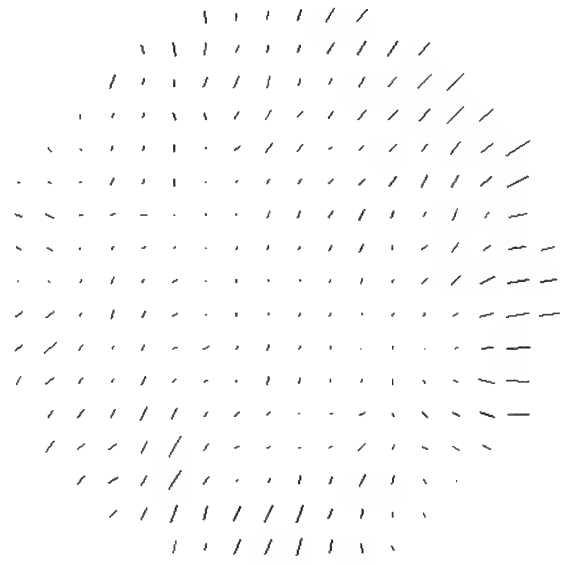

Orientation and Magnitude of the retardance

Polarization Diversity Active Imaging

R.A. Chipman, University of Alabama in Huntsville

Metal sphere

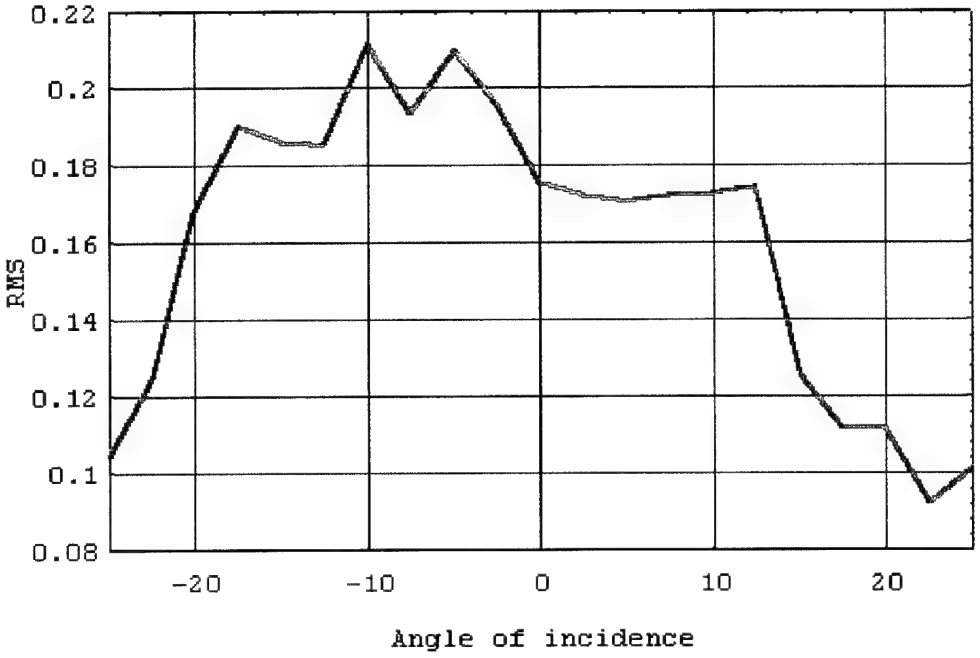

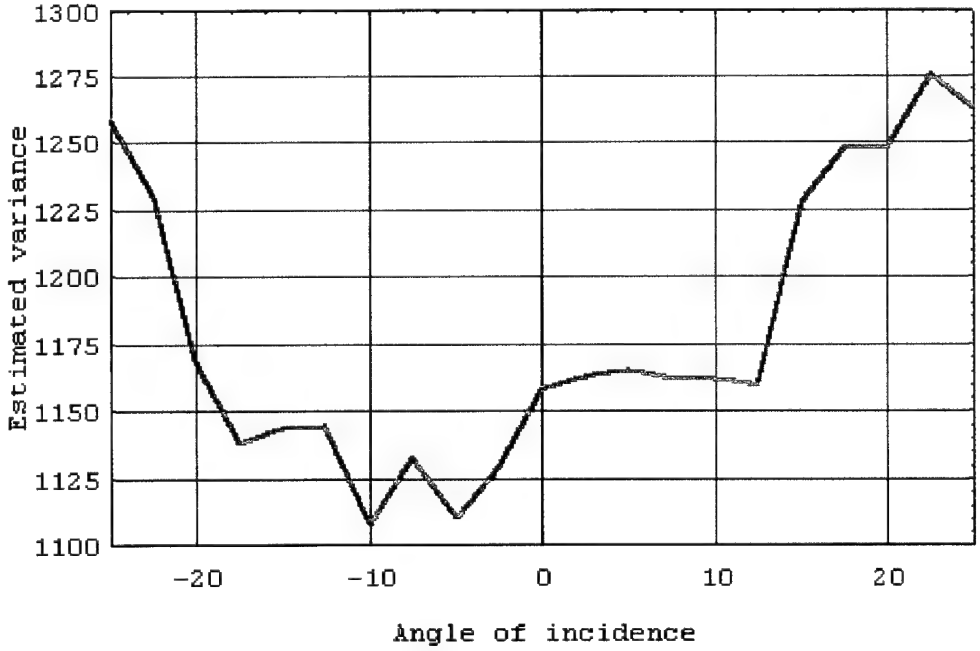

Polarization Diversity Active Imaging

R.A. Chipman, University of Alabama in Huntsville

Ping-pong ball

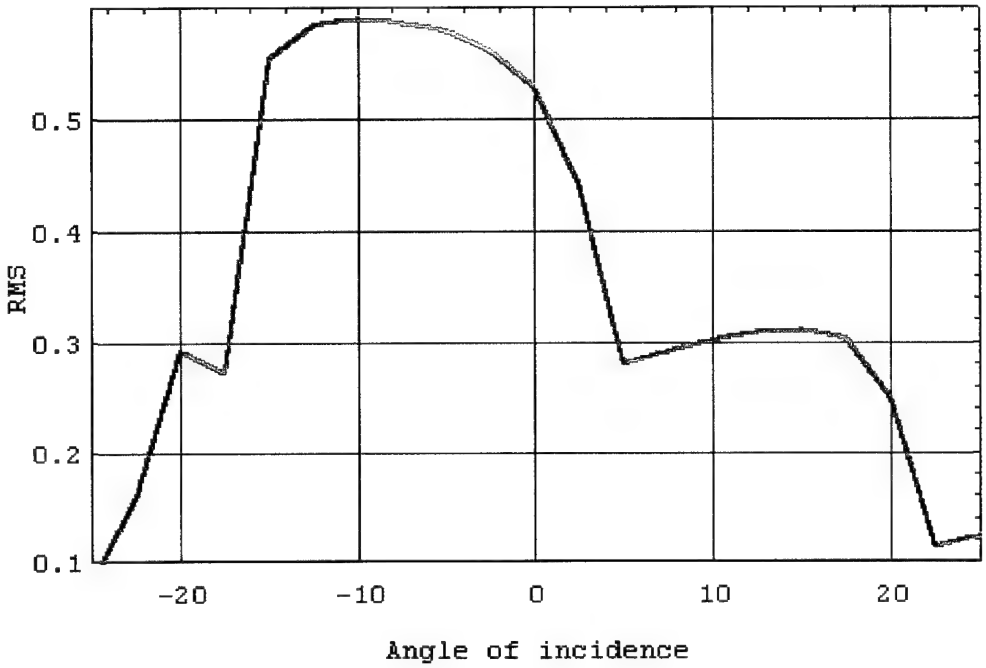

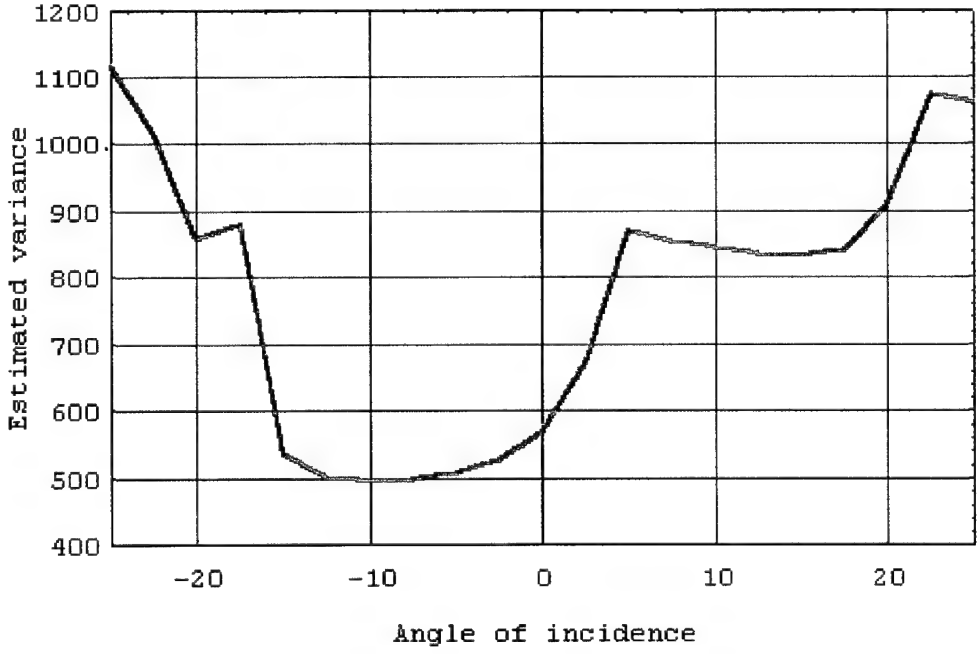

Polarization Diversity Active Imaging

R.A. Chipman, University of Alabama in Huntsville

Metal sphere

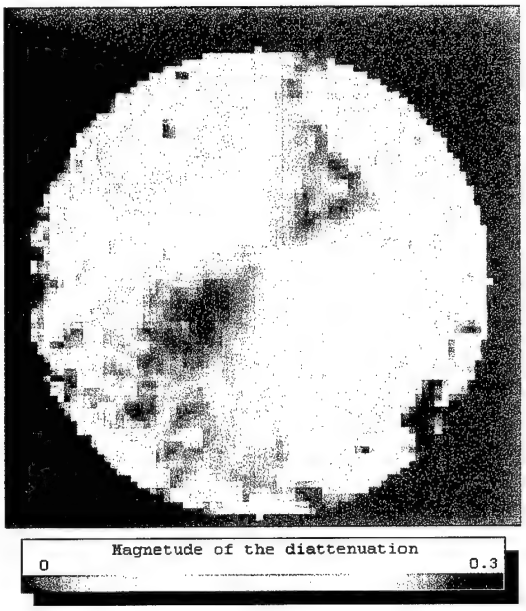

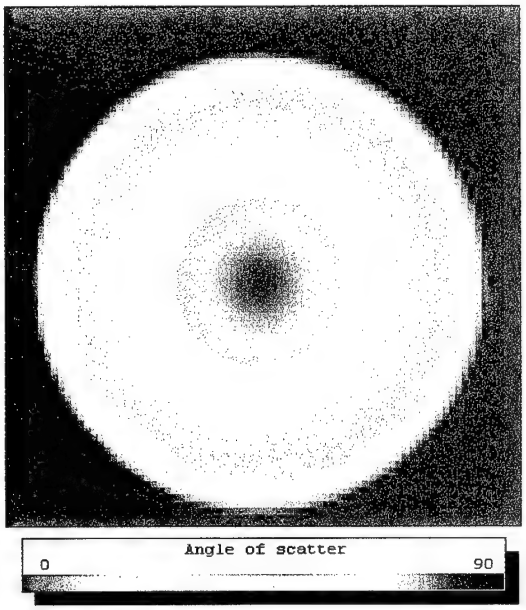

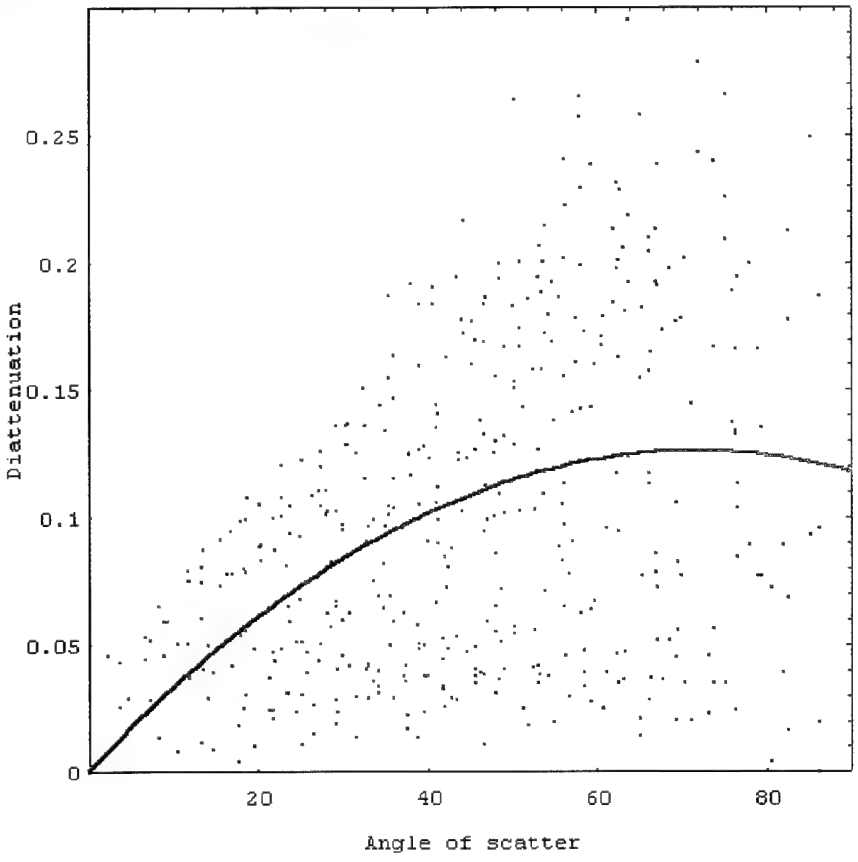

Polarization Diversity Active Imaging

R.A. Chipman, University of Alabama in Huntsville

Ping-pong ball

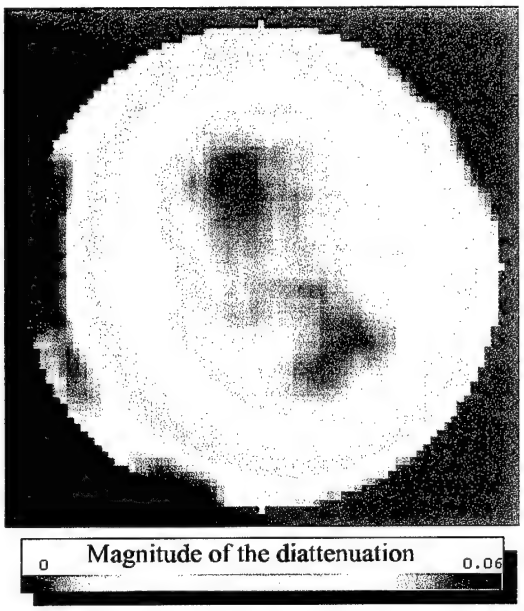

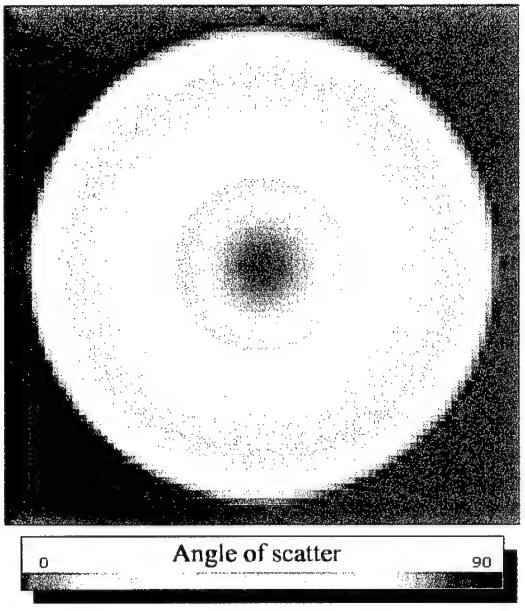

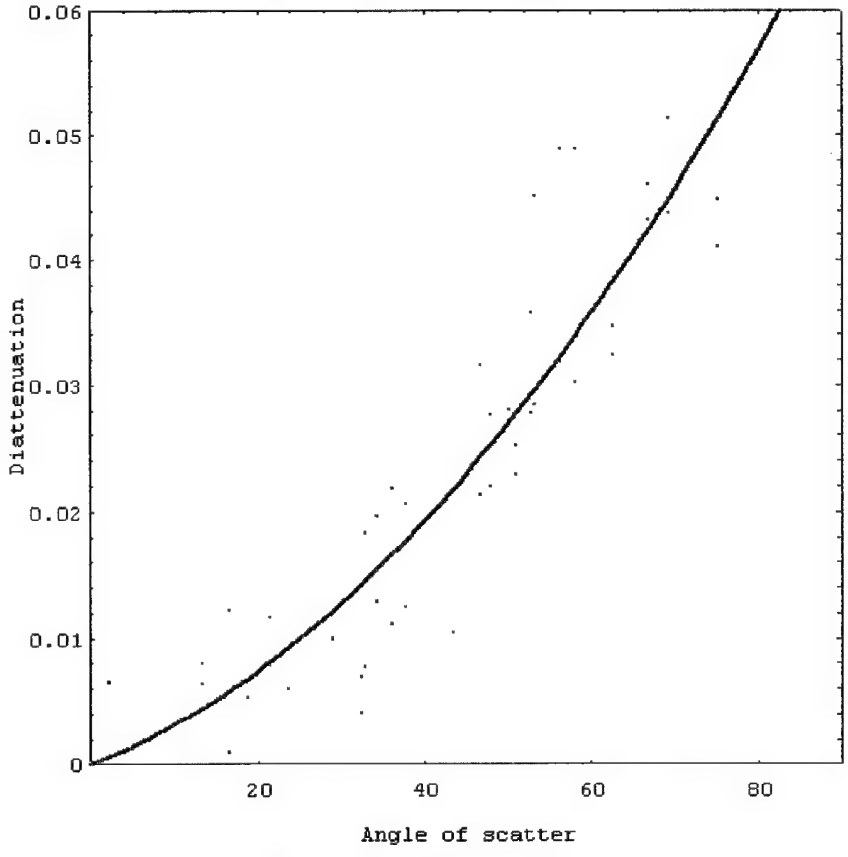

Polarization Diversity Active Imaging

R.A. Chipman, University of Alabama in Huntsville

Metal sphere

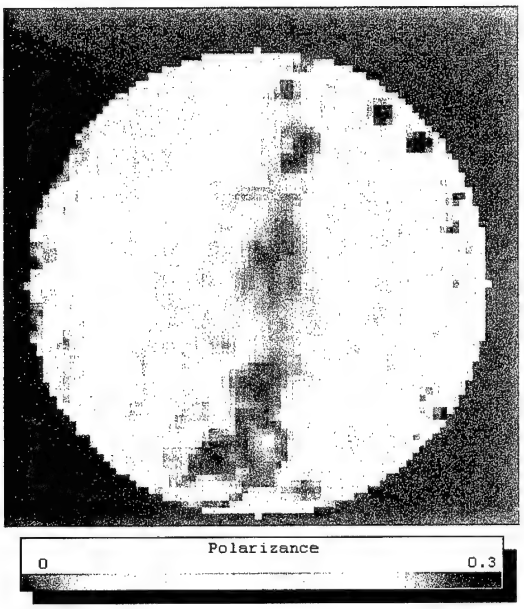

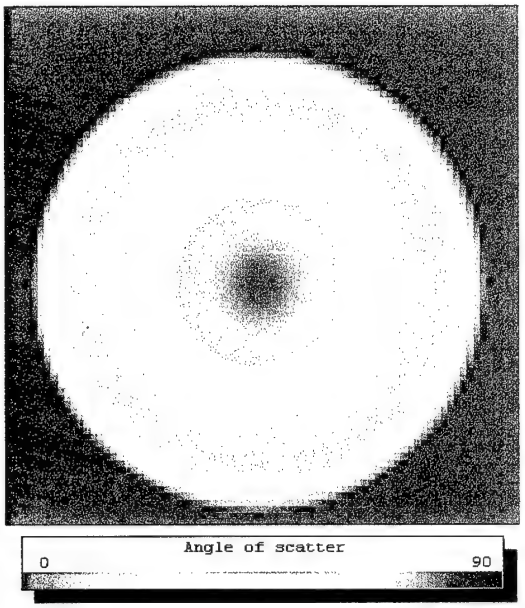

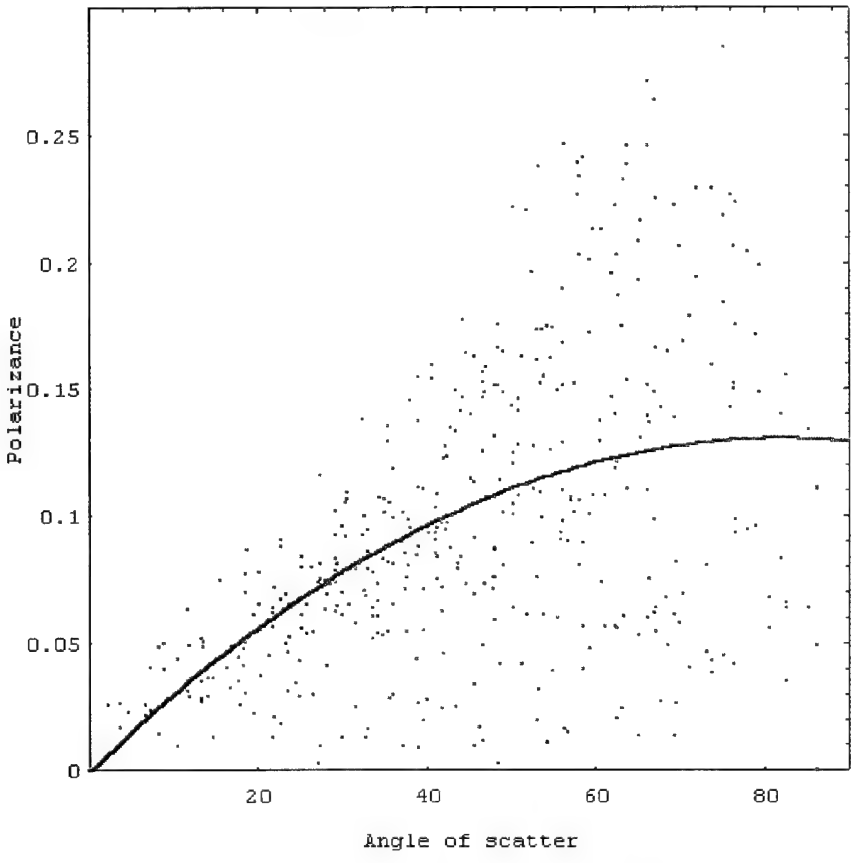

Polarization Diversity Active Imaging

R.A. Chipman, University of Alabama in Huntsville

Ping-pong ball

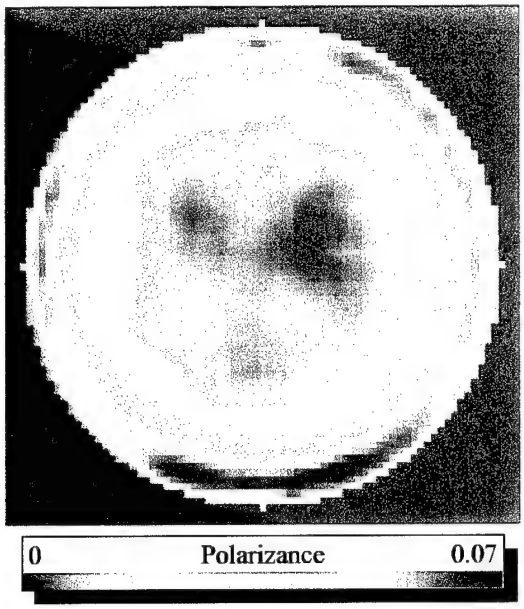

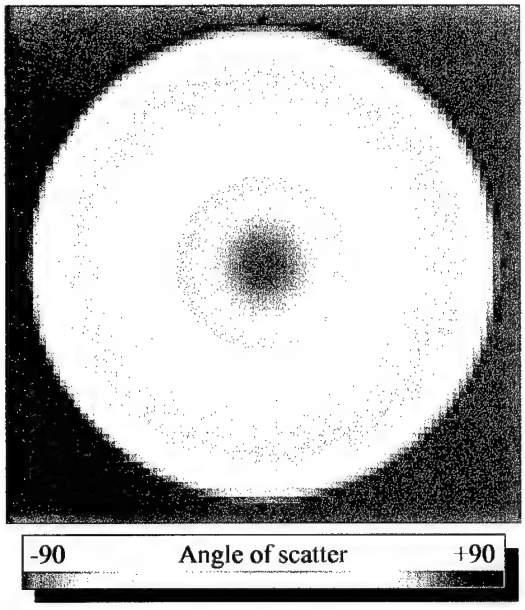

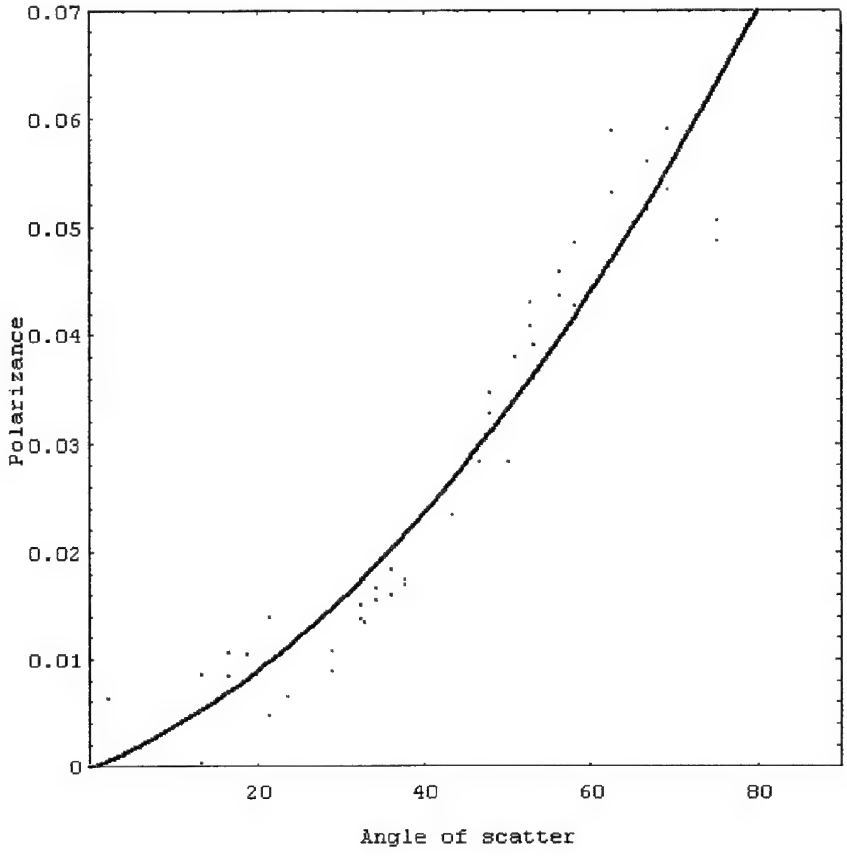

Polarization Diversity Active Imaging offers a wealth of previously unavailable information to an investigator. This study has demonstrated a strong potential of PDAI for estimating the material, geometry, and orientation of an object. As we continue to build our database of the polarization properties of various materials and geometrical shapes, the scope of PDAI's abilities will be uncovered.

2. Experimental methods

2.1. Intensity Mask

A black felt backdrop was placed behind the target to eliminate any reflected or scattered light from objects other than the target. The low intensity regions surrounding the target had very noisy signatures. To eliminate these regions an intensity mask was applied. The logarithm of intensity image was used to calculate the intensity mask for the polarization images. The images are thresholded at 25-35%. Low intensity regions were replaced with null values according to the mask calculated from this figure. The intensity mask is applied to the images during the smoothing and Mueller matrix decomposition routines. The masked values are usually shown as solid red or solid deep blue in the polarization property images.

2.2. Smoothed Mueller Matrix Images

The Mueller matrix describes all the polarizing and polarization-scrambling properties of an optical element. There are sixteen degrees of freedom in the Mueller matrix: one degree of freedom in intensity (transmission, reflection, or scattering), three degrees of freedom in retardance, three degrees of freedom in diattenuation, and nine degrees of freedom in depolarization. We have developed, with Air Force support, algorithms which decompose the Mueller matrix depolarizing, retarding, and diattenuating properties These algorithms are described in detail in References [1][8].

	Spherical targets			
	Metal	Pin-pong	Plastic	Wood
Size of the averaging filter	3-by-3	9-by-9	9-by-9	9-by-9

Table 1(a)

Polarization Diversity Active Imaging

R.A. Chipman, University of Alabama in Huntsville

Aluminum Cone (position 2, size filter : 3)

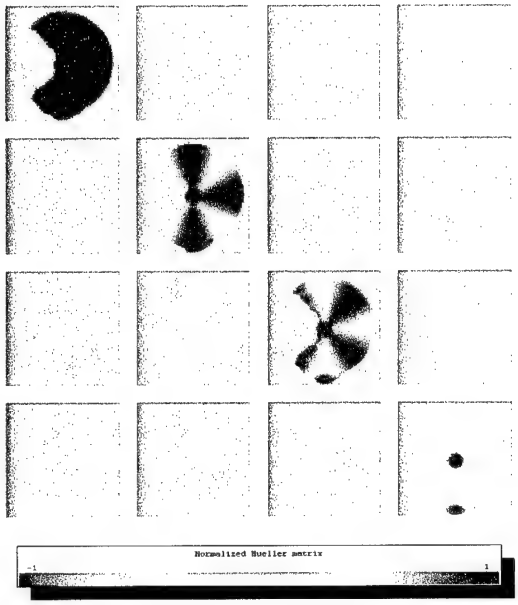

Smoothed normalized Mueller matrix

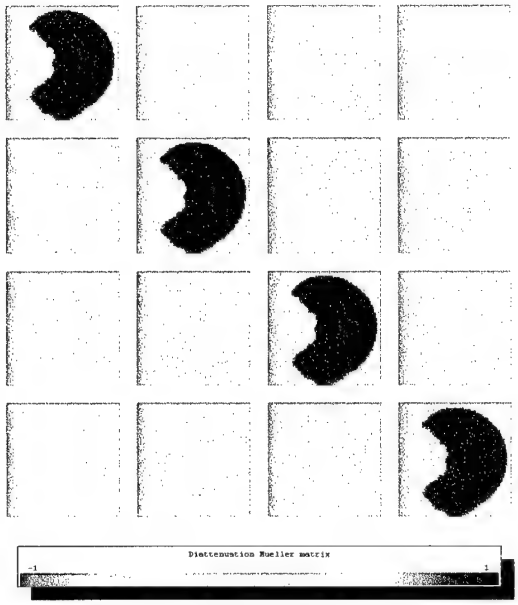

Smoothed diattenuation Mueller matrix

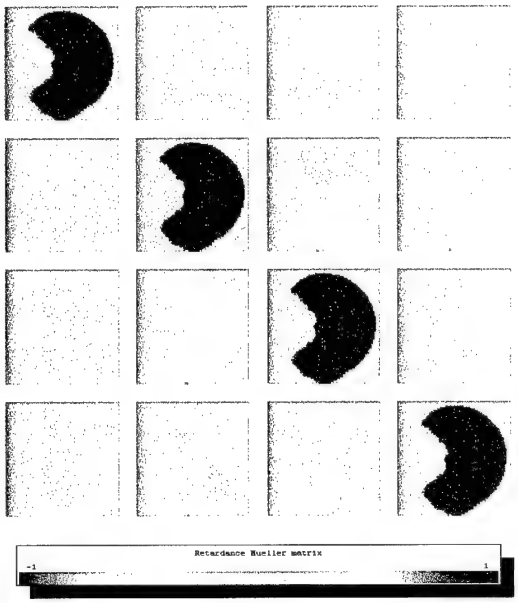

Smoothed retardance Mueller matrix

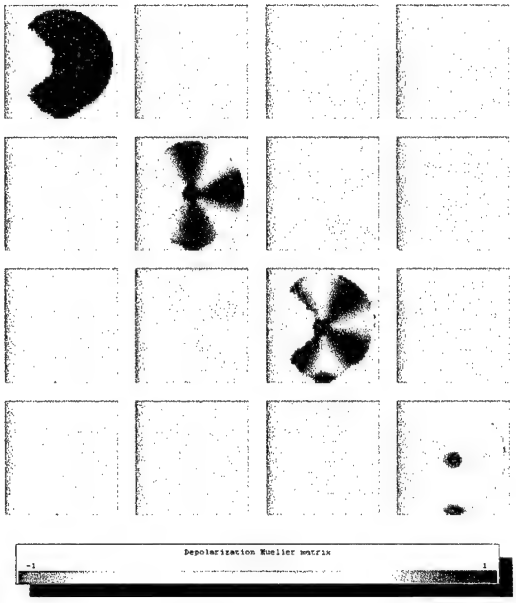

Smoothed depolarization Mueller matrix

To reduce image clutter, the Mueller matrix data in smoothed via a boxcar method using either 3-by-3, 5-by-5, or 9-by-9 image pixels to average adjacent image regions. We apply this smoothing to each of the sixteen images in the (unsmoothed) Mueller matrix. Table 1(a) and 1(b) report the size of the boxcar applied on each target. All of the property images in the remainder of this report were calculated from the smoothed Mueller matrix.

	Conical targets					
	Alum. 1	Black 1	Gold 1	Alum. 2	Black 2	Gold 2
Size of the averaging filter	3-by-3	3-by-3	3-by-3	3-by-3	5-by-5	5-by-5

Table 1(b)

2.3. Diattenuation Matrix Image

The diattenuation matrix is generated by the decomposition process by removing all the retardance and depolarization properties from the Mueller matrix. Diattenuation refers to the difference in attenuation between two orthogonal polarization states. Diattenuation has three degrees of freedom which can be expressed as the diattenuation magnitude, fast axis orientation and ellipticity or alternatively can be expressed as horizontal-vertical linear diattenuation, 45°-135° linear diattenuation and circular diattenuation. The d_{00} element is set to +1 during normalization.

2.4. Retardance Matrix Image

The retardance matrix is obtained following the precedent method by removing all the diattenuation and depolarization properties from the Mueller matrix. Retardance is the difference in phase accumulation between two polarizations states. The retardance has three degrees of freedom which can be expressed as the retardance magnitude, fast axis orientation, and ellipticity or alternatively can be expressed as horizontal-vertical linear retardance, 45°-135° linear retardance, and right-left circular retardance. The r_{00} element remains normalized to +1. The remaining first row (r_{01}, r_{02}, r_{03}) and first column (r_{10}, r_{20}, r_{30}) elements were set to zero during the decomposition.

2.5. Depolarization Matrix Image

The depolarizer matrix is generated by the decomposition process by removing all the retardance and diattenuation properties from the Mueller matrix. Depolarization is the property of coupling polarized light into partially-polarized or un-polarized light. Depolarization has nine degrees of freedom. The depolarizer matrix image is particularly useful to observe the type of depolarization behavior across the image. An isotropic depolarizer has equal elements along the diagonal of the matrix which means all incident polarized states are depolarized the same amount. An inhomogeneous depolarizer has different values along the diagonal which means the incident states are depolarized by differing amounts. The p_{00} element is set to +1 during normalization. The Mueller matrix decomposition algorithms automatically set the p_{01}, p_{02}, and p_{03} elements (which are related to diattenuation) to zero in the depolarizer matrix.

2.5.1. Depolarization Index Image

The depolarization index is the depolarization of the reflected and scattered light averaged for all possible incident polarized states[9]. The depolarization index for light exiting an optical element ranges from zero for light that remains completely polarized, to 0.5 for light that is 50% depolarized, to +1 for light that is completely depolarized.

2.5.2. Polarizance and Polarizance Vector

Polarizance and Polarizance Vectors [9] are both generated from the pure Mueller matrix (M) image. If we consider the case of an unpolarized incident state, the exiting state is determined only by the first column of M. The degree of polarization (DOP) of this exiting light resulting from unpolarized incident light is called the *polarizance*. Thus, the polarizance is given by :

$$\mathbf{P} = \frac{1}{\mathbf{m}_{\epsilon\epsilon}} \sqrt{\mathbf{m}_{\cap\epsilon}^{\parallel} + \mathbf{m}_{\parallel\epsilon}^{\parallel} + \mathbf{m}_{\sum\epsilon}^{\parallel}} \qquad (1)$$

The Polarizance vector $\vec{P}$ is then given by the first column of the Mueller matrix M. Physically, components of $\vec{P}$ are equal to the horizontal DOP, 45° DOP and circular DOP produced by unpolarized light.

The third component of the polarizance vector for all targets that were measured was equal to zero and showed the complete absence of circular polarizance. However, horizontal and 45° polarizance were observed. The polarization was a maximum for metal targets (25%-30% of linear polarizance) and a minimum for the ping-pong ball and the wood sphere (respectively 6% and 7%).

2.6. Retardance Images

The retardance images are calculated from the pure retardance matrix image discussed in Section 5. Retardance occurs when different polarized states have different phase shifts in their interaction with the target. The difference can result from different optical path lengths due to the curvature of the surface, optical properties of the surface material (*e.g.* birefringence), or angle of incidence differences across the incident beam. We are particularly interested in:

- the orientation of the linear retardance as related to the orientation of the target surface
- the magnitude of the linear retardance as related to the magnitude of the angle of incidence.

2.6.1. Orientation of Linear Retardance Fast Axis Image

The fast axis of the linear retardance represents the orientation of the linear state which will exit the sample (reflect from the target) with the least amount of retardance. Due to the curvature of the spherical and conical targets, different orientations of incident polarization will be the fast state across the image. As will be seen later in the diattenuation orientation image, the curvature and orientation of the reflecting surface gives distinct patterns to the polarization orientations.

2.6.2. Linear Retardance Magnitude Image

The linear retardance magnitude is the maximum difference in phase between linearly polarized states. We describe a commercial quarter-wave retarder, by saying it has 90° of linear retardance with a certain orientation of the fast axis. This linear retardance magnitude includes the horizontal-vertical retardance and 45°-135° linear retardance components.

2.6.3. Horizontal-Vertical Linear Retardance Image

The horizontal-vertical retardance is the relative phase introduced in scattering between horizontally polarized light and vertically polarized light. This is one of the three retardance components. If this component is > 0, then horizontal light has a smaller phase change through the reflection than vertical light. If this component is <0, then vertical light has the smaller phase change.

2.6.4. Circular Retardance Image

The circular retardance is the relative phase between right circularly-polarized (RCP) light and left circularly-polarized (LCP) light. If the circular retardance component is > 0, then RCP light travels has a smaller phase change on reflection than LCP light. The presence of circular retardance indicates that linearly polarized incident light will have its plane of polarization rotated on scattering.

2.7. Diattenuation Images

Diattenuation is the difference in the reflected intensity from the surface of the target between different incident polarized states. There are three degrees of freedom in diattenuation: magnitude, orientation (of the maximum reflected state), and ellipticity. Diattenuation can also be described by the three orthogonal components: horizontal-vertical linear diattenuation, 45°-135° linear diattenuation, and right-left circular diattenuation. We are particularly interested in:

Polarization Diversity Active Imaging

R.A. Chipman, University of Alabama in Huntsville

Aluminum Cone (position 2, size filter : 3)

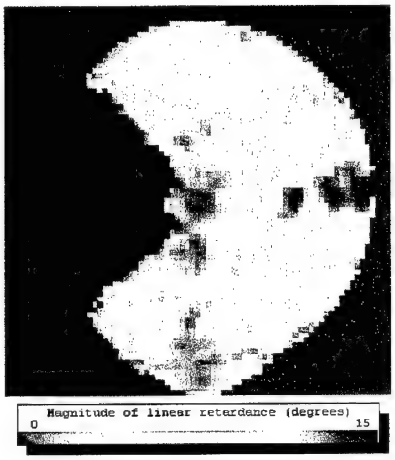

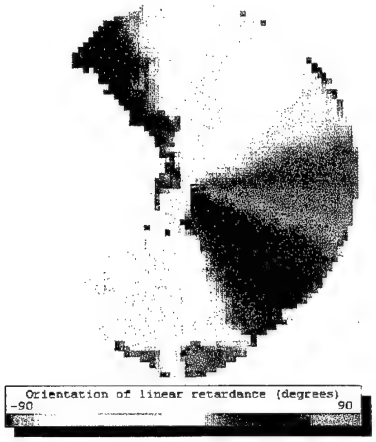

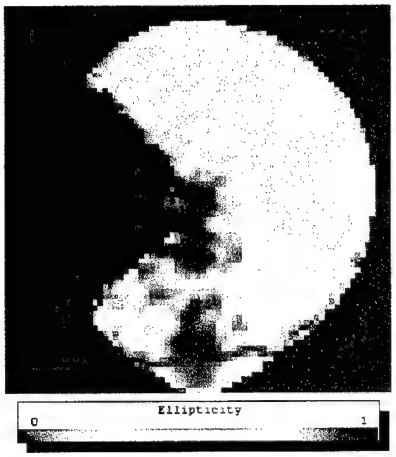

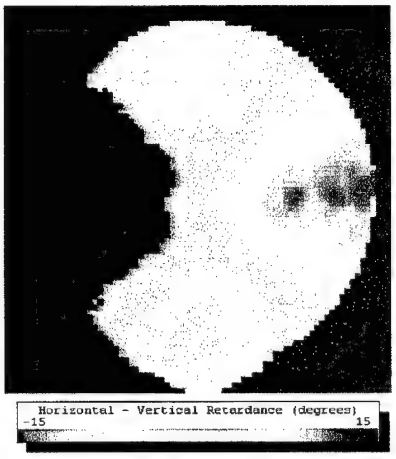

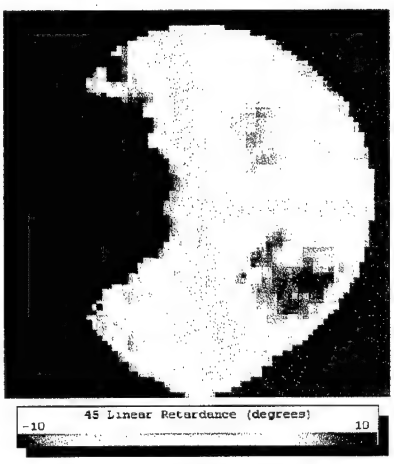

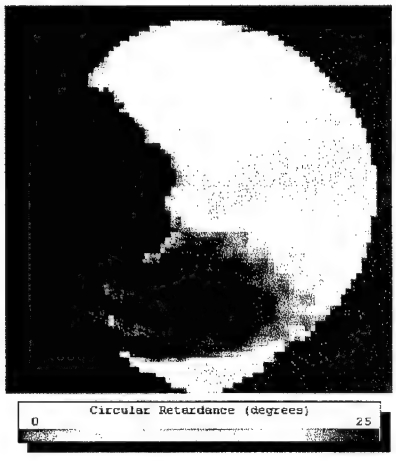

- the orientation of the linear diattenuation as related to the orientation of the target surface
- the magnitude of the linear diattenuation.

2.7.1. Orientation of Linear Diattenuation Image

The orientation of the linear diattenuation corresponds to the orientation of the linearly polarized state which has the greatest reflected intensity coefficient. This is analogous to the polarizer axis for transmitted light. Please note that an orientation of +90° is the same as an orientation of −90°. The orientation will be noisier in regions where the diattenuation magnitude approaches zero and the orientation is undefined.

2.7.2. Linear Diattenuation Magnitude Image

The linear diattenuation magnitude shows the difference in reflection intensities for all the linear polarization states. A commercial diattenuator (polarizer) is usually described by the relative transmittances (*e.g.* 0.99999 and <0.00001) and polarizer axis (*e.g.* vertical). A "perfect" polarizer has diattenuation equal to 1.

2.7.3. Horizontal−Vertical Diattenuation Image

The horizontal−vertical diattenuation component describes the difference in reflected intensity between horizontal and vertical polarized states. Zero values mean horizontal and vertical polarized light scatter with the same intensity. Positive values mean horizontal light is reflected more than vertical, and negative values mean vertical light is reflected more than horizontal.

2.7.4. Circular Diattenuation Image

The circular diattenuation is the difference in reflected intensity between incident right and left circularly-polarized light. Zero values mean there is no difference in reflected intensities,

Polarization Diversity Active Imaging

R.A. Chipman, University of Alabama in Huntsville

Aluminum Cone (position 2, size filter : 3)

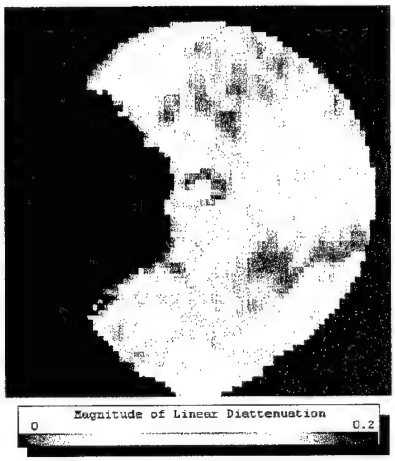

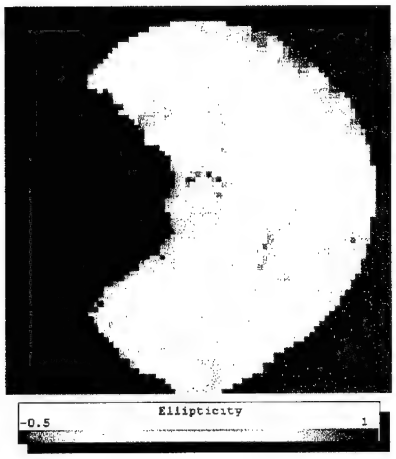

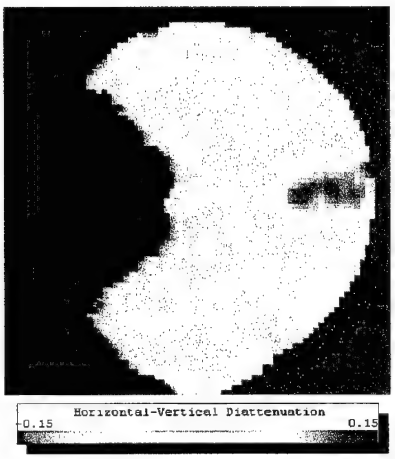

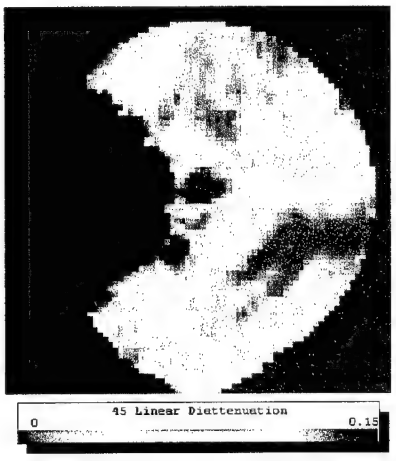

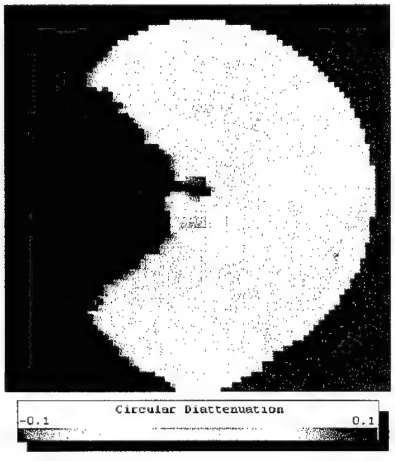

positive values mean RCP light is reflected more than LCP, and negative values mean LCP light is reflected more than RCP.

2.8. Polarization Crosstalk Images

Crosstalk occurs when light from one polarized state (e.g. horizontal) is coupled into the orthogonal polarized state (e.g. vertical). Four images of crosstalk are shown below:

- horizontal-to-vertical polarized state
- vertical-to-horizontal polarized state
- 45°-135° linear polarized state
- left-to-right circular polarized state.

2.8.1. Horizontal-to-Vertical Crosstalk

The horizontal-to-vertical crosstalk is derived from the Mueller matrix elements as:

$$\mathrm{Xtalk}_{\times\rho} = \frac{1}{2}\left[1 - \frac{\mathbf{m}_{\cap\epsilon} + \mathbf{m}_{\cap\cap}}{\mathbf{m}_{\epsilon\epsilon} + \mathbf{m}_{\epsilon\cap}}\right] \tag{2}$$

The values for the horizontal-to-vertical crosstalk range from 0 when the reflected light is horizontally polarized, to 0.5 when the reflected light is unpolarized, to +1 when the reflected light is vertically polarized.

2.8.2. Vertical-to-Horizontal Crosstalk

The vertical-to-horizontal crosstalk is derived from the Mueller matrix elements as:

$$\mathrm{Xtalk}_{\rho\times} = \frac{1}{2}\left[1 + \frac{\mathbf{m}_{\cap\epsilon} - \mathbf{m}_{\cap\cap}}{\mathbf{m}_{\epsilon\epsilon} - \mathbf{m}_{\epsilon\cap}}\right] \tag{3}$$

Polarization Diversity Active Imaging

R.A. Chipman, University of Alabama in Huntsville

Aluminum Cone (position 2, size filter : 3)

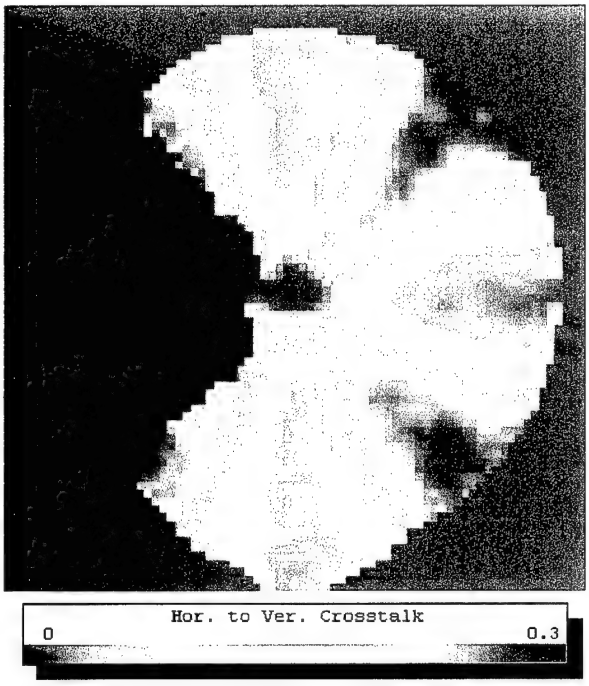

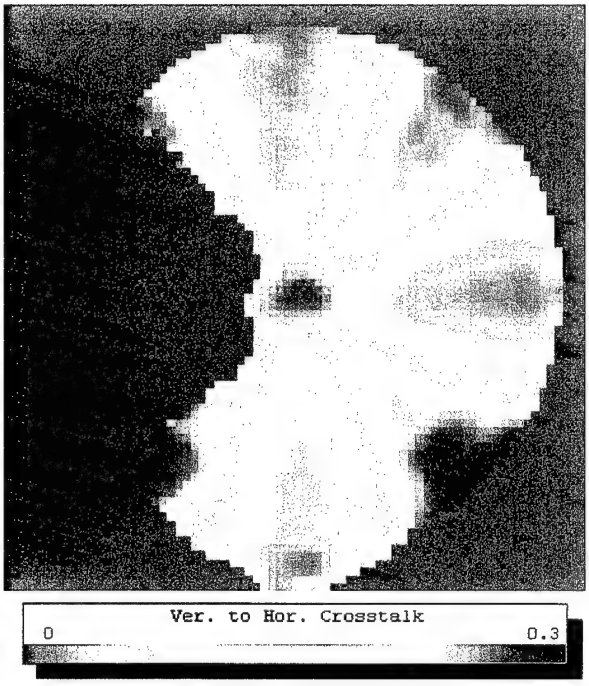

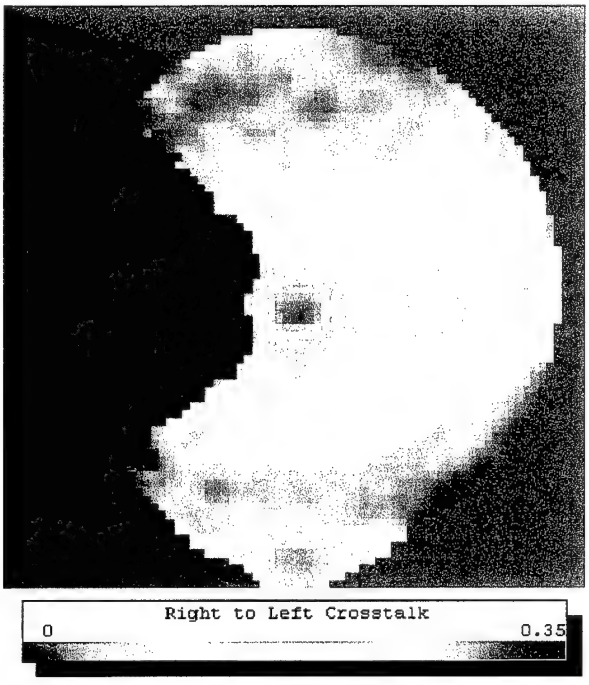

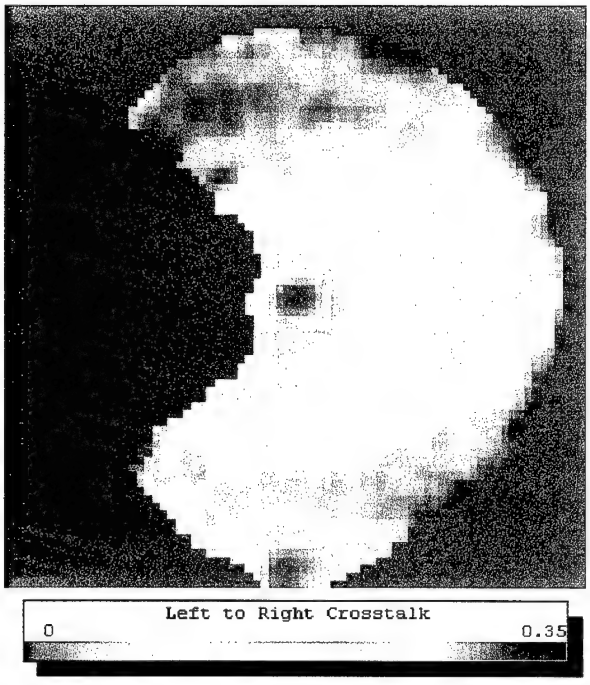

The values for the vertical-to-horizontal crosstalk range from 0 when the reflected light is vertically polarized, to 0.5 when the reflected light is unpolarized, to +1 when the reflected light is horizontally polarized.

2.8.3. 45°linear-to-135°linear Crosstalk

The 45°linear-to-135°linear crosstalk is derived from the Mueller matrix elements as:

$$\mathrm{Xtalk}_{\infty\neg\cap\sum\neg} = \frac{1}{2}\left[1 - \frac{\mathbf{m}_{\|\epsilon} + \mathbf{m}_{\|\|}}{\mathbf{m}_{\epsilon\epsilon} + \mathbf{m}_{\epsilon\|}}\right] \tag{4}$$

The values for the 45°linear-to-135°linear crosstalk range from 0 when the reflected light is polarized at 45°, to 0.5 when the reflected light is unpolarized, to +1 when the reflected light is polarized at 135°.

2.8.4. Right-to-Left Circular Crosstalk

Circularly polarized light is described by two orthogonal states: right circularly polarized and left circularly polarized. These two states have opposite helicity ("handedness") and will interact with optical elements and surfaces differently. The right-to-left circular crosstalk is derived from the Mueller matrix elements as:

$$\mathrm{Xtalk}_{\not\nabla} = \frac{1}{2}\left[1 - \frac{\mathbf{m}_{\sum\epsilon} + \mathbf{m}_{\sum\sum}}{\mathbf{m}_{\epsilon\epsilon} + \mathbf{m}_{\epsilon\sum}}\right] \tag{5}$$

The values for the right-to-left circular crosstalk range from 0 when the reflected light is right-circularly polarized, to 0.5 when the reflected light is unpolarized, to +1 when the reflected light is left-circularly polarized.

2.8.5. Fraction of polarized light returned

The following table gives the fraction of polarized light returned for each crosstalk. The percentage is determined by averaging each crosstalk on all the surface of the object. The values for each crosstalk range from 0% to 100%. The fraction of polarized light returned is equal to 0% when the reflected light corresponds to the first polarized state (e.g. Horizontal) of the crosstalk, and 100% when it corresponds to the coupled orthogonal polarized state (e.g. vertical). When the reflected light is unpolarized the percentage of crosstalk is equal to 50%.

Target	Hor. To Ver.	Ver. To Hor.	45° to 135°	Right to Left	Polarizance
Alum. cone 1	14.3%	14.1%	15.9%	25.1%	5.6%
Alum. cone 2	14.2%	13.9%	16.7%	25.1%	3.5%
Black cone 1	9.5%	9.4%	11.8%	14.4%	3.6%
Black cone 2	9.7%	9.4%	11.8%	14.8%	3.4%
Gold cone 1	21.7%	21.6%	23.5%	36.9%	12%
Gold cone 2	20%	18.7%	21.5%	34.5%	10.2%
Metal sphere	11.5%	11.2%	12.4%	19.6%	9.4%
Ping-pong ball	46.1%	45.9%	46%	48.4%	3%
Plastic sphere	41.7%	41.6%	41.8%	43.6%	6.9%
Wood sphere	41.2%	40.1%	44.4%	47.4%	2.4%

Table 2: Fraction of polarized light returned for each crosstalk

The last three targets (Ping-pong ball, Plastic and Wood spheres) behave like a totally depolarizing medium. Whatever the crosstalk, the percentage of polarized light returned is closed to 50%. Cones and stainless steel sphere do not depolarize completely the polarized light returned. For each of these targets the reflected light behaves like the first polarized state of the crosstalk. Only the right to left crosstalk seems to be a little more depolarizing.

2.9. Cone Image Highlights

In addition to the spherical objects, three cones were imaged. Due to the curvature and orientation of the surfaces, the cones gave a distinct signature especially for the orientations of the retardance and diattenuation axes. The cones were measured in two different positions as seen in Figure 1 on next page. In position 1, the incident light beam is head-on to the tip of the cone, and the polarization analyzer collects light at 15° to the cone orientation. In position 2, the incident light is at 15° to the cone orientation, and the polarization generator collect light parallel to the tip of the cone.

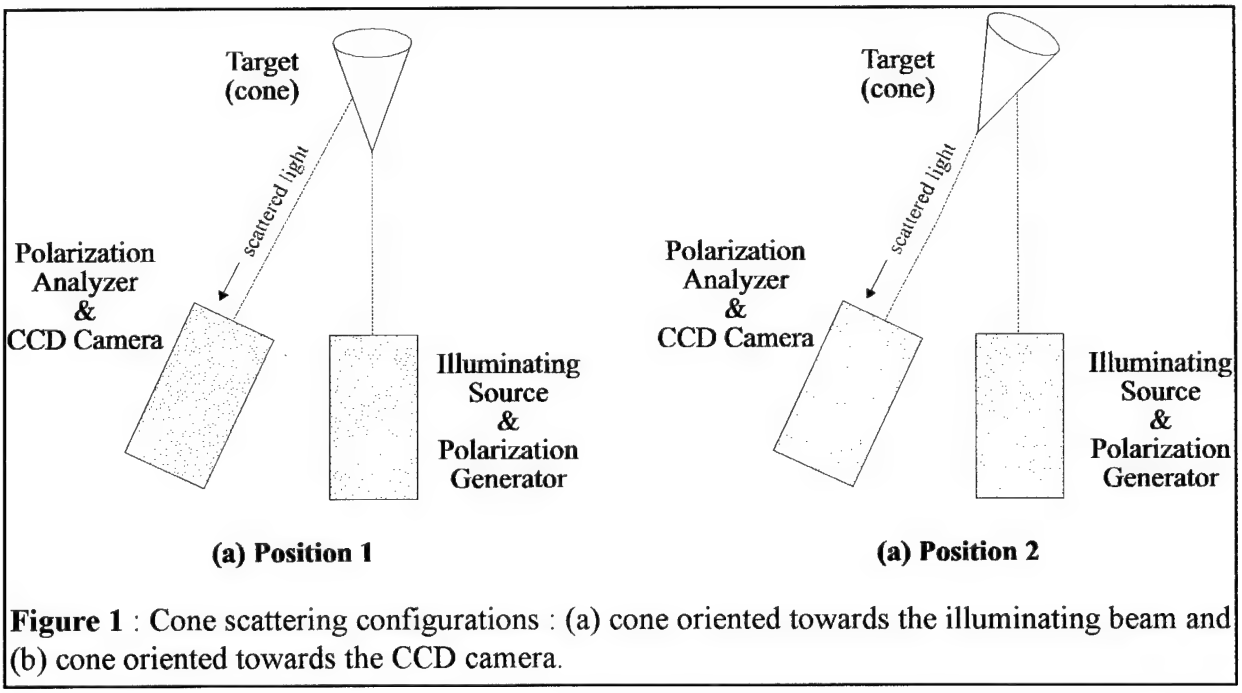

Figure 1 : Cone scattering configurations : (a) cone oriented towards the illuminating beam and (b) cone oriented towards the CCD camera.

2.10. Incidence and Scatter Angle-Polarization Parameters Correlation

Retardance and diattenuation orientations are strongly correlated to the surface orientations of the targets. Angle of incidence and angle of scatter functions are calculated for spherical targets and correlated with the polarization parameters. This polarimetric scatter is expected to show a

quadratic relationship between retardance and angle of incidence and diattenuation and angle of incidence for the monostatic configuration. If so, then this quadratic relationship can be applied to angle of incidence for estimation in active imaging.

The retardance orientation and diattenuation orientation are correlated with the orientation of the plan of incidence and the plan of scatter at the target. Estimations obtained from spherical target data sets show an obvious correlation.

2.10.1. Diattenuation orientation-angle of scatter correlation

To determine the correlation between the Diattenuation orientation and the scatter plane orientation, we first generated a scatter angle pattern of a spherical object (Figure 2). This image is determinated with the same size characteristics as the experimental diattenuation orientation image (same radius and center of sphere). These characteristics are calculated by a routine that determines pixel coordinates of the center (X_0, Y_0) and radius (R) of a spherical object from the logarithm of the intensity image. This is the same image used to define the intensity mask. The orientation of the scatter plan is then deduced by the following expression :

$$\theta_{\text{scatter}} = \text{ArcTan}\left(\frac{Y - Y_c}{X - X_c}\right) \qquad \text{for } (X - X_c)^2 + (Y - Y_c)^2 \le R^2 \qquad \textbf{(6)}$$

$$\theta_{\text{scatter}} = 0 \qquad \text{for } (X - X_c)^2 + (Y - Y_c)^2 > R^2$$

Next, we correlate these theoretical angles of scatter with actual angle-of-diattenuation data from a series of the spherical targets.

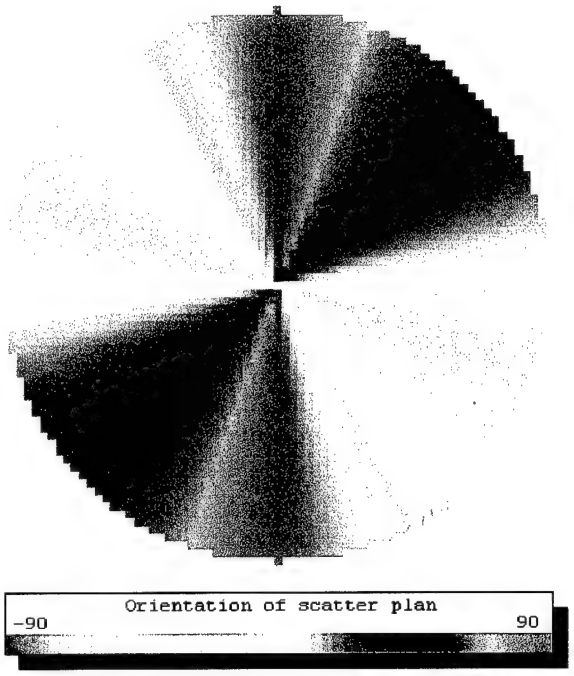

Figure 2 : Angle of scatter pattern of a spherical object.

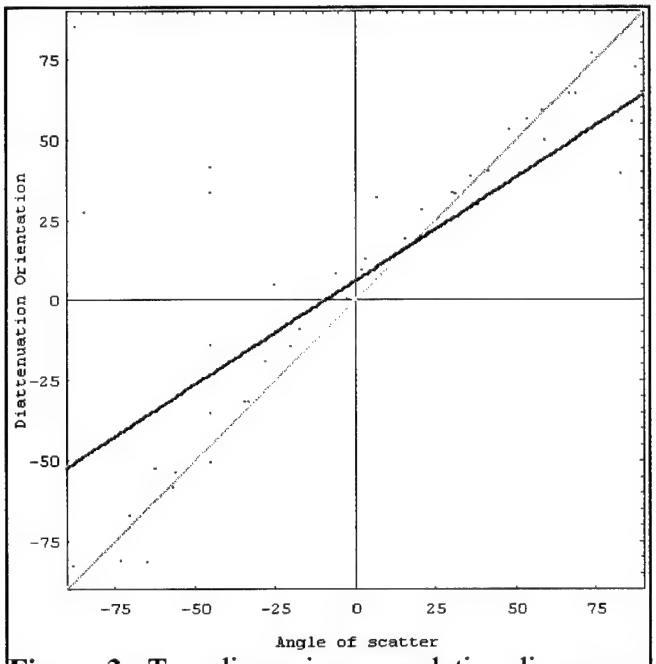

Figure 3 : Two dimensions correlation diagram of Ping-pong ball (diattenuation orientation-Angle of scatter)

Figure 3 plots the theoretical angle of scatter versus the measured diattenuation orientation for a ping-pong ball. A large number of points are seen to lie on the line of unity. The best fit line through the data is also plotted (green line). The correlation coefficient (r) for this data set is calculated to be 0.64 and corresponds to the slope of the best fit line. Note that the correlation coefficient becomes 0 for uncorrelated data, and equal to 1 if the two data sets are linearly related. Each correlation is obtained from the smoothed images which are beforehand sampled every n x n pixels; n being the size of the mask used for the smoothing procedure.

The best correlation between angle of scatter and diattenuation orientation (Table 2) were obtained for the Ping-pong ball and the Plastic sphere. The data from the other targets (Metal sphere and Wood sphere) contained irregularities in the diattenuation orientation images which degraded the value of the correlation coefficient.

Type of target	Correlation Coefficient (r)
Metal sphere	0.38
Ping-pong ball	0.64
Plastic sphere	0.83
Wood sphere	0.61

Table 2: Correlation coefficient of each spherical target

A two dimensional diagram is also used to determine a mask representing regions corresponding to the best correlation between the Diattenuation orientation and the scatter plane. Image shown in Figure 4 represents areas for which the difference between diattenuation orientation and scatter plane does not exceed ±5% of the theoretical value.

By applying this mask on the diattenuation orientation image of the ping-pong ball, it is found that about 50% of the experimental image correlates well with the theoretical pattern. It is also found that the highest correlation occurs near the edges of the sphere.

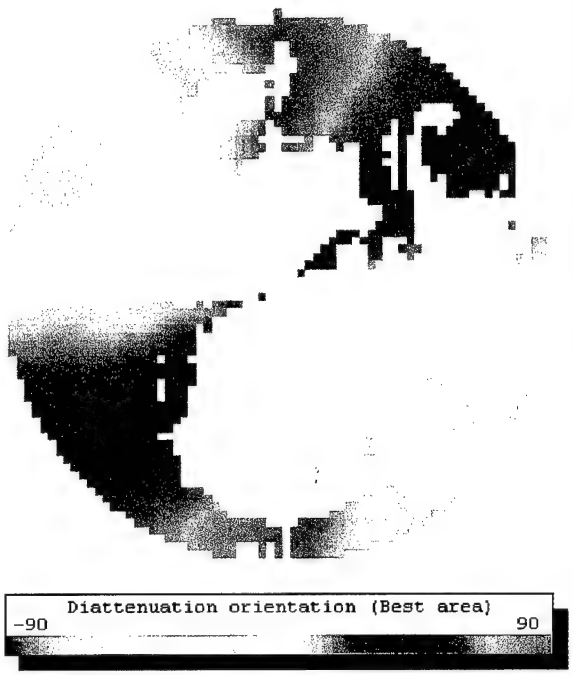

Figure 4 : Representation of the best area of Ping-pong ball Diattenuation orientation after correlation.

2.10.2. Correlation between Diattenuation orientation and angle of incidence

In a manner similar to the previous section, we calculate the correlation factor between the angle of incidence and the Diattenuation orientation. The angle of incidence pattern (Figure 5) is calculated by projecting the angle of scatter pattern in the direction of the incidence angle θ_i (Figure 6). The expression of the angle of incidence then becomes :

$$\theta_{\text{AOI}} = \text{ArcTan}\left(\frac{Y-Y_{\epsilon}+(R-Z[X-X_{\epsilon},Y-Y_{\epsilon}])\text{Sin}\theta_{\phi}}{X-X_{\epsilon}}\right) \quad \text{for } (X-X_{\epsilon})^2+(Y-Y_{\epsilon})^2 \le R^2 \tag{7}$$

$$\theta_{\text{AOI}} = 0 \quad \text{for } (X-X_{\epsilon})^2+(Y-Y_{\epsilon})^2 > R^2$$

with $Z(X,Y) = R-\sqrt{R^2-X^2-Y}$

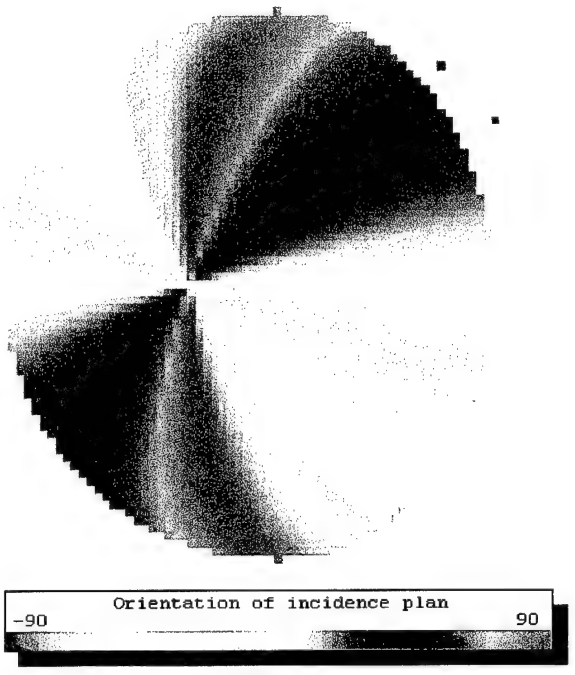

Figure 5 : Angle of incidence pattern of a spherical target, $\theta_{AOI}=20°$

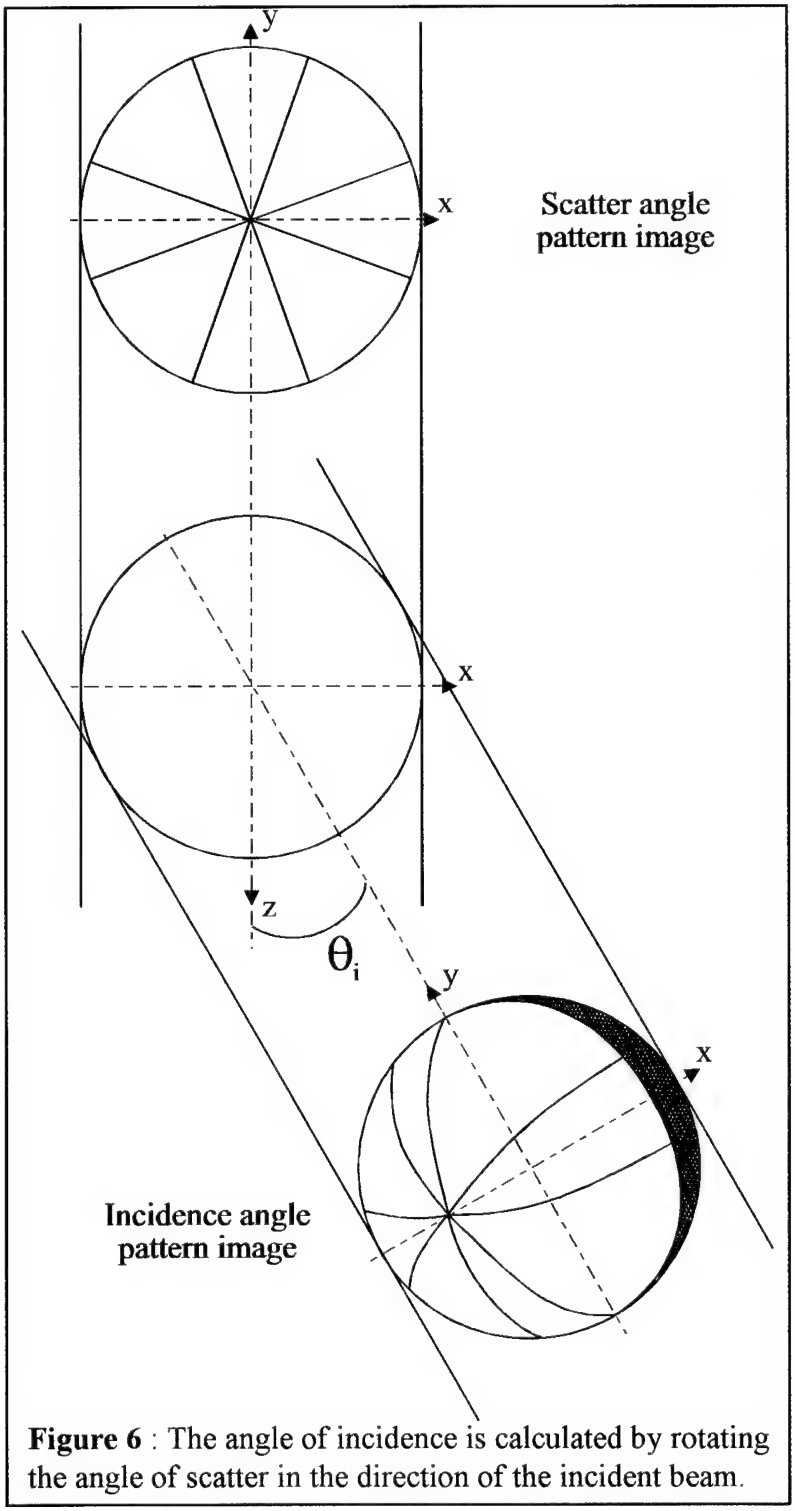

Figure 6 : The angle of incidence is calculated by rotating the angle of scatter in the direction of the incident beam.

The correlation is then determined for different incidence angle values between -25° and 25°. For each value, we determine the residual mean squared (also called coefficient of determination) and the estimated variance. Remember that the polarimetric signatures of each target have been taken for an incidence angle of about -15°.

To verify the consistency of the method, it was applied to a theoretical data set corresponding to an angle of incidence of -10°. Figure 7 shows that the angle of incidence is easily determinated. This determination is much more difficult from the experimental data sets due to the presence of noise, but an estimation of this angle was possible.

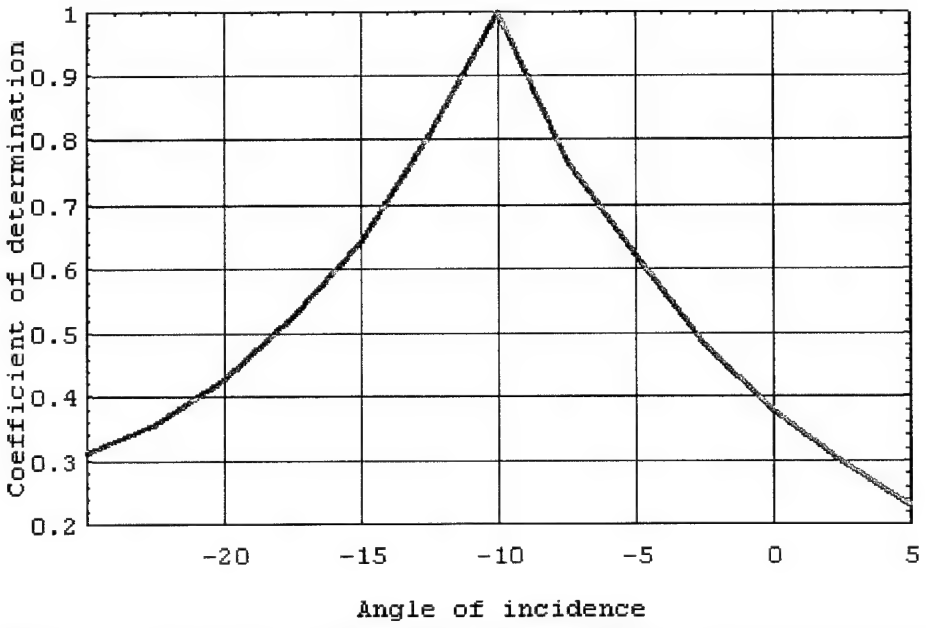

Figure 7 : Coefficient of determination obtained from a theoretical data set corresponding to an angle of incidence of -10°.

Figure 8 plots the coefficient of determination calculated from the ping-pong ball data set. The best correlation is obtained for an angle of incidence of -10°, the experimental value of this angle was about -15°. This angle of incidence has not been detected from the Wood sphere data set, the best correlation is obtained for the opposite value of the angle of incidence used (15°).

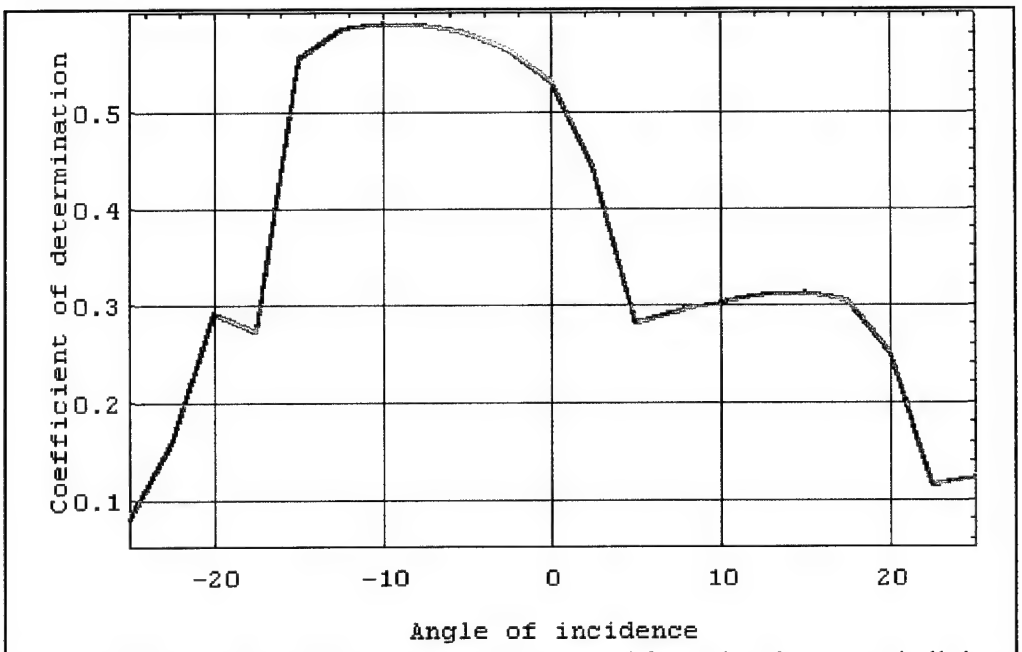

Figure 8 : Coefficient of determination obtained from the ping-pong ball data set.

2.10.3. Correlation between retardance and diattenuation magnitude and angle of scatter

The polarimetric scatter is expected to show a quadratic relationship between retardance and diattenuation magnitude and the angle of scatter (Figure 9). To correlate these two parameters, we apply the method previously developed. In the present case, the angle of scatter is defined by:

$$\theta_{\text{scatter}} = \text{ArcTan}\left(\frac{Z[X,Y]}{\sqrt{X^2+Y^2}}\right) \qquad \textbf{(8)}$$

The correlation function is represented by a second order function resulting from a quadratic fit between theoretical and experimental data. Only the retardance magnitude of the Metal sphere (figure 10) seems to present a quadratic relationship with the angle of scatter. Diattenuation magnitude of ping-pong ball and plastic sphere both present a quadratic relationship.

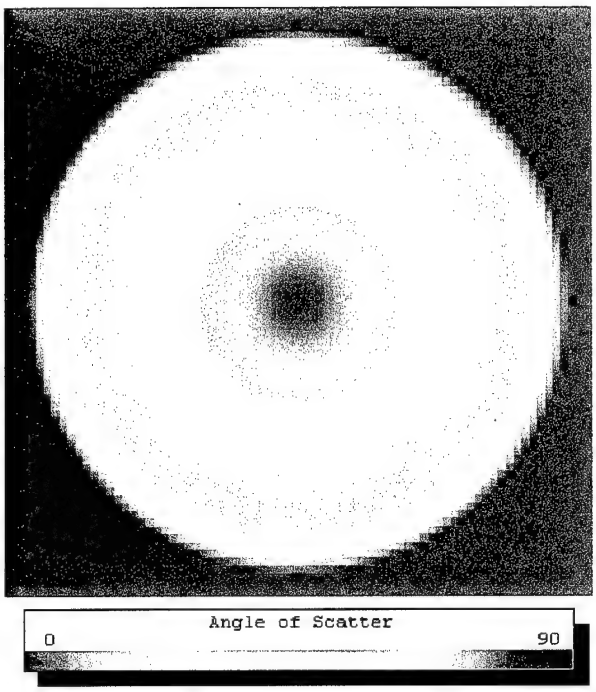

Figure 9 : Angle of scatter pattern

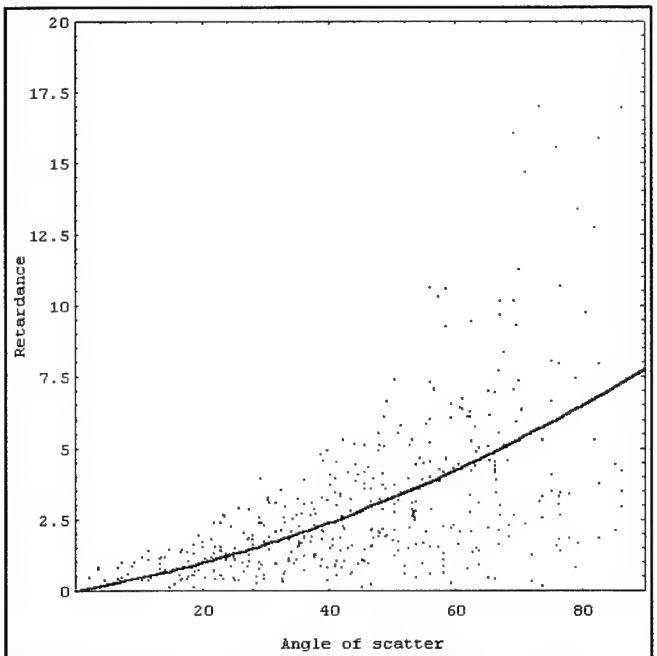

Figure 10 : Two dimensions correlation diagram of metal sphere (retardance magnitude-Angle of scatter)

2.10.4. Correlation between Polarizance and angle of scatter

The correlation between Polarizance and the angle of scatter is also expected to be a quadratic relationship. The best correlations were obtained for the Ping-pong ball (figure 11) and the Plastic sphere for which the Polarizance images had a radial symmetry. The two other targets (the Metal sphere and the Wood sphere) did not have radially symmetric polarizance patterns, and therefore correlated poorly with the angle of scatter.

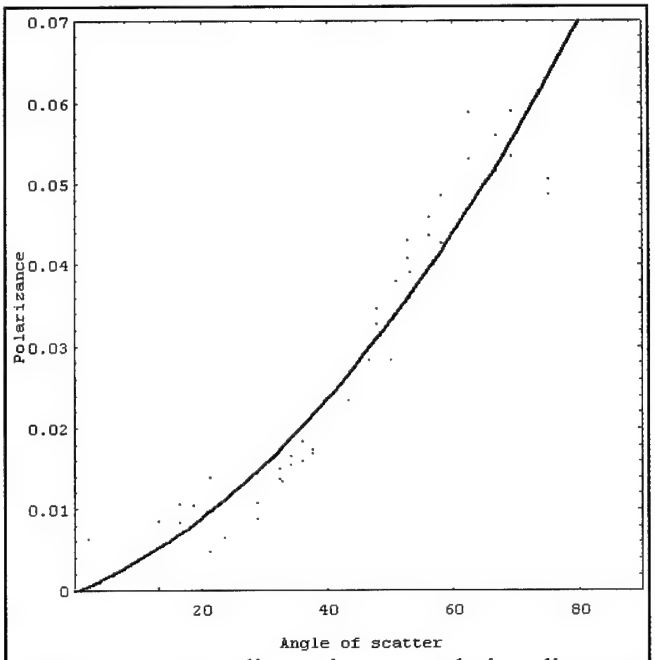

Figure 11 : Two dimensions correlation diagram of ping-pong ball (Polarizance-Angle of scatter).

2.11. Mueller Matrix Imaging Polarimeter

2.11.1. Principle

The Mueller Matrix Imaging Polarimeter (MMIP) was constructed at UAH under an AFOSR grant issued in 1989 by program manager Lee Giles. The Mueller Matrix Imaging Polarimeter took three years to assemble and calibrate before accurate Mueller matrix images were

being routinely measured, an indication of the complexity of the technique. The instrument formed the basis for Larry Pezzaniti's dissertation, which contains a wealth of information on the technique. The Mueller matrix imaging polarimeter has become the most successful instrument in the Polarization Laboratory and has been involved in over 30 papers.

The Mueller Matrix Imaging Polarimeter is an accurate instrument for measuring polarization properties over a field of view in visible and near-infrared light. The MMIP can measure the polarization and polarization scrambling properties of optical elements at a high resolution [2]. This instrument can be configured for measurements in transmission, reflection, retro reflection, and variable-angle scattering. The MMIP has been used for characterization of polarization elements, beam splitter cubes[3], scattering surfaces [4], liquid crystal modulators[5], electro-optic PLZT modulators [6], GaAs waveguide devices[7], and entire optical systems.

For Polarization Diversity Active Imaging the sample becomes a target, and the polarization generator and polarization analyzer are configured for bistatic scattering measurements. All of the polarization altering properties of the sample, the diattenuation, retardance, depolarization, and polarizance, may be computed from the Mueller matrix. Diattenuation refers to the difference in attenuation between two orthogonal polarization states (sometimes referred to as the polarizing efficiency), retardance is the difference in phase accumulation between two polarization states, depolarization is the coupling of polarized light into unpolarized light, and polarizance is the coupling of unpolarized light into polarized light.

Shown in figure 12 in its current configuration for scattering measurements, the polarimeter may be divided into three sections: a polarization state generator, a sample compartment, and a polarization state analyzer. The polarization state generator includes a spatially filtered laser whose coherence has been scrambled by a spinning groung glass plate in order to remove speckle effects. The instrument presently operates with a 633nm He-Ne 5mw laser, a 1064 nm YAG laser (200 mW), a 543 nm 15 mW HeNe, and a 850nm 25mw diode laser, although configuring the instrument with a new source is straightforward.

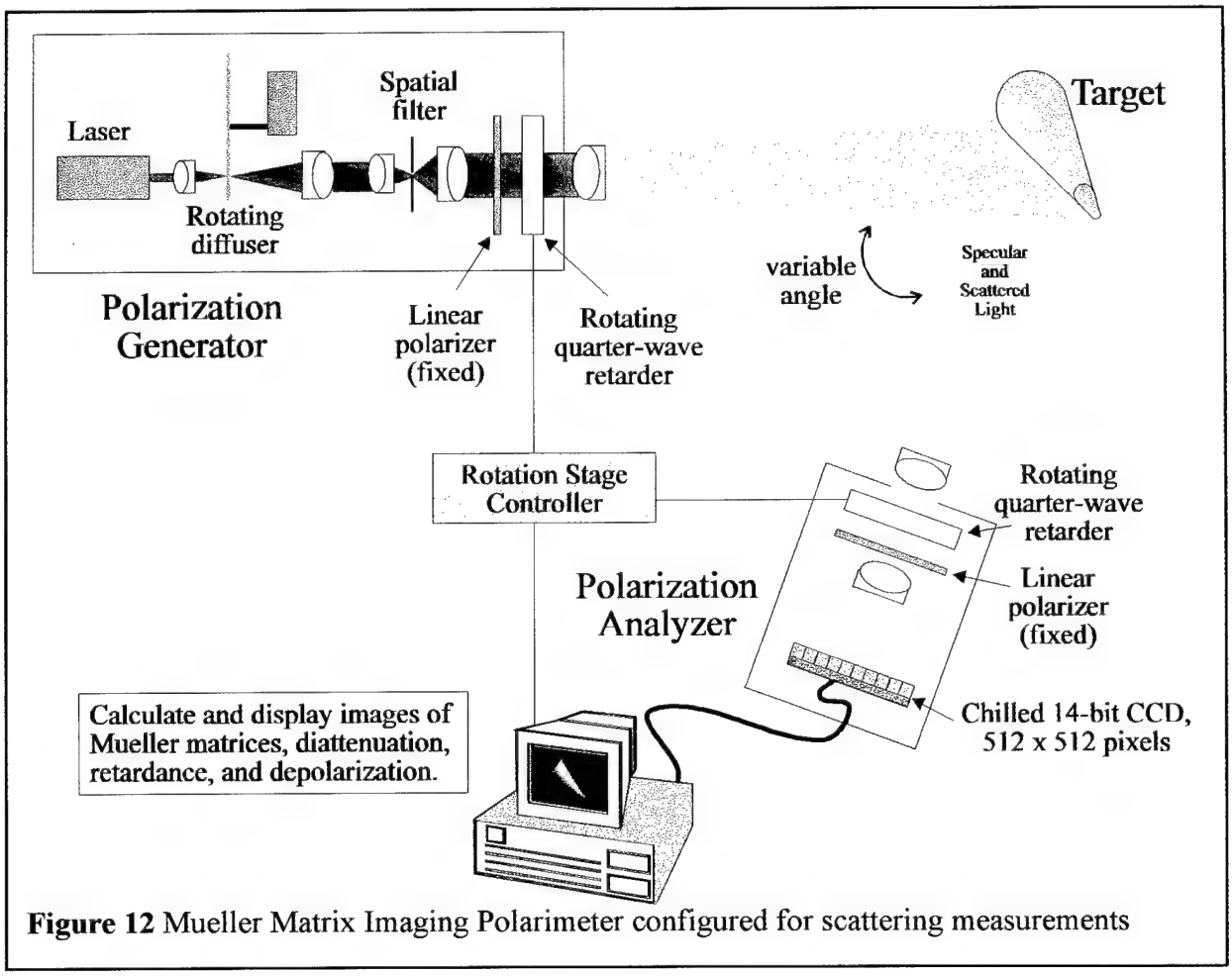

Figure 12 Mueller Matrix Imaging Polarimeter configured for scattering measurements

The MMIP is a dual-rotating retarder polarimeter which illuminates a sample with known polarized states and then analyzes the exiting polarized state over a spatially-resolved image of the sample. Highly calibrated polarization optics are used in the measuring instrument, and an extensive calibration procedure is followed to ensure the accuracy of the measurements. A set of 60 spherical waves with different polarization states are sequentially launched into the sample. Between subsequent measurements, the first retarder is rotated 6 degrees and the second retarder is rotated 30 degrees. With this 5:1 ratio scheme, the polarization information is encoded onto Fourier components of the detected intensities. The 60 recorded images are then analyzed pixel by pixel to compute a 16-element Mueller matrix image[8] using a Mathematica® package of data reduction and analysis algorithms developed by our research group.

The 4-by-4 Mueller matrix, **M**, relates an incident polarized state described by Stokes vector $\vec{S}$ to the exiting (reflected, transmitted, scattered) state with Stokes vector $\vec{S}'$:

$$\vec{S}' = \begin{bmatrix} S'_{\epsilon} \\ S'_{\cap} \\ S'_{\parallel} \\ S'_{\Sigma} \end{bmatrix} = \mathbf{M}\vec{S} = \begin{bmatrix} m_{\epsilon\epsilon} & m_{\epsilon\cap} & m_{\epsilon\parallel} & m_{\epsilon\Sigma} \\ m_{\cap\epsilon} & m_{\cap\cap} & m_{\cap\parallel} & m_{\cap\Sigma} \\ m_{\parallel\epsilon} & m_{\parallel\cap} & m_{\parallel\parallel} & m_{\parallel\Sigma} \\ m_{\Sigma\epsilon} & m_{\Sigma\cap} & m_{\Sigma\parallel} & m_{\Sigma\Sigma} \end{bmatrix} \begin{bmatrix} S_{\epsilon} \\ S_{\cap} \\ S_{\parallel} \\ S_{\Sigma} \end{bmatrix} \quad (9)$$

The Mueller matrix can be written as the multiplication of a pure depolarizing matrix, **D**, a pure retarder matrix, **R**, and a pure diattenuating (polarizing) matrix, **P**:

$$\mathbf{M} = \mathbf{D} \cdot \mathbf{R} \cdot \mathbf{P} \quad (10)$$

These 4-by-4 matrix images can then be decomposed into images of the depolarization, retardance, and diattenuation[9]. These maps give a spatially-resolved description of the polarization performance of the sample.

The illuminating source for these measurements was a 5mW HeNe laser operating at a wavelength of 632.8nm. The target (sphere or cone) is illuminated with collimated light; the specularly reflected and scattered light passes through the polarization analyzer and is detected on the CCD array. The angle between the incident and collected beams was 15°.

2.11.2. Identification of pixels or regions with suspicious data quality

To check the data integrity of each measurement set, we evaluate a least square estimation of the total intensity fluctuation of the sixty intensity images. This fluctuation comes from the instability of the laser source and from the shot noise and thermal noise of the CCD camera. The least square estimation function takes the following form :

16 Dimensional Mueller Matrix Space

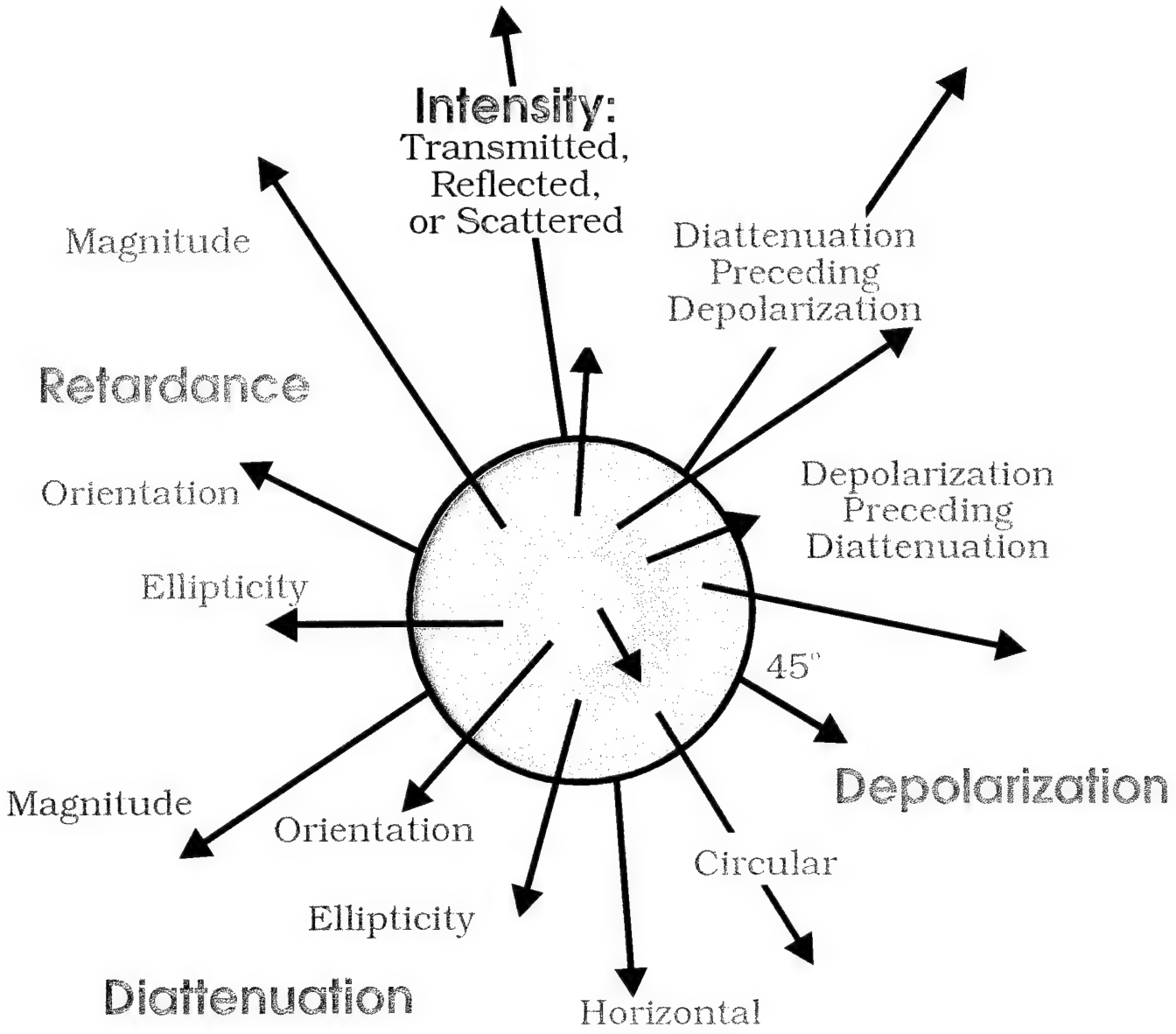

- There are 16 degrees of freedom in the Mueller matrix.
- Extracting the polarization properties from the Mueller matrix is a complex task.
- These measurements concentrate on the retardance magnitude and retardance orientation.

$$\Delta_{\phi\Gamma} = \sqrt{\frac{1}{30}\sum_{\Gamma=0}^{\Sigma\epsilon}\left(\frac{I_{\Gamma+\Sigma\epsilon}(i,j)-I_{\Gamma}(i,j)}{I_{\Gamma+\Sigma\epsilon}(i,j)-B_{\supset\prec\subset}(i,j)}\right)^{\parallel}} \quad (11)$$

Δ_{ϕ} represents the total intensity fluctuation of the pixel located at the (i,j) position. $I_k(i,j)$ is the pixel intensity of the k th image. $B_{gnd}(i,j)$ represents the dark current background level.

A set of 60 images is used to determine the Mueller matrix. The two retarders are rotated in angular increments with a 5:1 ratio. Since the angular increment of the polarization generator retarder being 6°, the measured intensities become redundant after the thirtieth position which explains the summation limit of the estimation function. Therefore, the Δ_{ϕ} function is a measure of the similarity between the first half and the second half of the 60 measurements. The maximum errors occurred in regions of low intensity surrounding each target. Intensity fluctuations corresponding to the signature of the target usually did not exceed 5%.

3. Discussion and Conclusions

3.1. Imaging polarization in a movie studio

The Mueller Matrix Imaging Polarimeter will be modified to measure Mueller matrices of small scattering targets in a "movie studio" we will construct. Initial targets will be simple geometric shapes such as spheres, cones, plates, and cylinders with correspondingly simple angle of incidence functions. Target roughness will be characterized in a Wyko profilometer, and refractive index measured with our visible spectropolarimeter to provide materials characterization of the scattering surfaces. Mueller matrix images and movies will then be taken of the targets in a variety of configurations, and retardance, diattenuation, and depolarization images produced and studied. First, we seek to demonstrate that for some surfaces the Mueller matrix images can be inverted to determine surface orientation. Later work will develop principles which underlie polarimetric scatter, so that a theoretical understanding will emerge on the accuracy at which this technique can operate and the polarimeter requirements for useful measurements.

3.2. Imaging polarization in a monostatic configuration

This contract will only make measurements in the bistatic configuration. After successful demonstration of Polarization Diversity Active Imaging in the bistatic configuration, we plan to develop the monostatic configuration shown on the next page in a later contract. This configuration is needed to support other Air Force programs in active imaging and laser radar which operate in the monostatic mode. This is a far more difficult configuration, requiring an excellent nonpolarizing beam splitter and beam dump. The monostatic calibration is far more involved than the bistatic calibration and the accuracy is not as great.

Imaging Polarization Movie Studio

R.A. Chipman, University of Alabama in Huntsville

For Missile Models:

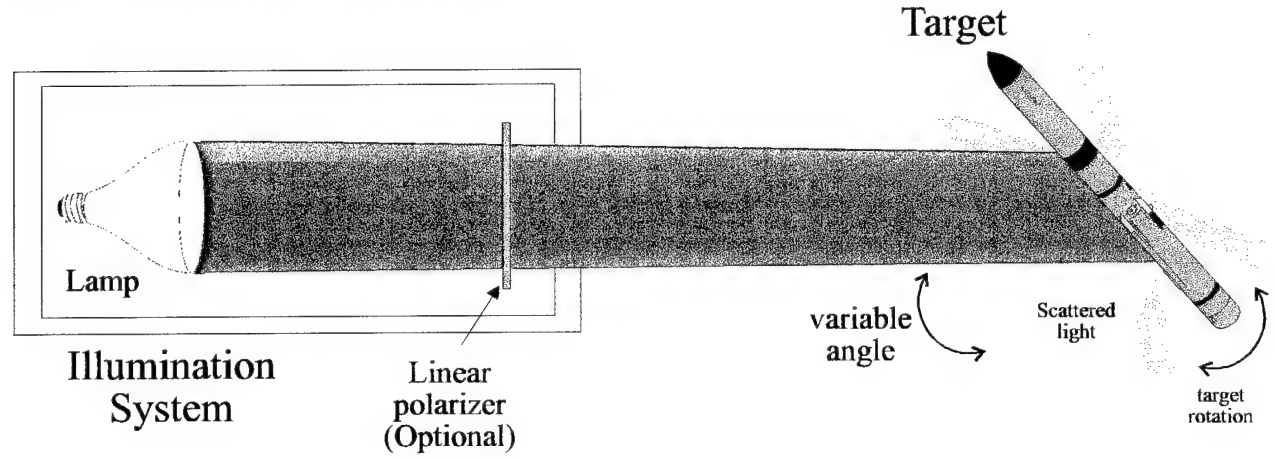

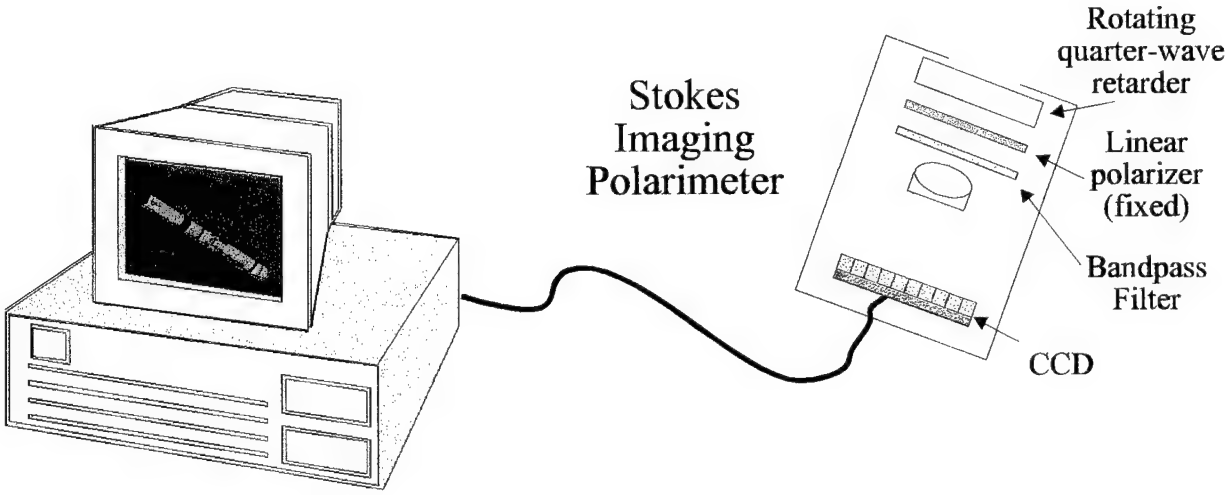

- Measure Stokes Vector movies of target models and other samples.
- Polarization images acquired as target rotates.
- Measure images of polarization orientation, degree of linear and circular polarization.
- Investigate relationship of polarization orientation to object geometry.
- Estimate object orientation and study texture effects.
- Two axes of rotation to simulate tumbling objects, study orientation.

Polarization Diversity Active Imaging

R.A. Chipman, University of Alabama in Huntsville

Experimental Configuration for Monostatic Imaging:

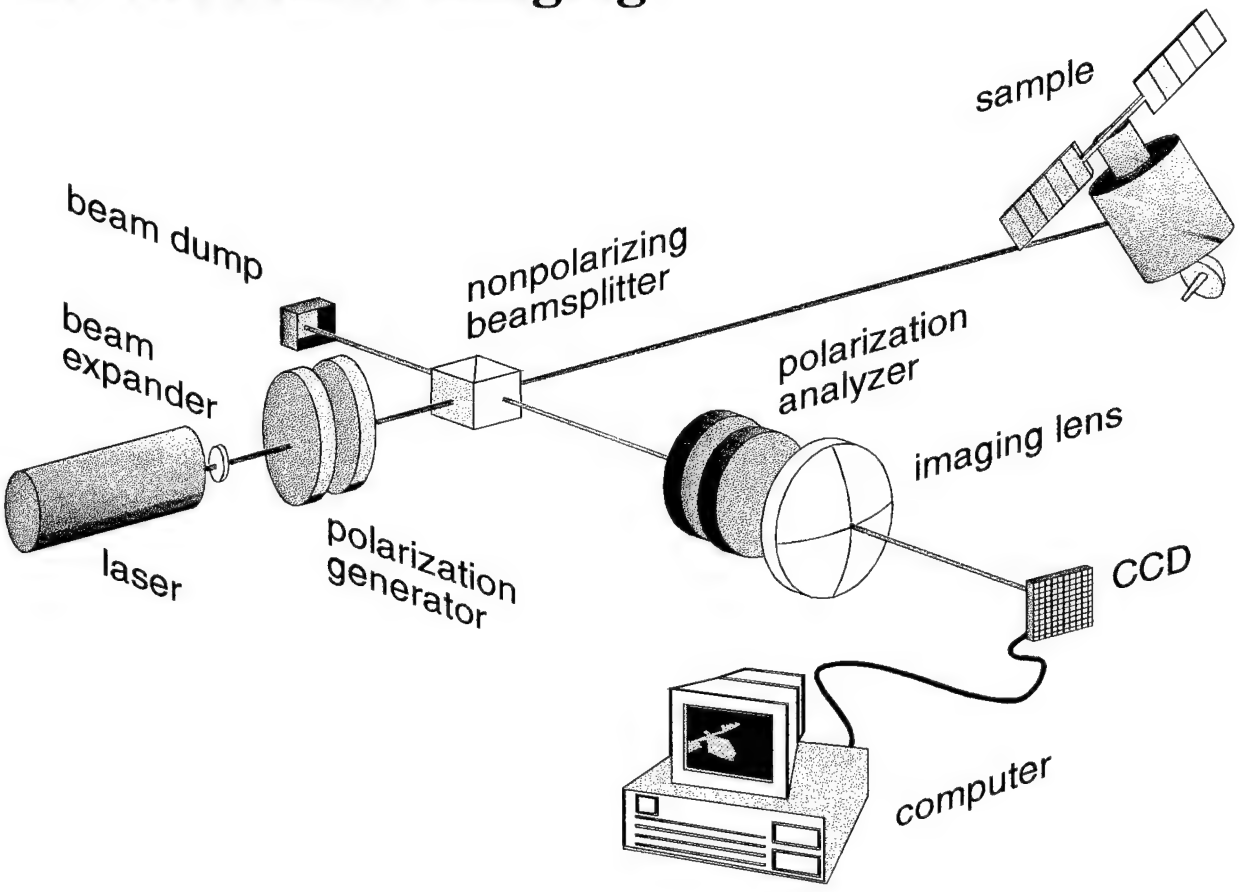

- Measures Mueller matrix images of a target in retroreflection.
- Requires an excellent low-scatter, nonpolarizing beamsplitter and beam dump.
- Involves considerable calibration challenges.

3.3. Classes of retroreflected satellite returns

One objective of Polarization Diversity Active Imaging is to classify pixels in images. The figure on the next page shows a classification system for light retro reflected or reflected from a satellite. By making Polarization Diversity Active Images of the satellite, it should be possible to classify pixels into these categories based on differences in polarization.

Specular beams including the glints, roof mirrors, corner cube structures, and other multiple reflections tend to be bright. Roof mirrors and corner cubes have a larger angular acceptance than glints, so even though they may not be common structures, they light up over considerable illuminating solid angles. Specular reflections follow Fresnels equations.

Glints reverse the helicity of circular polarized light, converting right circularly polarized light into left and vice versa. The plane of linearly polarized light is unchanged.

Roof mirrors do not reverse the helicity, it changes once on the first reflection, and again on the second reflection. Folding mirrors are retarders, and to a lesser extend diattenuators. Therefore roof mirrors have twice the retardance of a folding mirror, oriented along the s-plane of the mirrors. Thus the retardance orientation yields the orientation of the roof mirror axis, with an uncertainty of 90 degrees. Since s-reflectance is greater than p-reflectance, the diattenuation can resolve this 90 degree ambiguity. The ratio of the retardance to the diattenuation provides a constraint on the possible values of the refractive index. The depolarization yields information on the ratio of specular to diffuse (from roughness) reflectance.

Corner cubes have three reflections and so reverse helicity as do glints. But three retardances acting 120 degrees apart in orientation do not cancel, but instead yield an elliptical retarder. Thus corner cubes can be separated from glints and roof mirrors by this elliptical retardance. Similarly they act as elliptical diattenuators, with the ratio of diattenuation to retardance providing constraints on the refractive index of a corner cube formed from a single material.

Classes of Retroreflected Satellite Returns

Glints

Light reflected at normal incidence from small areas

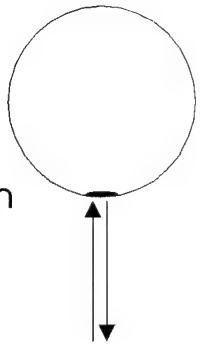

Diffuse Scatter

Portion of diffuse scatter which propagates in retroreflected direction

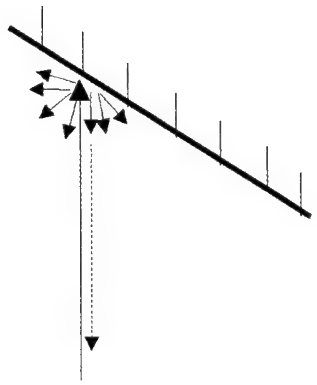

Roof Mirror

Two reflecting surfaces 90° apart illuminated in the plane containing both normals

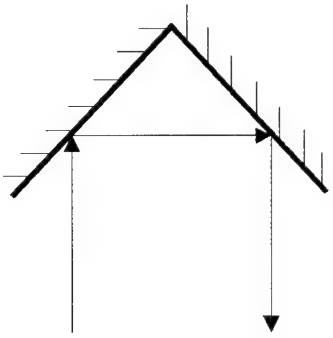

Corner Cube

Three reflecting surfaces 90° apart arranged as a vertex of a cube

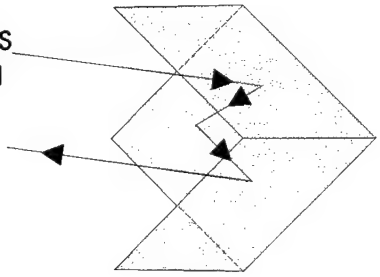

Higher Order Reflections

Four or more reflections which retroreflect a beam

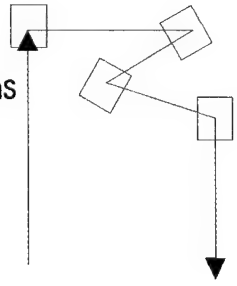

Diffusely scattered light does not follow Fresnels equations. Materials show a very large range of scatter polarization behavior based on roughness, texture, grating structures, cracks, inhomogeneities, bulk scatter, etc. Nevertheless, useful generalizations will doubtless emerge for paints, finished metals, natural materials (trees, dirt, etc) and other common materials. In my laboratory from limited measurements, mostly of paints in retro reflection, I have observed the following: (1) the diffuse scattering interaction is a partial polarizer (diattenuator) in the s-p plane, which increases quadratically in strength from normal incidence. (2) There is a weak linear retardance also in the s-p plane. (3) Depolarization is usually dominant.

Thus from Mueller matrix measurements in a Polarization Diversity Active Imaging apparatus, these classes of light/target interactions should be identifiable by the different polarization characteristics. This work will allow careful scientific data to be acquired in controlled laboratory settings to investigate this hypothesis. Note that this classification is not possible with passive imaging or illumination with a single polarization state.

3.4. Conclusions

Tables 3 and 4 give the most important results about the depolarization power of each target. The tables also present the main characteristics of the retardance and diattenuation orientation images which can be used to determine the surface orientation of the targets. From these results, general statements can be made:

- rough objects (e.g., wood ball and pin-pong ball) scatter nearly unpolarized light and have very irregular polarization patterns,
- smoother objects have well-defined polarization signatures, with more predictable patterns.

Estimation of the surface orientation of the target can be only obtained if the polarization signatures are sufficiently obvious. From our results, it appears that diattenuation orientation is better for determining the surface orientation of an object than the retardance orientation. Both properties, however, appear promising and warrant further investigation.

	Depolarization Index	**Polarizance vector**	**Linear Retardance Orientation**	**Linear Diattenuation Orientation**
Metal sphere	Weakly depolarizing	$-0.25 \leq H^* \leq 0.25$ $-0.25 \leq V^* \leq 0.25$ $C^* = 0$	Easy to distinguish a scatter angle pattern	Easy to distinguish a scatter angle pattern
Plastic sphere	Weak in the specular direction. Strong in the scattering direction.	$-0.15 \leq H \leq 0.15$ $-0.15 \leq V \leq 0.15$ $C = 0$	Completely irregular, impossible to distinguish a scatter angle pattern	Good scatter angle pattern, with unusual "double-center"
Ping-pong ball	Strongly depolarizing	$-0.06 \leq H \leq 0.06$ $-0.06 \leq V \leq 0.06$ $C = 0$		
Wood sphere	Strongly depolarizing	$-0.035 \leq H \leq 0$ $-0.07 \leq V \leq 0.07$ $C = 0$	Very irregular, difficultly interpreted	Very irregular at the center

Table 3

* H and V are respectively the magnitude of the horizontal and vertical component, C being the magnitude of the circular component.

Angle of incidence and angle of scatter functions have been calculated for our spherical targets and correlated with the measured polarimetric parameters. From the polarimetric signatures sufficiently significant, the degree of correlation is relatively high between theoretical and experimental data set. Quadratic relationships expected between diattenuation (retardance) magnitude and angle of scatter are mainly visible from metal and plastic objects. The correlation is difficultly interpretable for the wood sphere which the polarimetric signatures are very irregular.

	Depolarization Index	**Polarizance vector**	**Linear Retardance Orientation**	**Linear Diattenuation Orientation**
Aluminum Cone Position 1	Weak in the specular direction (tip). ≈0.25 in the other direction.	$-0.1 \leq H \leq 0.1$ $-0.15 \leq V \leq 0.15$ $C = 0$	Excellent pattern, can be interpreted	Irregular pattern, difficultly interpretable
Black Cone Position 1	≈0.25 whatever the direction	$-0.1 \leq H \leq 0.1$ $-0.1 \leq V \leq 0.1$ $C = 0$	Irregular pattern, impossible to interpret it	Irregular pattern, impossible to interpret it
Gold Cone Position 1	Weak in the specular direction (tip). ≈0.5 in the other direction.	$-0.3 \leq H \leq 0.3$ $-0.3 \leq V \leq 0.3$ $C = 0$	Excellent pattern, can be interpreted	Excellent pattern, can be interpreted
Aluminum Cone Position 2	Weak in the specular direction (tip). ≈0.25 in the other direction.	$-0.12 \leq H \leq 0.12$ $-0.12 \leq V \leq 0.12$ $C = 0$	Half of the pattern is interpretable, the second part corresponds to the shadow	Irregular pattern, impossible to interpret it
Black Cone Position 2	≈0.25 whatever the direction	$-0.05 \leq H \leq 0.05$ $-0.05 \leq V \leq 0.05$ $C = 0$	Irregular pattern, difficultly interpretable	Does not present a typical pattern
Gold Cone Position 2	Weak in the specular direction (tip). ≈0.5 in the other direction.	$-0.25 \leq H \leq 0.25$ $-0.25 \leq V \leq 0.25$ $C = 0$	Half of the pattern is interpretable, the second part corresponds to the shadow	Excellent pattern, can be interpreted

Table 4

Some of the series of the spherical targets present excellent patterns of retardance and diattenuation orientation. The estimation of their correlations with the angle of incidence and the angle of scatter patterns is more complex due to the conical shape of these objects. These estimations will be the object of further investigation.

We have shown that it was possible to correlate the orientation and the magnitude of retardance or diattenuation with the angles of incidence and scatter to estimate the shape of an object. In some cases, these polarimetric parameters are not sufficient because of irregularities on their respective patterns. However, these parameters can be completed by others, also correlated to the surface of the target (e.g. polarizance).

The next step will investigate methods to identify and separate specular pixels from majority of diffusely scattering pixels. These specular pixels may be useful for refractive index estimation, one of the essential parameters for the determination of shape and orientation of the object.

4. References

1. Russell A. Chipman, "Polarimetry," in the *Handbook of Optics*, Chap. 22, (McGraw-Hill, New York, 1994).

2. J.L. Pezzaniti and R.A. Chipman, "Mueller matrix imaging polarimetry," *Opt. Eng.* **34**(6), 1558-1568 (1995).

3. J.L. Pezzaniti and R.A. Chipman, "Angular dependence of polarizing beam splitter cubes," *Appl. Opt.* **33**(10), 1916-1929 (1994).

4. J.L. Pezzaniti and R.A. Chipman, "Mueller matrix scatter polarimetry of a diamond-turned mirror," *Opt. Eng.* **34**(6), 1593-1598 (1995).

5. J.L. Pezzaniti, S.C. McClain, R.A. Chipman, S.-Y. Lu, "Depolarization in a liquid crystal TV's," *Opt. Lett.* **18**(23), 2071-2073 (1993).

6. E.A. Sornsin and R.A. Chipman, "Mueller matrix polarimetry of PLZT electro-optic modulators," *Proc. SPIE* **2873**, (1996).

7. M.H. Smith, E.A. Sornsin, R.A. Chipman, T.J. Tayag, "Polarization characterization of self-imaging GaAs/AlGaAs waveguide beamsplitters using Mueller matrix imaging polarimetry," submitted to SPIE Photonics West '97 (Optoelectronics, 1997).

8. R.A. Chipman, "Polarimetry," in the *Handbook of Optics*, Chap. 22 (McGraw-Hill, New York, 1994).

9. S.-Y. Lu and R.A. Chipman, "Interpretation of Mueller matrices based on polar decomposition, *J. Opt. Soc. Am. A* **13**(5) (1996).

Appendix A:

Line Graphs of Diattenuation and Retardance Orientation Images

Polarization Diversity Active Imaging

R.A. Chipman, University of Alabama in Huntsville

Aluminum cone

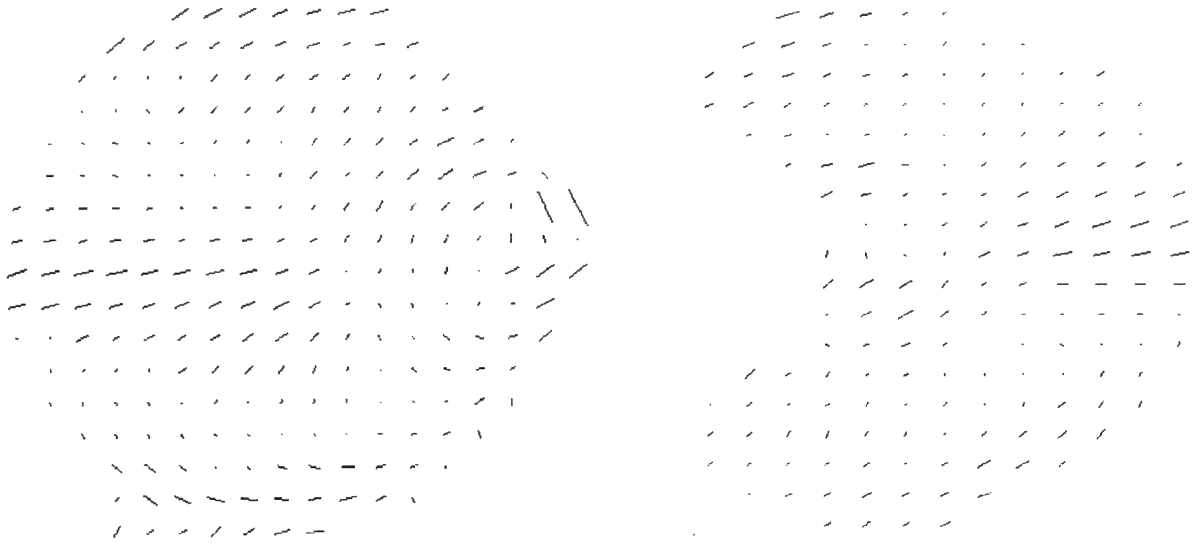

Orientation and Magnitude of the diattenuation

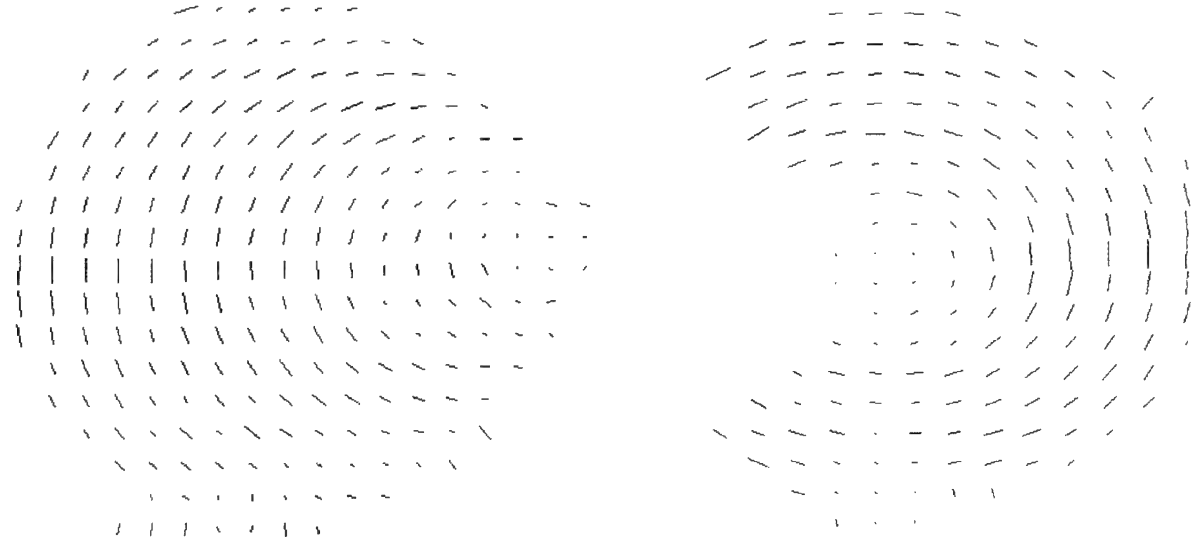

Orientation and Magnitude of the retardance

Polarization Diversity Active Imaging

R.A. Chipman, University of Alabama in Huntsville

Black cone

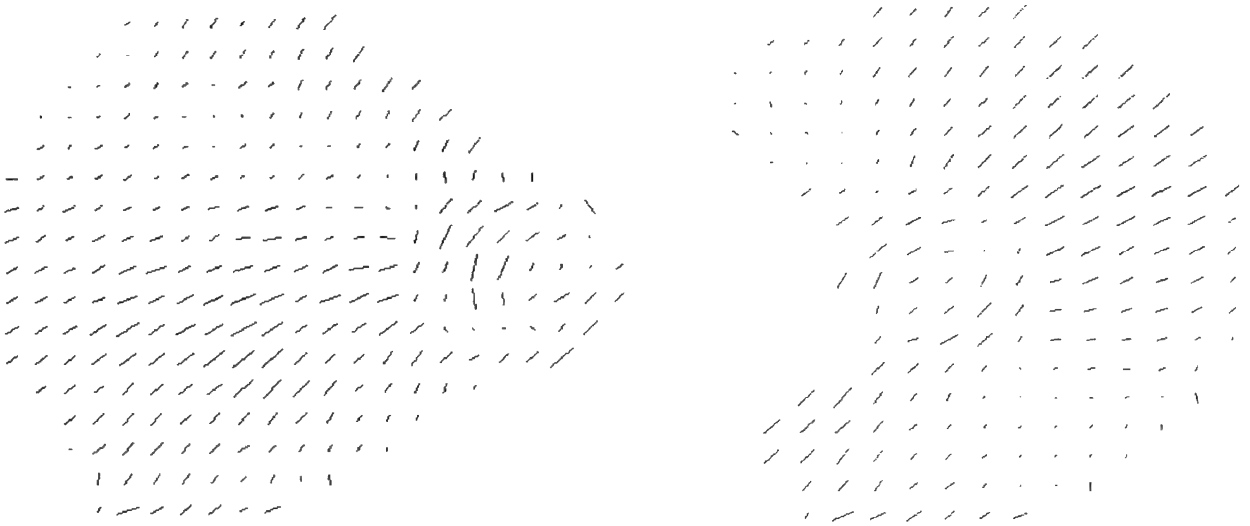

Orientation and Magnitude of the diattenuation

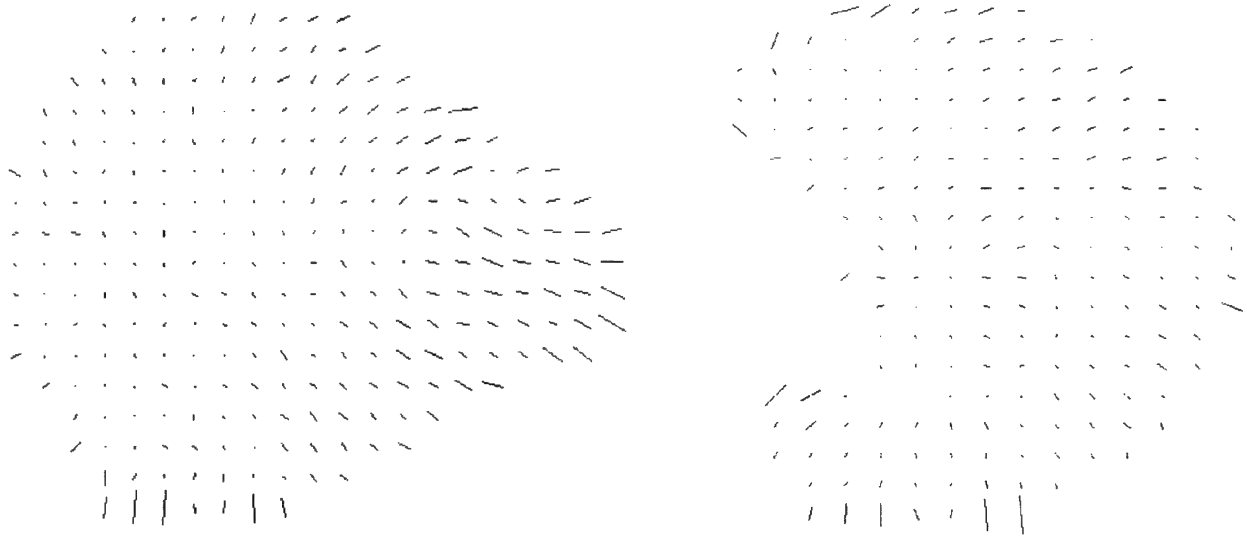

Orientation and Magnitude of the retardance

Polarization Diversity Active Imaging

R.A. Chipman, University of Alabama in Huntsville

Gold cone

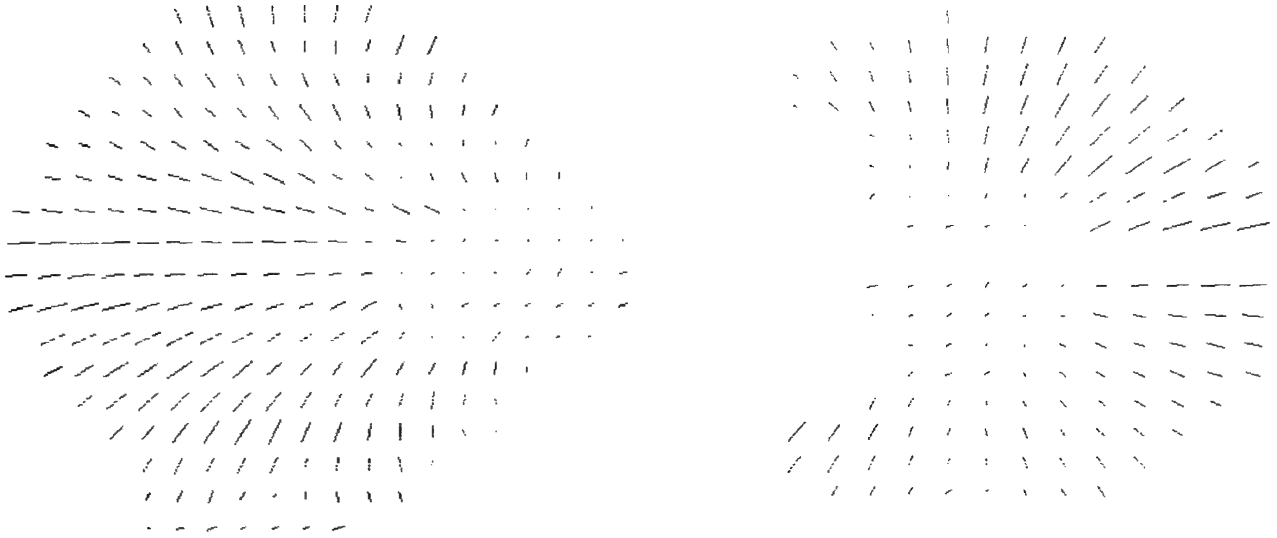

Orientation and Magnitude of the diattenuation

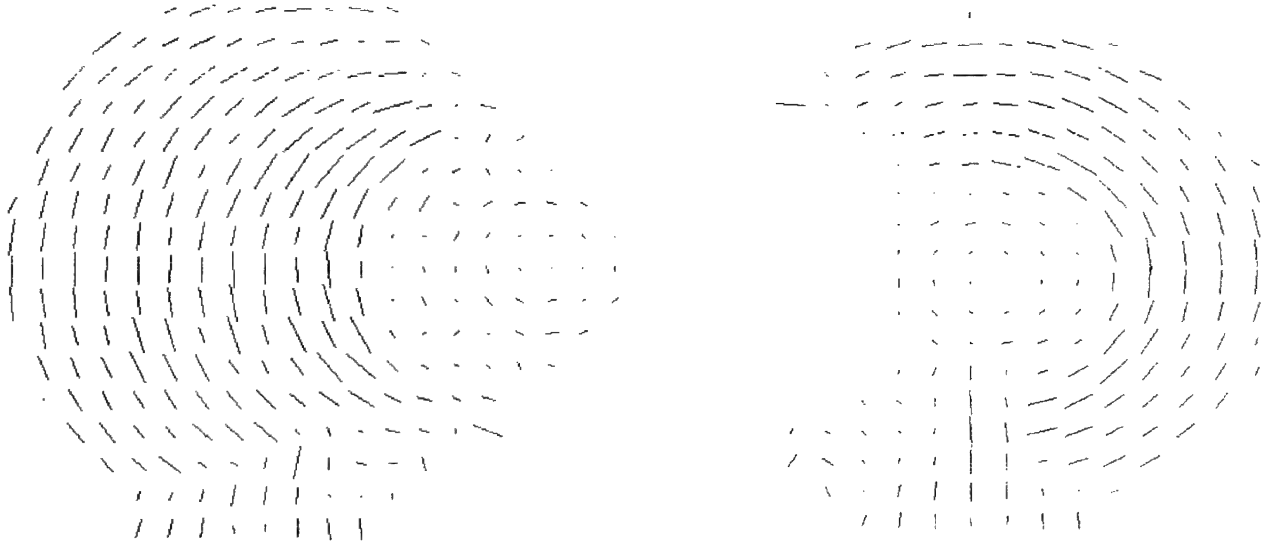

Orientation and Magnitude of the retardance

Appendix B:

Polarizance Images

Polarization Diversity Active Imaging

R.A. Chipman, University of Alabama in Huntsville

Polarizance

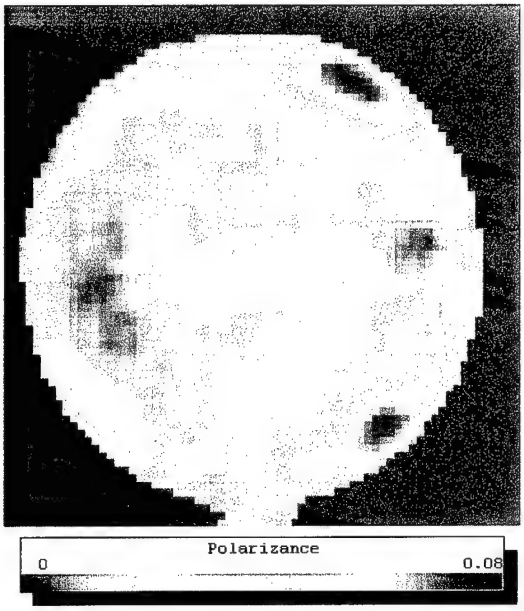

Wood sphere

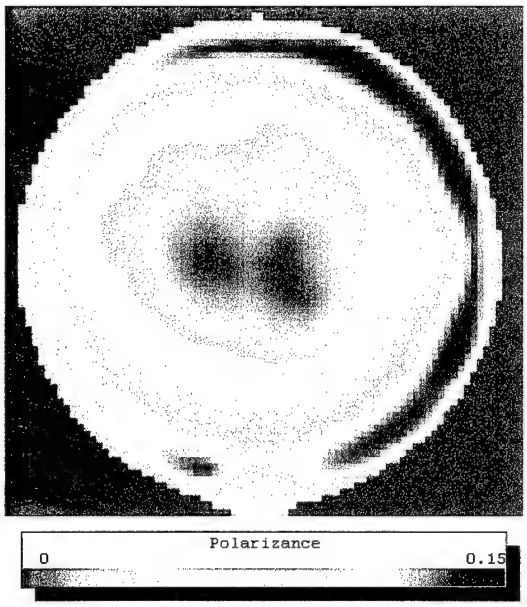

Plastic sphere

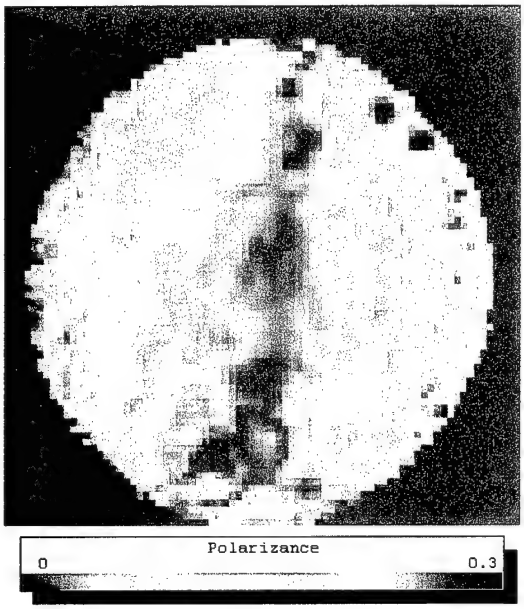

Metal sphere

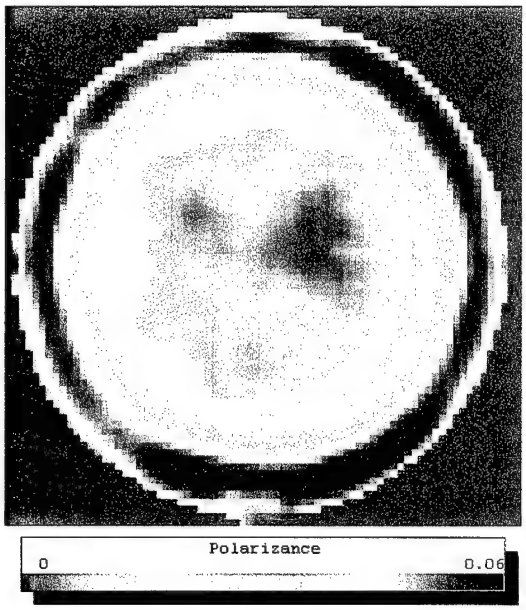

Ping-pong sphere

Polarization Diversity Active Imaging

R.A. Chipman, University of Alabama in Huntsville

Polarizance

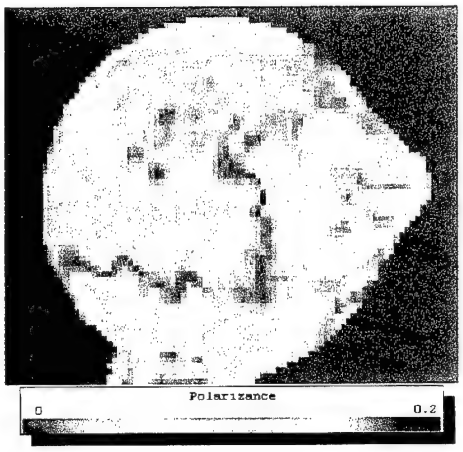

Aluminum Cone

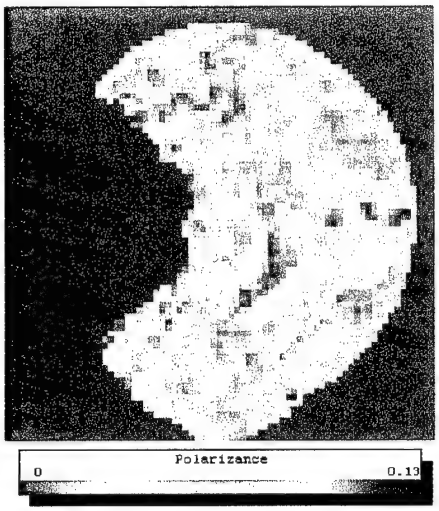

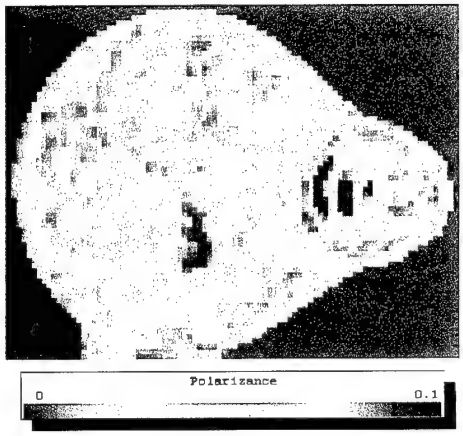

Black Cone

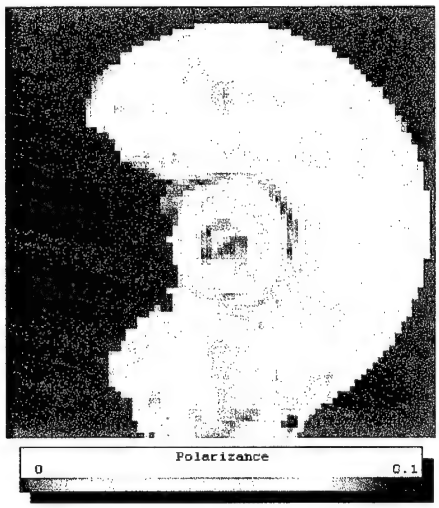

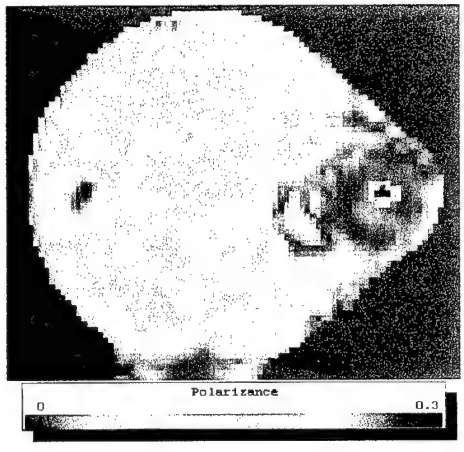

Gold Cone

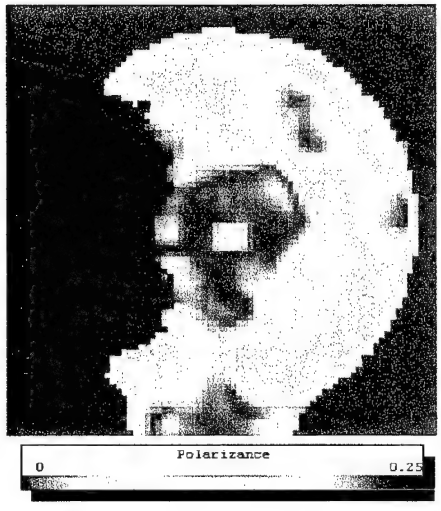

Appendix C:

Polarizance Vector Images

Polarization Diversity Active Imaging

R.A. Chipman, University of Alabama in Huntsville

Polarizance Vector
Aluminum cone

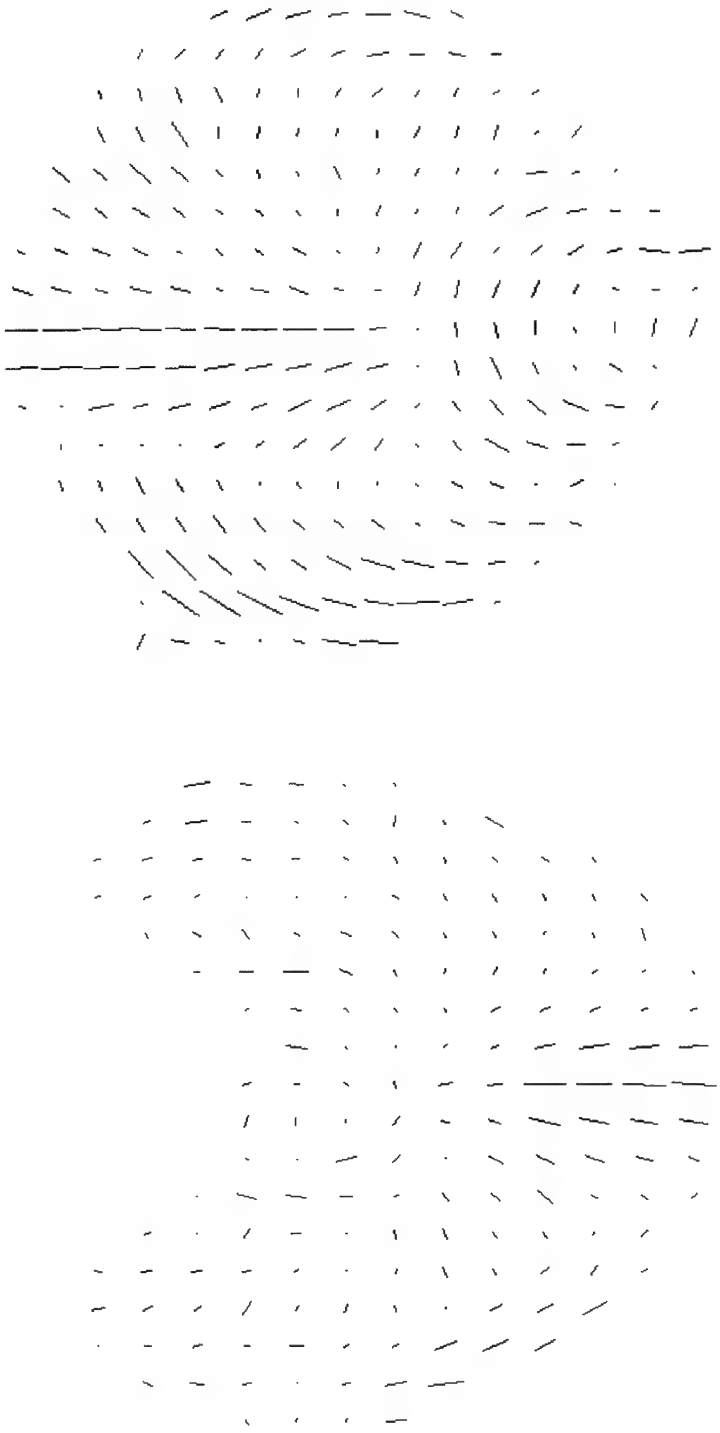

Polarization Diversity Active Imaging

R.A. Chipman, University of Alabama in Huntsville

Polarizance Vector
Black cone

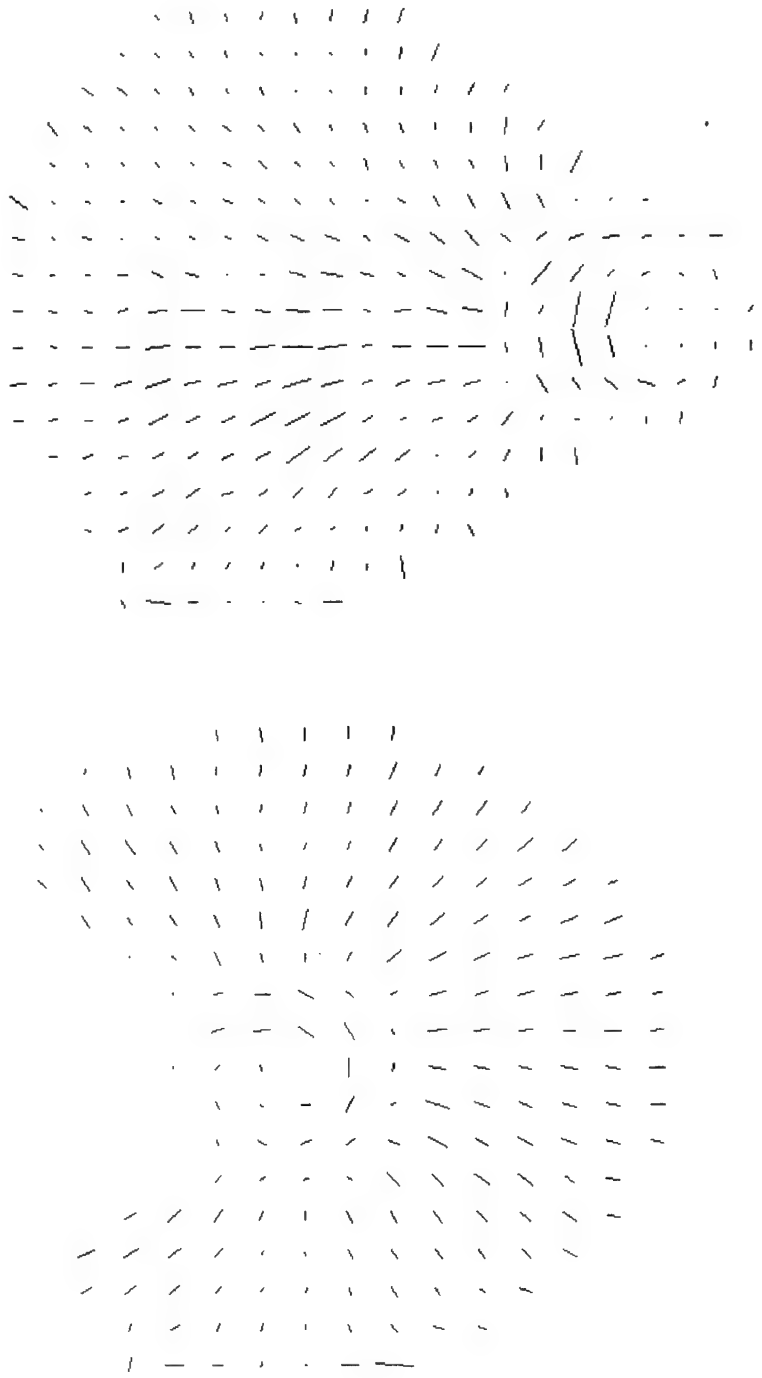

Polarization Diversity Active Imaging

R.A. Chipman, University of Alabama in Huntsville

Polarizance Vector
Gold cone

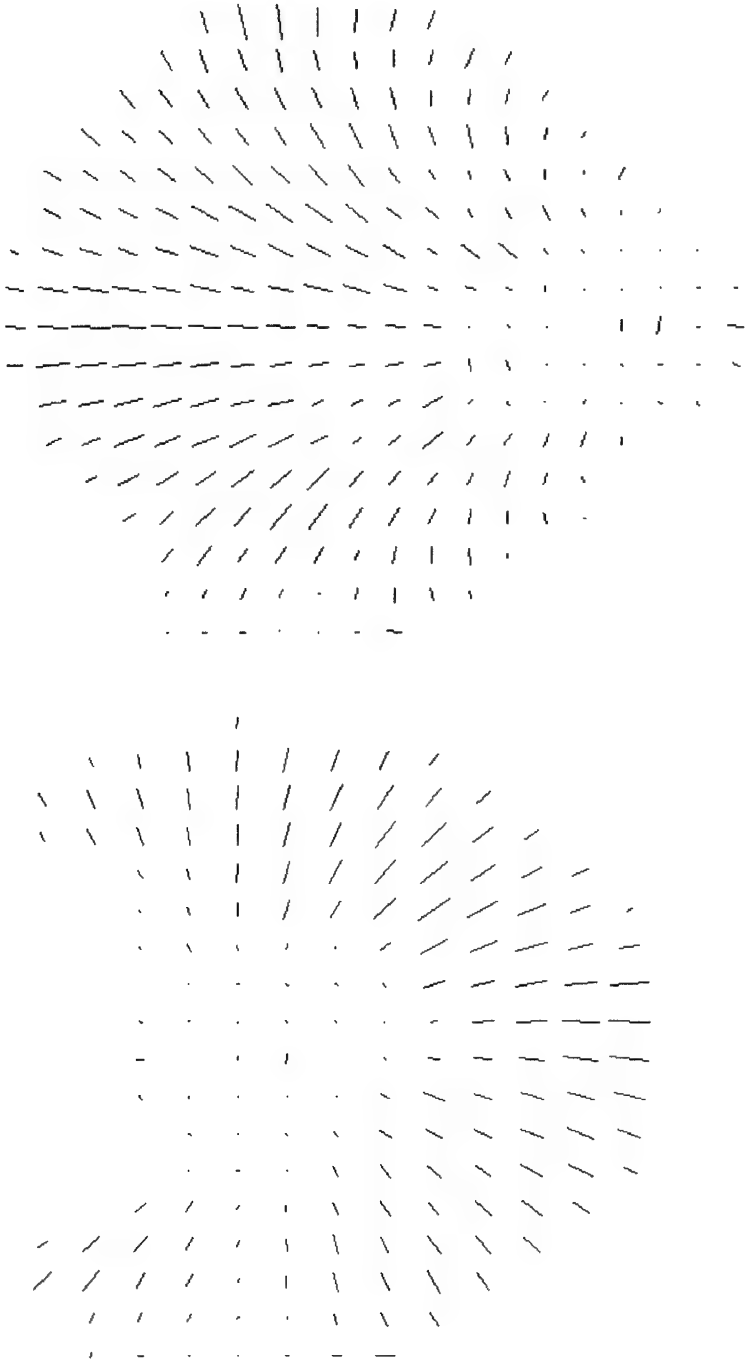

Appendix D:

Correlation between Diattenuation orientation and Angle of Scatter

Polarization Diversity Active Imaging

R.A. Chipman, University of Alabama in Huntsville

Metal sphere

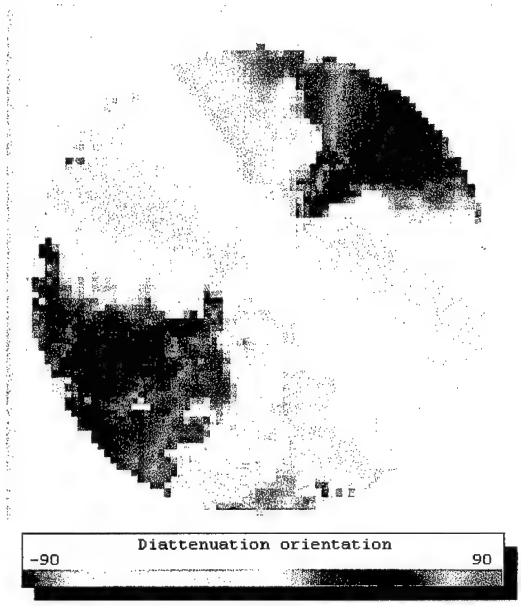

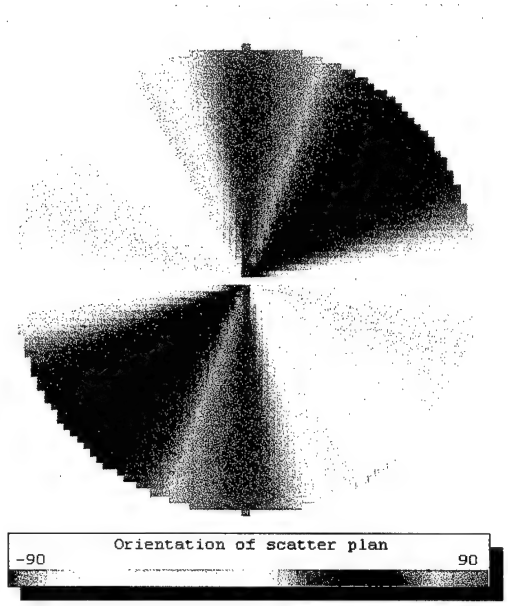

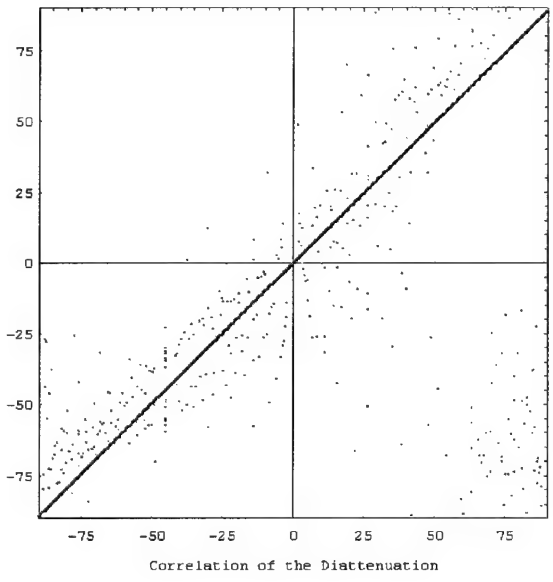

Polarization Diversity Active Imaging

R.A. Chipman, University of Alabama in Huntsville

Ping-pong ball

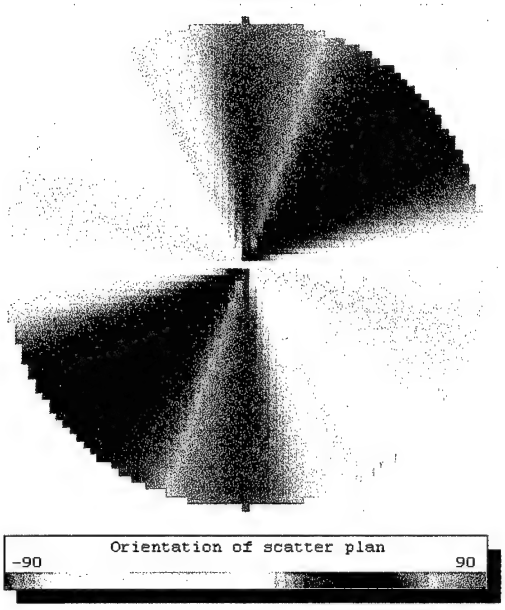

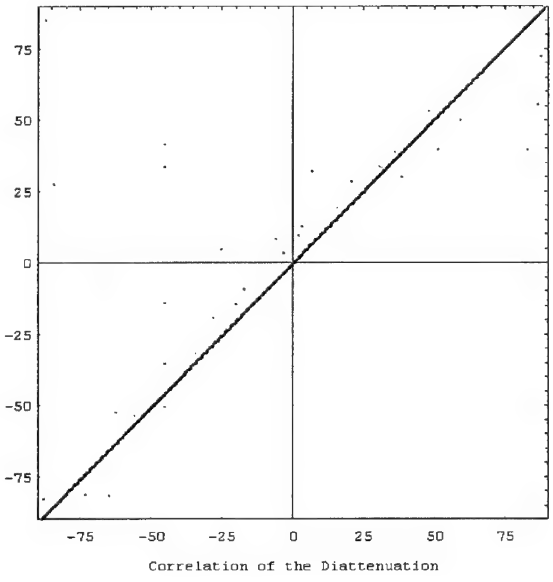

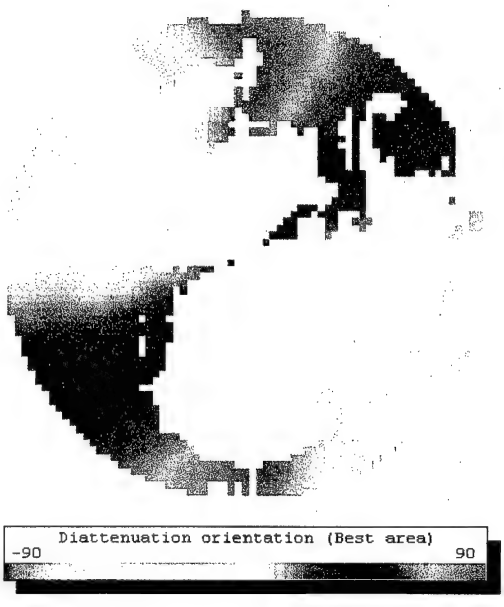

Polarization Diversity Active Imaging

R.A. Chipman, University of Alabama in Huntsville

Plastic sphere

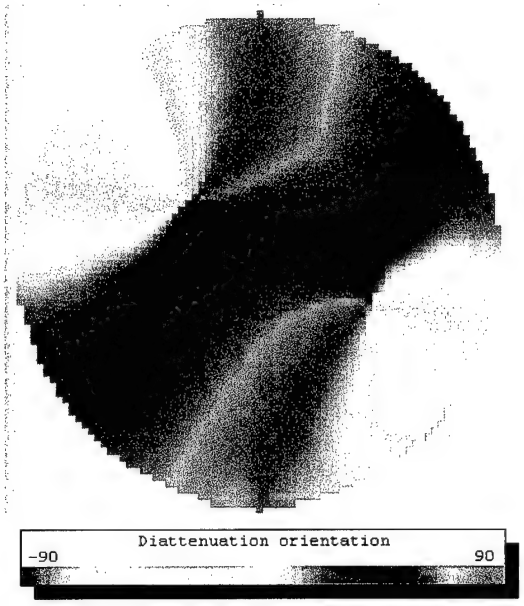

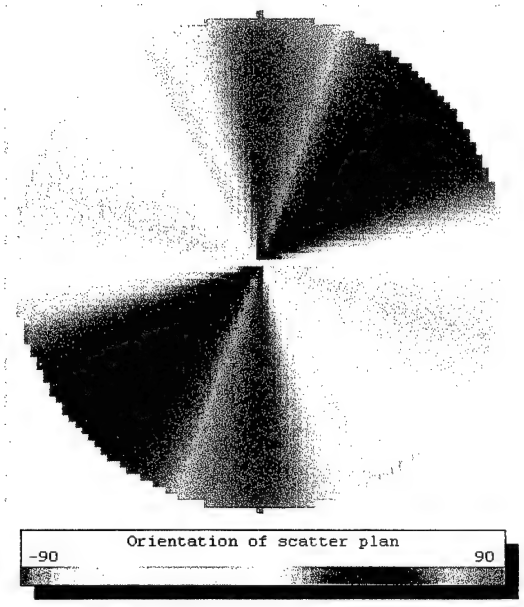

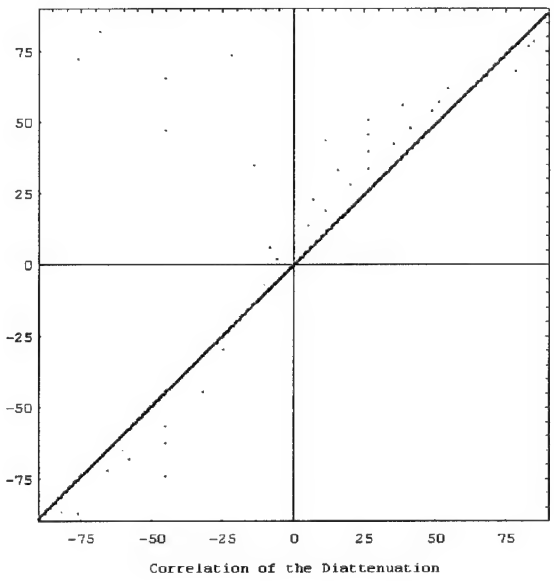

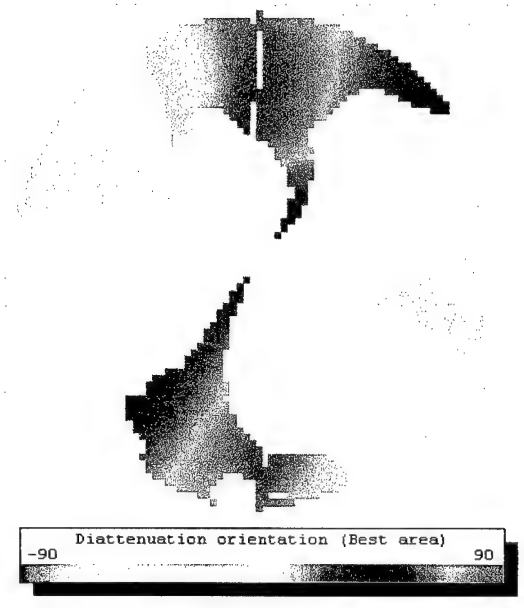

Polarization Diversity Active Imaging

R.A. Chipman, University of Alabama in Huntsville

Wood sphere

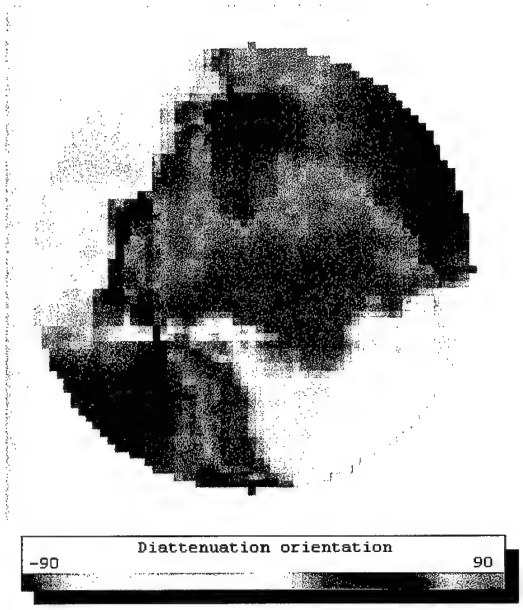

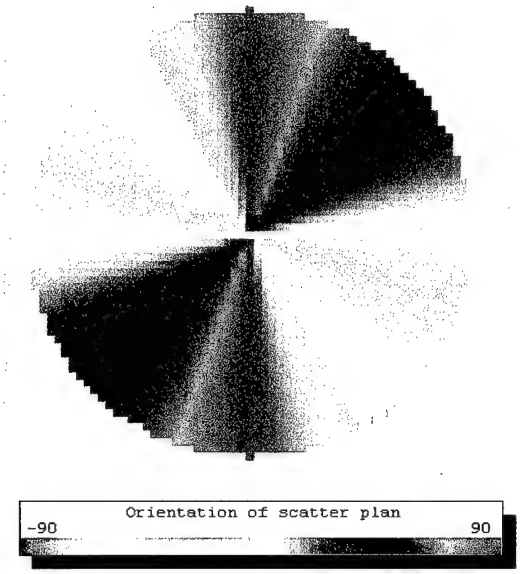

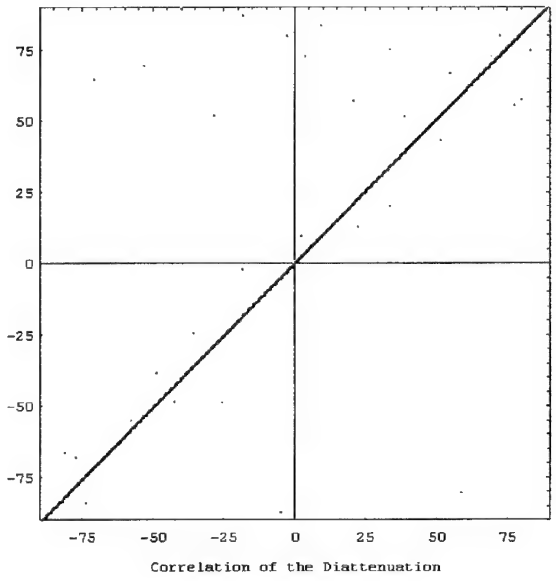

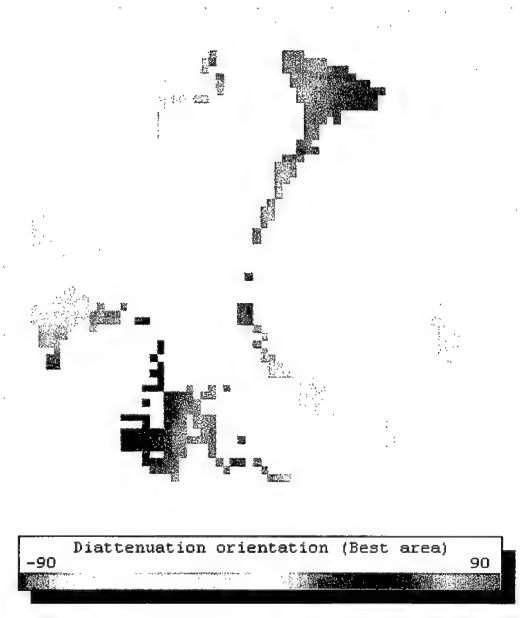

Appendix E:

Correlation between Diattenuation orientation and Angle of Incidence

Polarization Diversity Active Imaging

R.A. Chipman, University of Alabama in Huntsville

Plastic sphere

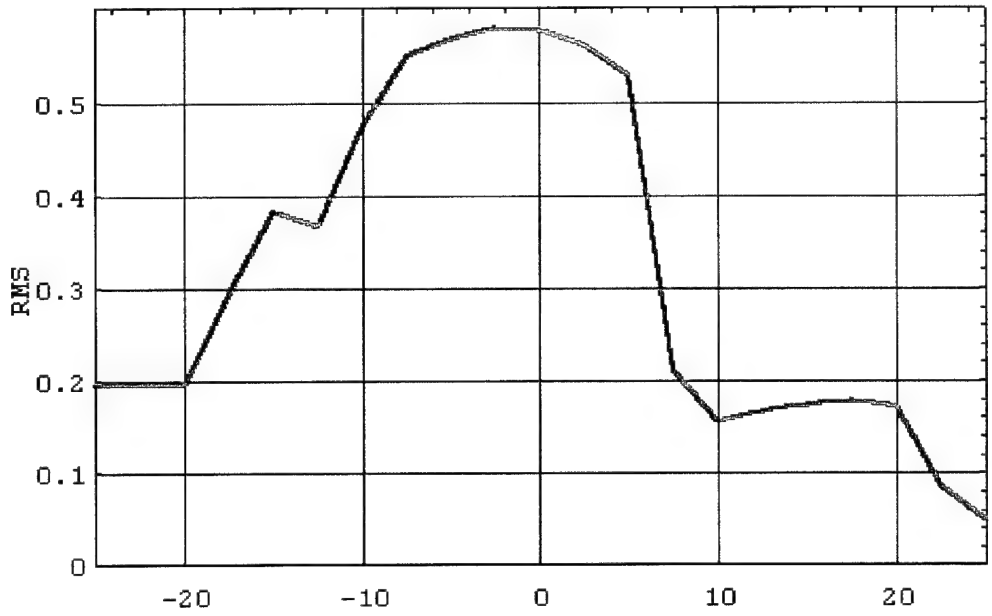

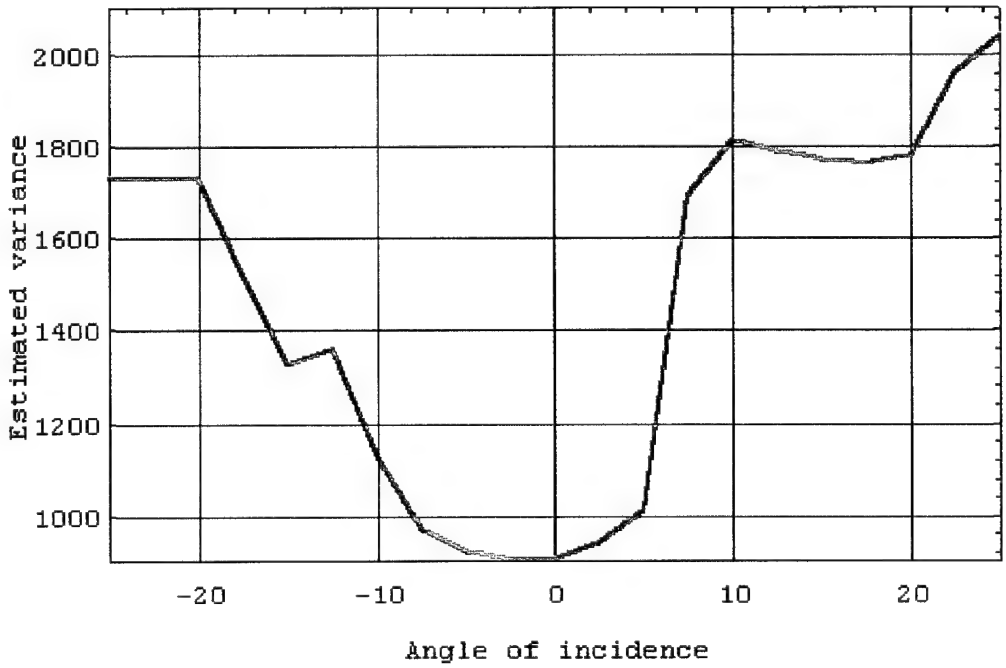

Polarization Diversity Active Imaging

R.A. Chipman, University of Alabama in Huntsville

Wood sphere

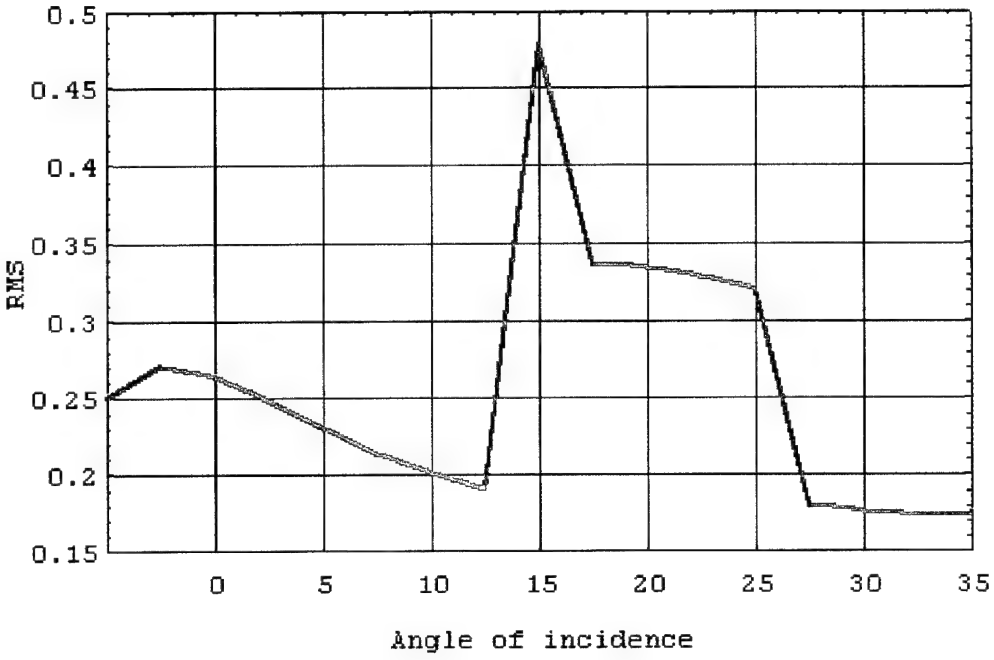

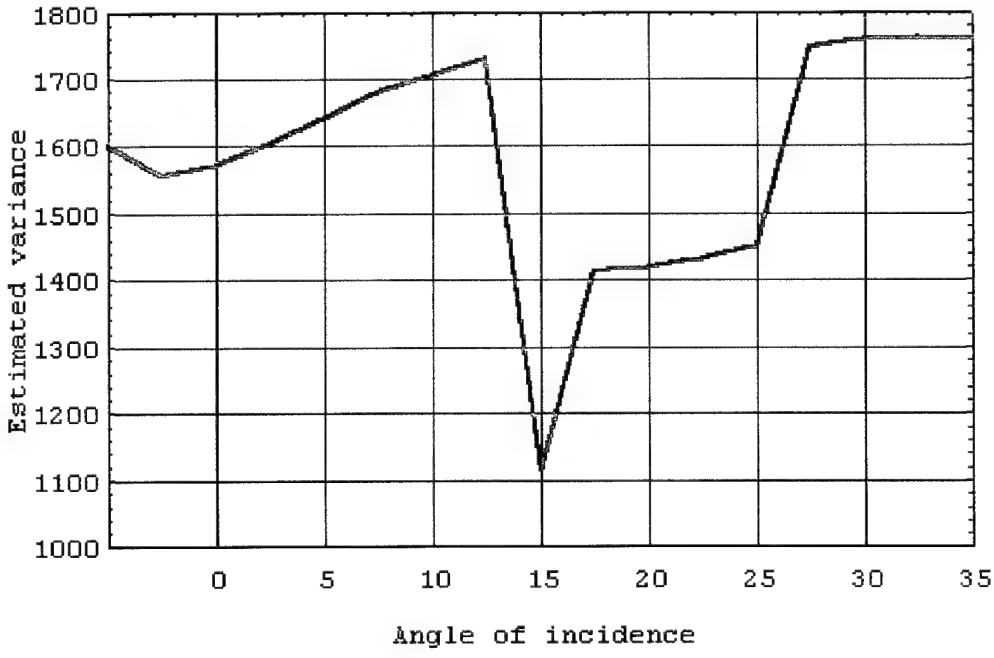

Appendix F:

Correlation between Retardance magnitude and Angle of Scatter

Polarization Diversity Active Imaging

R.A. Chipman, University of Alabama in Huntsville

Metal sphere

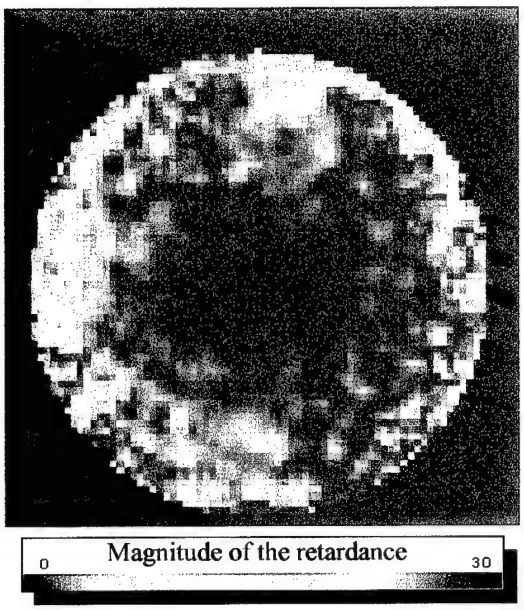

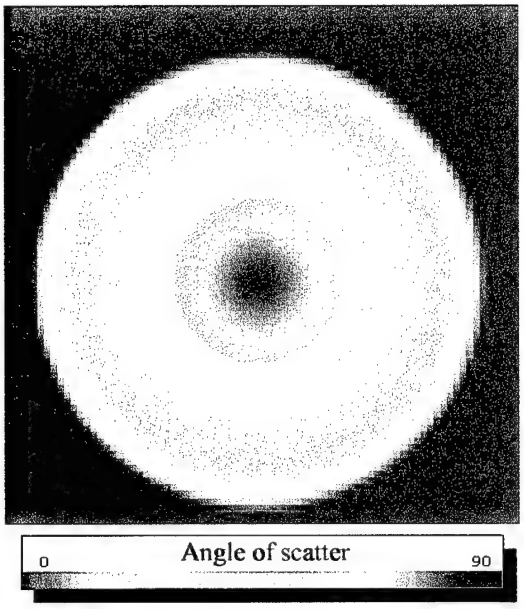

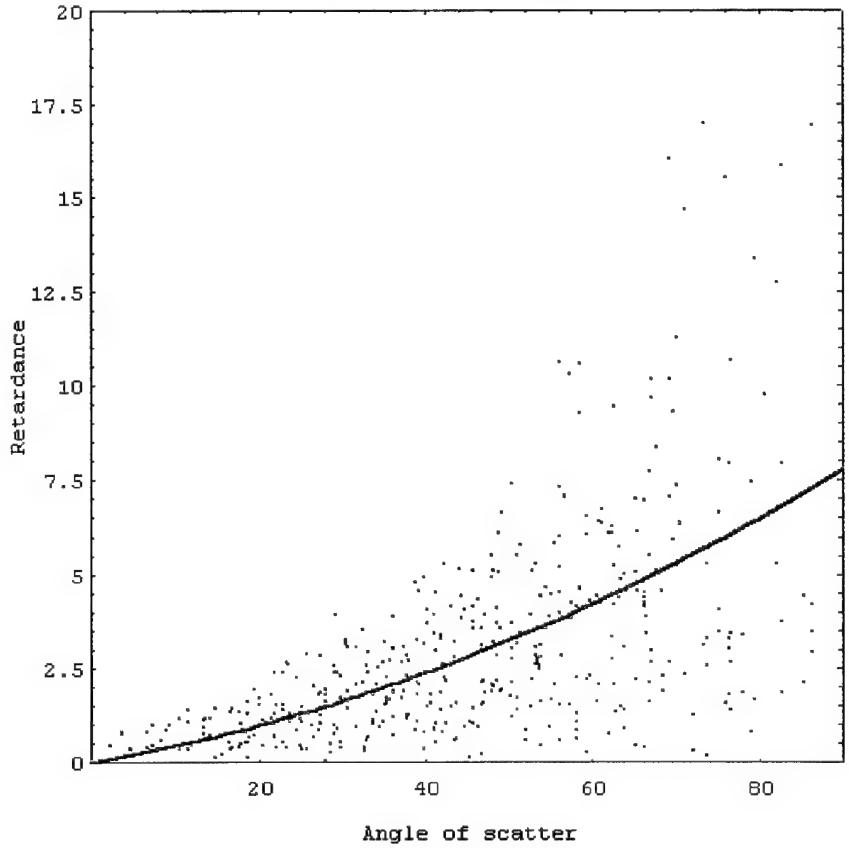

Polarization Diversity Active Imaging

R.A. Chipman, University of Alabama in Huntsville

Ping-pong ball

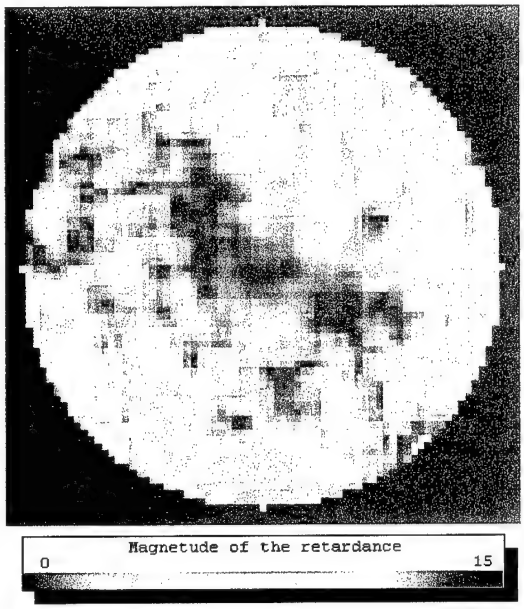

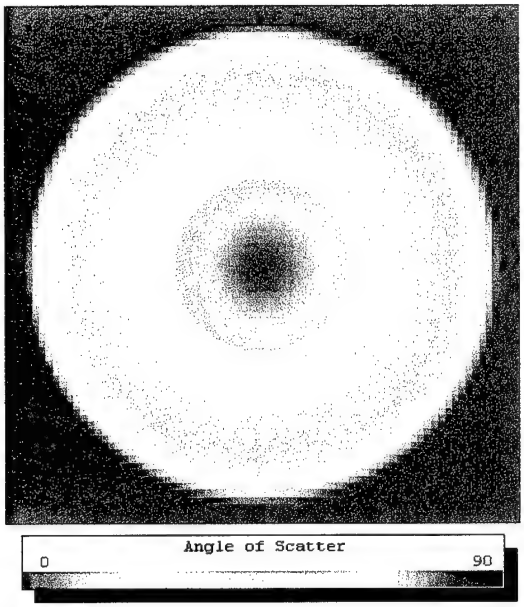

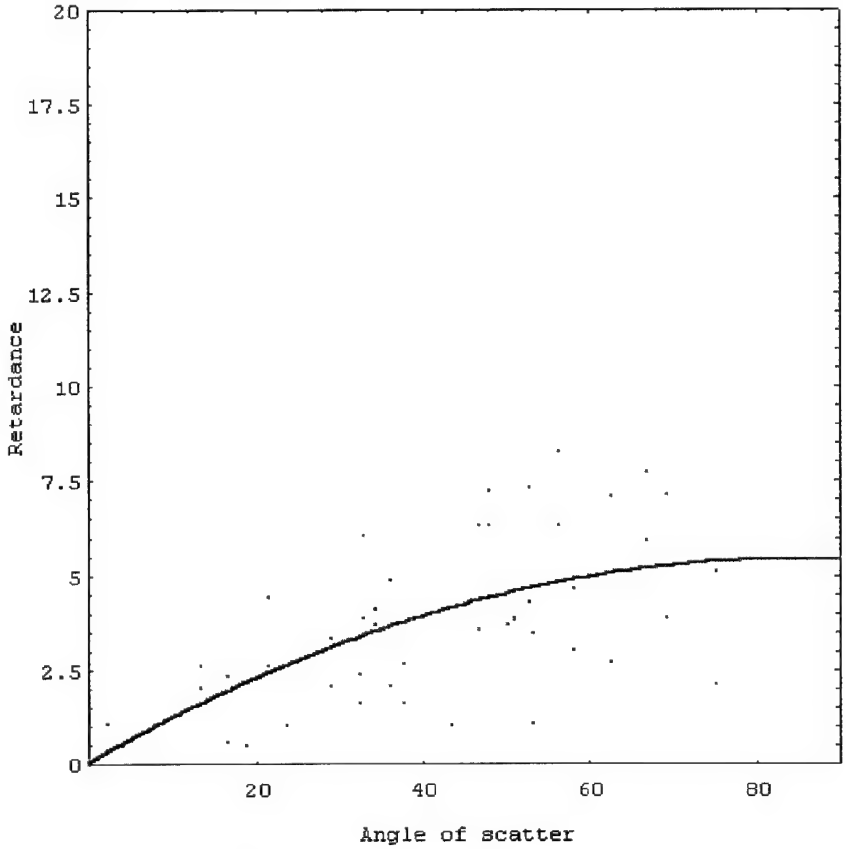

Polarization Diversity Active Imaging

R.A. Chipman, University of Alabama in Huntsville

Plastic sphere

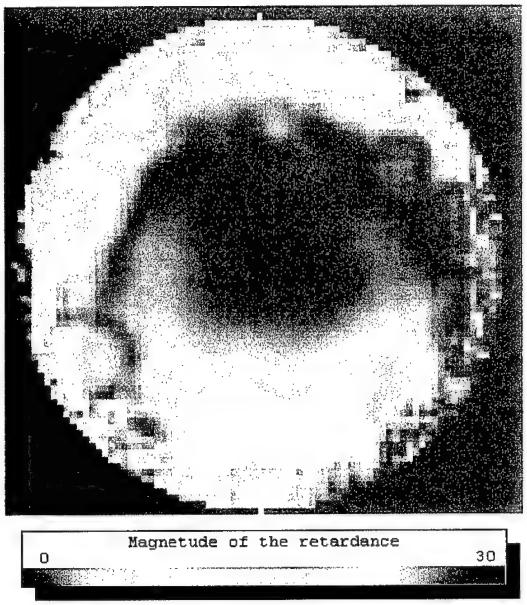

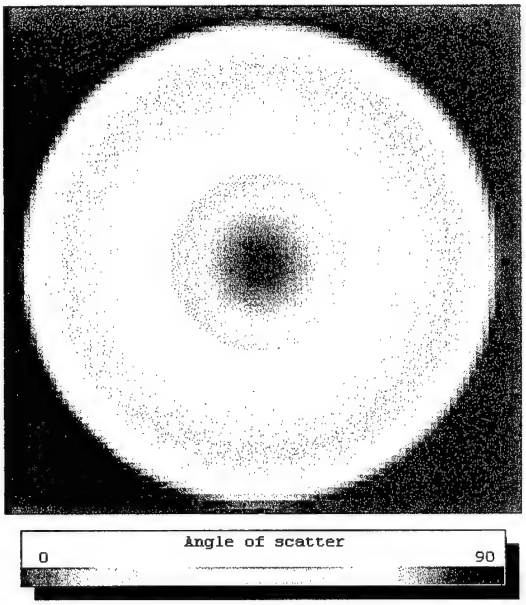

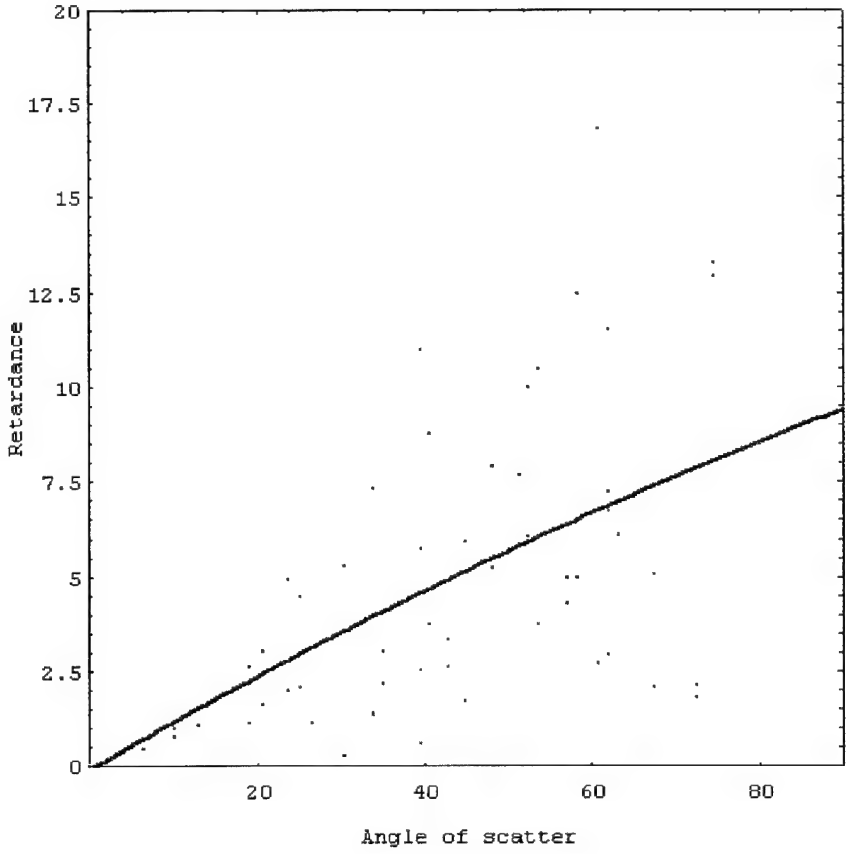

Polarization Diversity Active Imaging

R.A. Chipman, University of Alabama in Huntsville

Wood sphere

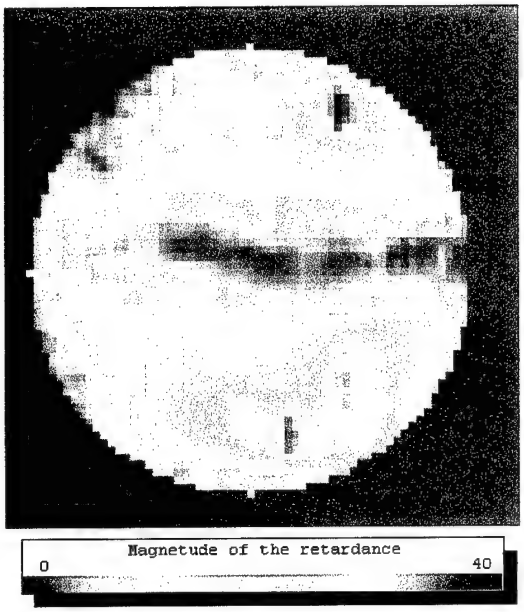

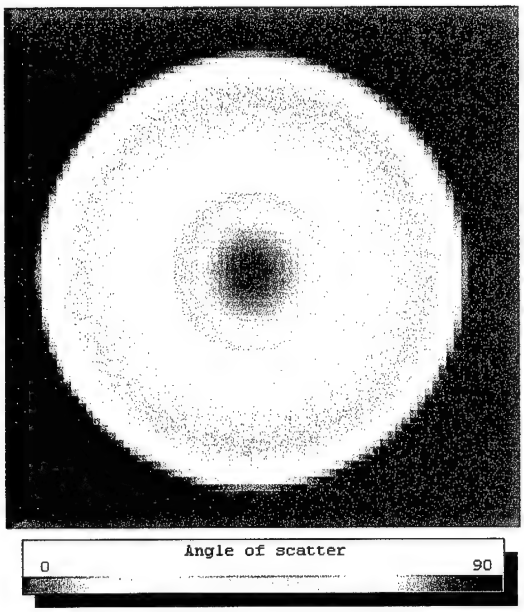

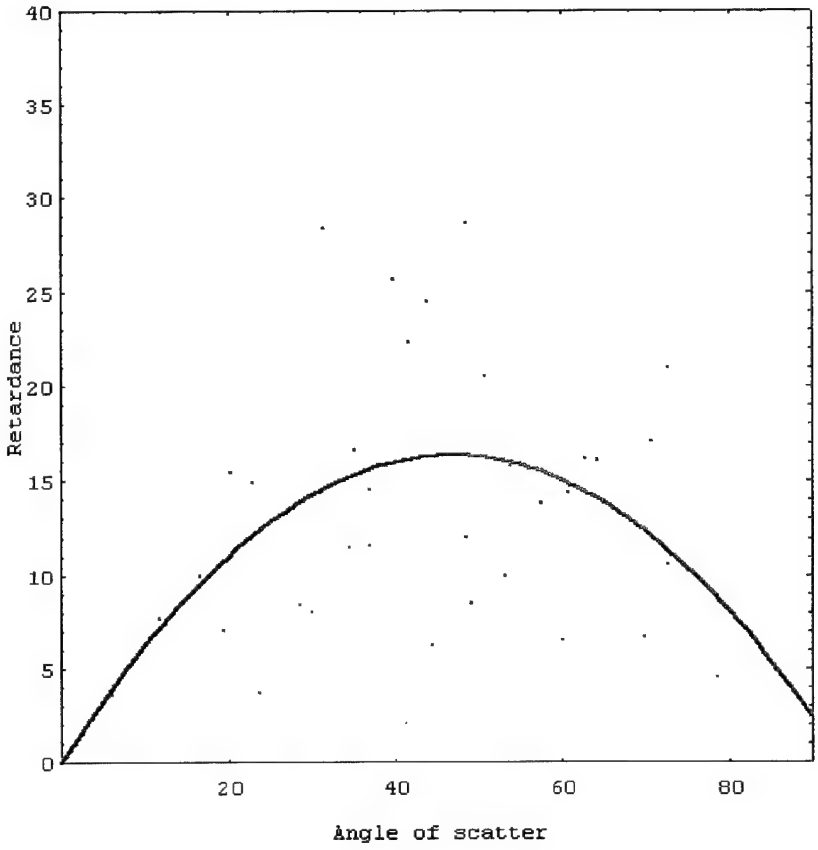

Appendix G:

Correlation between Diattenuation magnitude and Angle of Scatter

Polarization Diversity Active Imaging

R.A. Chipman, University of Alabama in Huntsville

Wood sphere

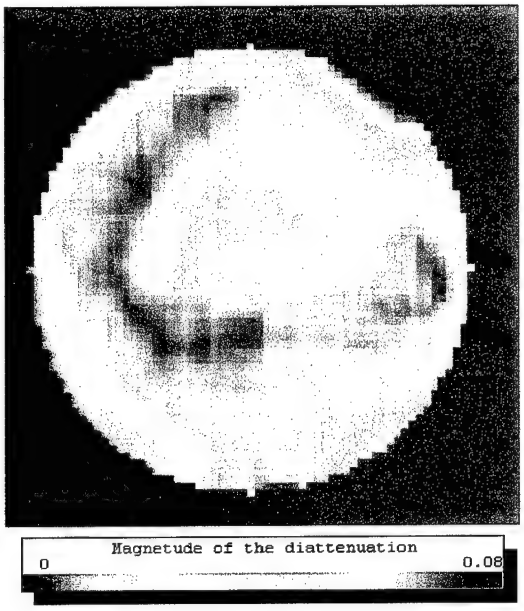

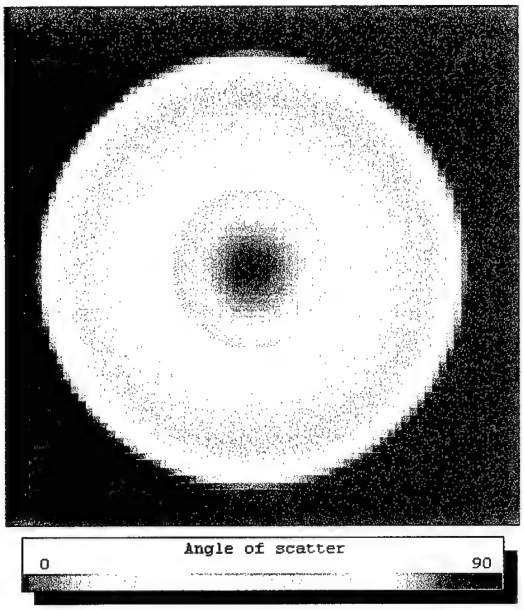

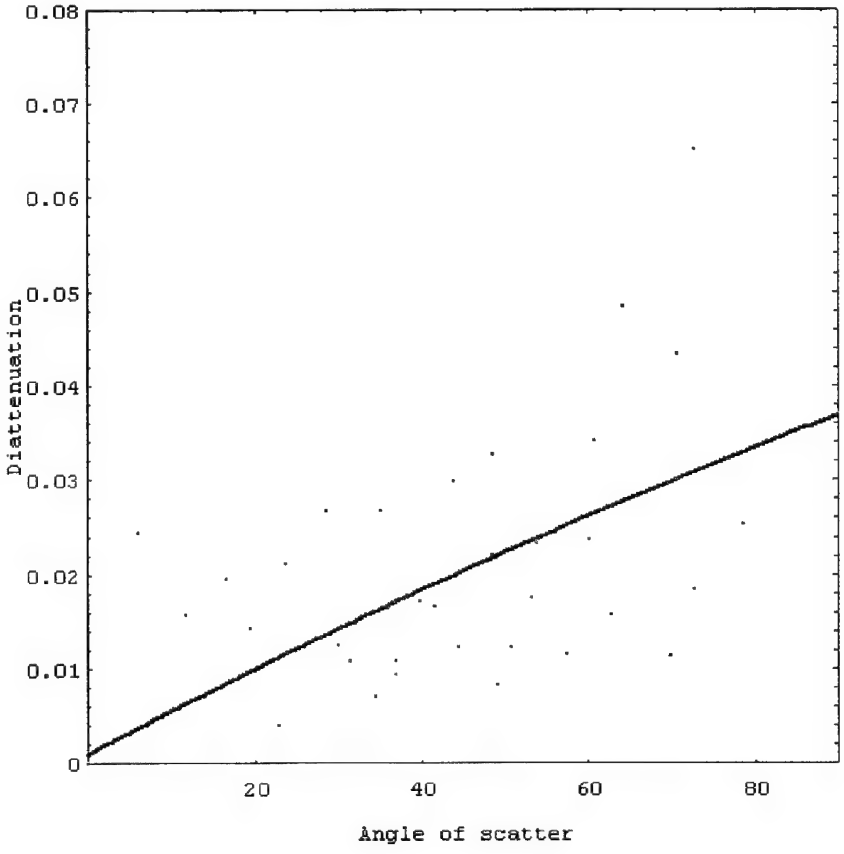

Polarization Diversity Active Imaging

R.A. Chipman, University of Alabama in Huntsville

Plastic sphere

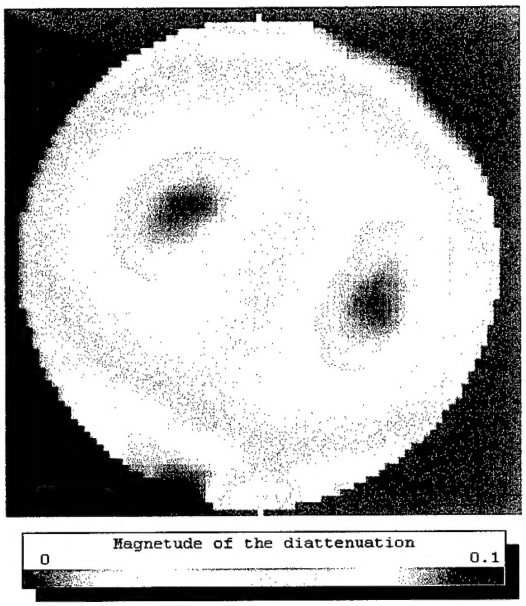

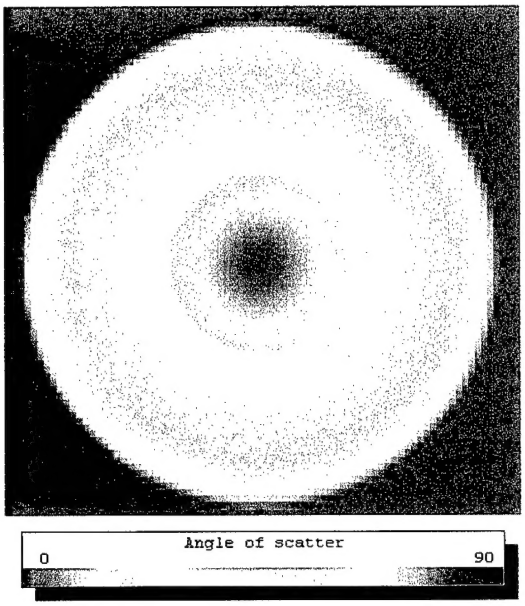

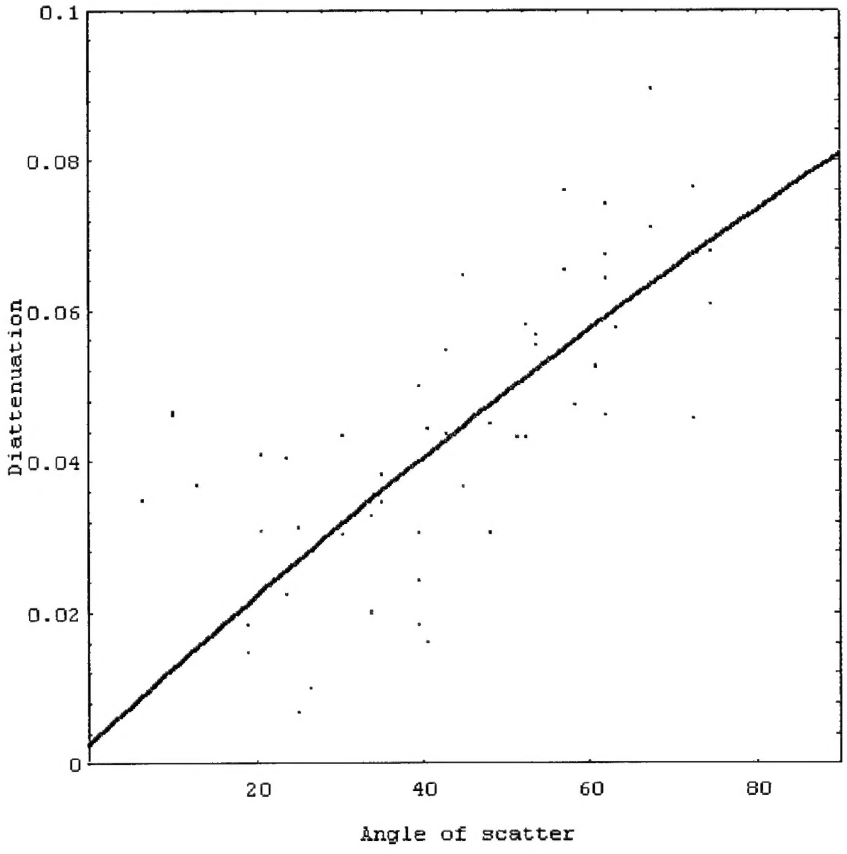

Appendix H:

Correlation between Polarizance and Angle of Scatter

Polarization Diversity Active Imaging

R.A. Chipman, University of Alabama in Huntsville

Plastic sphere

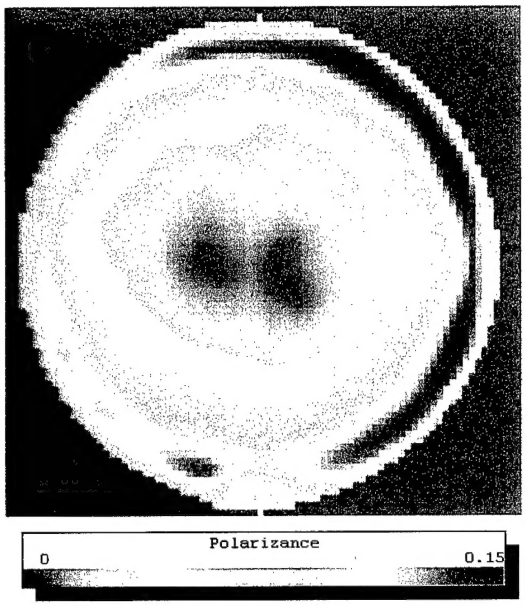

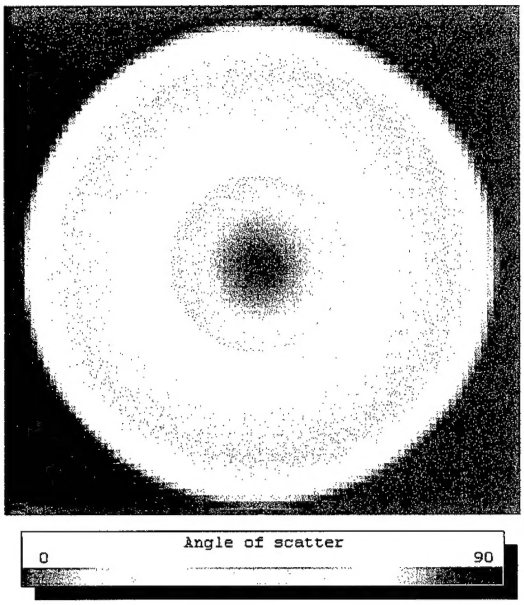

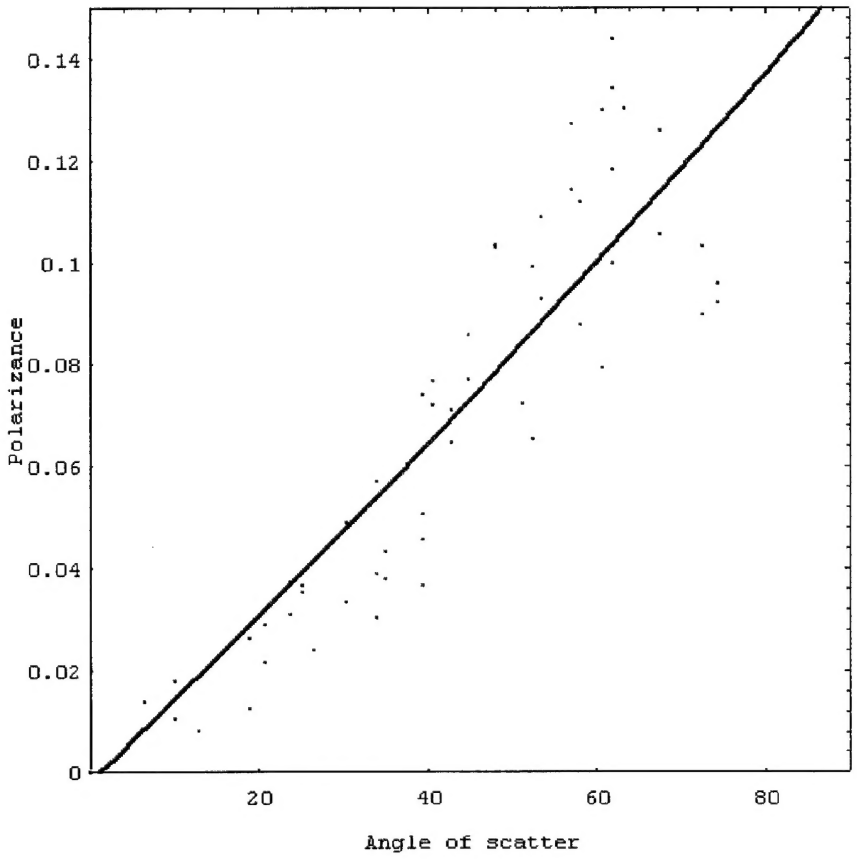

Polarization Diversity Active Imaging

R.A. Chipman, University of Alabama in Huntsville

Wood sphere